Cellular localization and characterization of Cyclooxygenase-2 in interstitial cells of the kidney

Dissertation

ZUR ERLANGUNG DES DOKTORGRADES DER NATURWISSENSCHAFTEN (DR.RER.NAT) DER FAKULTÄT FÜR BIOLOGIE UND VORKLINISCHE MEDIZIN DER UNIVERSITÄT REGENSBURG

vorgelegt von

Michaela Alexandra Anna Fuchs

aus

Regensburg

im Jahr

2019

All boundaries are conventions

Die vorliegende Arbeit entstand im Zeitraum von Juli 2015 bis Juli 2019 unter Anleitung von Herrn Prof. Dr. med. Armin Kurtz am Institut für Physiologie der Universität Regensburg.

Promotionsgesuch eingereicht am: 10.07.2019

Die Arbeit wurde angeleitet von: Herr Prof. Dr. med. Armin Kurtz

Unterschrift

(Michaela Fuchs)

Content

1 Introduction 8

1.1 The kidney, structure and primary function 8

1.2 Cyclooxygenase 11

1.2.1 Structure and Subtypes, Prostaglandin production and regulation 11

1.2.2 Localization of Cox in the kidney 14

1.2.3 Function and regulation of Cyclooxygenase-2 in the kidney 14

1.2.4 Pharmacological inhibition of Cyclooxygenase 15

1.2.5 Models for the functional investigation of Cox-2 in the kidney 16

1.3 Aims of this study 18

2 Material and Methods 20

2.1 Material 20

2.1.1 Instruments 20

2.1.2 Consumables 21

2.1.3 Commercial kits, enzymes and chemicals 22

2.1.4 Buffers and Solutions 24

2.1.5 Primer for genotyping and real time pcr 26

2.1.6 Probes for *in-situ* hybridization and antibodies 27

2.1.7 Software and internet services 28

2.2 Methods 29

2.2.1 Animals 29

2.2.1.1 Mouse strains and animal breeding 29

2.2.1.2 Genotyping of mice 30

2.2.1.3 Induction of Cre-Recombinase activity with tamoxifen 31

2.2.1.4 High salt diet 32

2.2.1.5 Treatment with low salt diet and Enalapril 32

2.2.1.6 Adenine-induced kidney fibrosis 32

2.2.1.7 Water deprivation for 24h 32

2.2.1.8 Unilateral ureteral obstruction 32
2.2.1.9 GFR measurement 32
2.2.2 Retrograde arterial perfusion of mice 33
2.2.3 Zonal dissection of kidneys 34
2.2.4 Tail cuff blood pressure measurement 34
2.2.5 Metabolic cages 34
2.2.6 Spot urine collection and analysis 35
2.2.6.1 Osmolality measurement 35
2.2.6.2 Sodium and potassium measurement in urine 35
2.2.7 Histological methods 35
2.2.7.1 Embedding of tissue in paraffin 35
2.2.7.2 Section of paraffin embedded tissue 36
2.2.7.3 Immunofluorescence staining 36
2.2.7.4 Sirius Red staining 37
2.2.8 *In-situ* hybridization utilizing the RNAscope® technique 37
2.2.8.1 Chromogenic and duplex RNAscope 37
2.2.8.2 RNAscope® Multiplex Fluorescent Assay 39
2.2.9 Microscopy 39
2.2.9.1 Microscopy for fluorescent dyes 39
2.2.9.2 Microscopy for RNAscope® 2.5 HD Reagent Kit (brow/duplex) 39
2.2.10 Molecular biology methods 40
2.2.10.1 Measurement of mRNA expression levels and cDNA synthesis 40
2.2.10.2 Quantitative real time PCR 41
2.2.11 Measurement of plasma parameters 41
2.2.11.1 Blood sample collection 41
2.2.11.2 Renin-ELISA 42
2.2.12 Statistics 42
3 Results 43

3.1 Localization of Cox-2 in the kidney and characterization of Cox-2 expressing cells 43
3.2 Regulation of Cox-2 expression in the kidney 48
3.3 Importance of Cox-2 for kidney development and function 52
3.3.1 Function of Cox-2 investigated by conditional gene deletion in specific compartments 52
3.3.1.1 Conditional deletion of Cox-2 in all cells of the adult kidney 52
3.3.1.2 Functional consequences of Cox-2 deletion in normally developed kidneys 54
3.3.2 Importance of Cox-2 in the FoxD1 compartment during nephrogenesis 56
3.3.2.1 Renin cell recruitment in FoxD1$^{+/Cre}$ Cox2$^{fl/fl}$ mice 59
3.3.3 Function of Cox-2 in PDGFR-β^{+} interstitial medullary cells 59
3.3.3.1 Functional relevance of interstitial Cox-2 expression under normal conditions 60
3.3.3.2 Handling of high dietary sodium in mice deficient for Cox-2 in PDGFR-β^{+} cells 62
3.4 Role of Cox-2 in kidney fibrosis 67
3.4.1 Progression of adenine induced fibrosis in mice deficient for Cox-2 67
3.4.2 Effects of Cox-2 deletion in PDGFR-β^{+} cells in the UUO model 71
4 Discussion 72
4.1 Cox-2 expression and regulation in cells of the kidney 73
4.2 Different functions of Cox-2 in the kidney 76
4.2.1 Cox-2 in the adult kidney 76
4.2.2 Role of Cox-2 in the stromal progenitor compartment 77
4.2.3 Function of medullary Cox-2 expression with different dietary sodium intake 79
4.5 Cox-2 in two models of kidney fibrosis 82
4.5.1 Influence of Cox-2 deletion in PDGFR-β^{+} cells on adenine induced nephropathy 82
4.5.2 Role of Cox-2 in PDGFR-β^{+} interstitial cells during 5d UUO 84

5 Summary 86
6 Bibliography 88
7 Annex 102
7.1 Abbreviations 102
7.2 Congress contributions 104
7.3 Declaration 105
8 Acknowledgement 106

1 Introduction

1.1 The kidney, structure and primary function

The kidneys of mammals are paired organs located in the lower abdominal cavity behind stomach and intestines on the left and right side of the spine. The huge number of different cell types present in the kidney gives an impression of the different physiological functions fulfilled by these organs.

The central function of the kidneys is the excretion of urinary metabolic waste products and keeping the acid/base and water homeostasis in the body. Closely connected to this is the control of systemic blood pressure and the renin-angiotensin-aldosterone system (RAAS) (Figure 1).

Other important functions are the production and release of hormones such as erythropoietin (EPO) for the formation of new red blood cells and calcitriol, the active metabolite of vitamin D, a central hormone for the bone metabolism[1,2].

Contained in a capsule of connective tissue, the mammalian kidney can be divided into three major zones: the cortex, the outer and the inner medulla. The most prominent functional subunit of the kidney is the nephron, including the glomerulus as the site of primary urine filtration and the following tubular system for urinary concentration. The human kidney contains about 1 million glomeruli, the murine kidney averages about 12.000 to 16.000 glomeruli.[3]

The primary urine is filtered in the capillary slings of the glomerulus by a system of three cooperative membranes, the fenestrated capillary endothelium, the basal membrane and the slit membrane between the long foot processes of the podocytes. Each glomerulus is surrounded by a bowman capsule and embedded in between other glomeruli, capillaries, interstitial cells and the proximal tubules in the kidney cortex. From the glomerulus, the primary urine is transported along the proximal tubule through the loop of Henle to the distal tubule and into the collecting duct (CD). During the passage of the urine through the different parts of the tubular system, important electrolytes such as sodium, potassium and glucose as well as the majority of the filtered water are reclaimed by an osmotic countercurrent system between the tubules and the adjacent blood vessels.

The function of the macula densa cells is the sensing of luminal ion concentrations, especially chloride, and the appropriate adjustment of glomerular filtration and electrolyte reuptake[4,5]. These cells are a specialized subtype of the cortical thick

ascending loop of Henle (cTAL) and are located in close proximity to the renin producing cells at the vascular pole of the glomerulus. Together with the renin producing cells and extra-glomerular mesangial cells, they form the juxtaglomerular apparatus (JGA)[6].

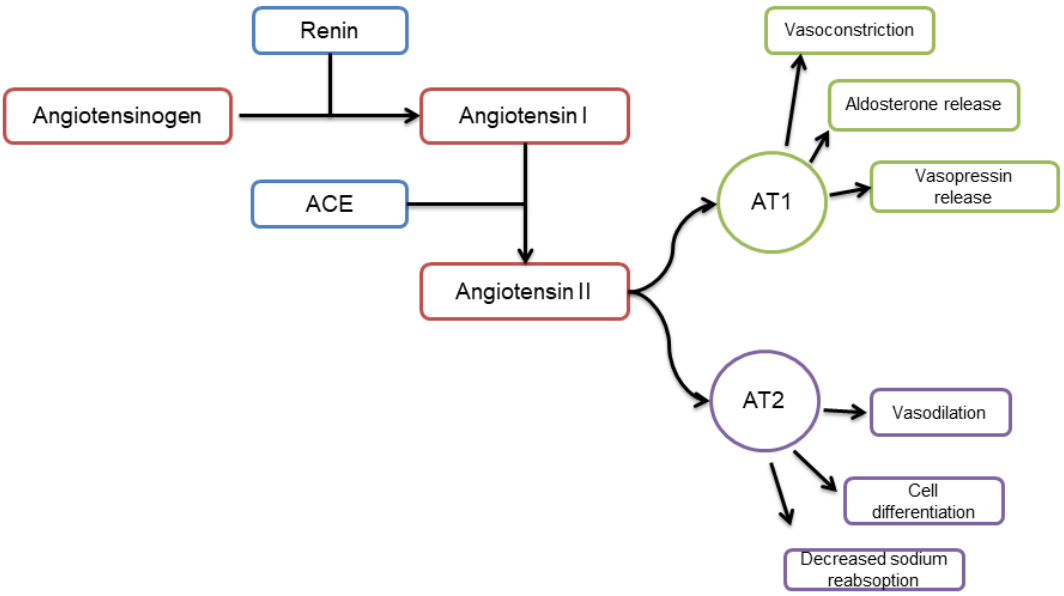

Figure 1: Schematic overview of the RAAS and its most important physiological effectors; after generation of ANGI by renin the ACE converts it to ANGII that exerts the physiological effects through binding to AT1 or AT2 receptors

Depending on the luminal chloride concentration, the cells of the macula densa control the synthesis and release of renin from the adjacent cells[4,7]. Renin, an aspartyl protease the rate limiting enzyme of the RAAS converts angiotensinogen, produced in the liver, to angiotensin I by cleaving a decapeptide of the N-terminal end[8–10] (Figure 1). Angiotensin I is then further processed by the angiotensin-converting-enzyme (ACE) to angiotensin II (ANG II) which can bind to two different angiotensin receptors (AT1 or AT2) in humans. After binding to its receptors, ANG II exerts a broad spectrum of effects such as vasoconstriction leading to a reduced renal blood flow, release of aldosterone for a heightened reabsorption of sodium in the proximal tubule and vasopressin release leading to water retention. All these effects are aimed toward maintaining blood pressure and water homeostasis under varying conditions such as changed dietary salt intake or an acute volume challenge[7].

Beside tubular cells, the most numerous cell type in the kidney are interstitial pericytes and fibroblast-like cells. These cells are located between the tubules and small vessels across all kidney zones and uphold the kidney structure[3,11].

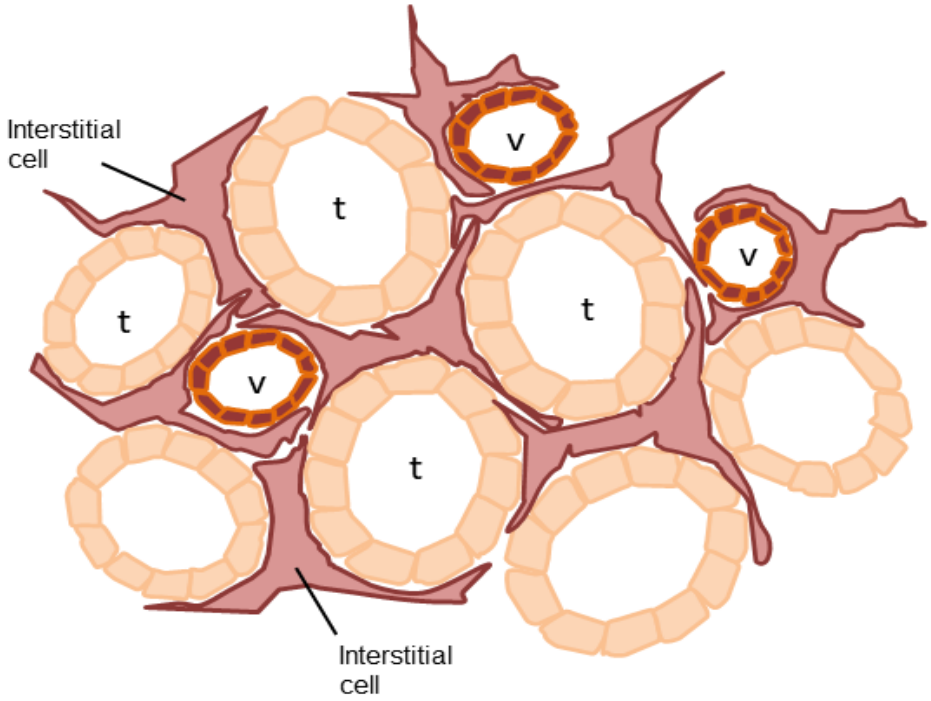

Figure 2: Stylized view of interstitial fibroblast-like cells in the kidney; interstitial cells are located between tubules (t) and vessels (v) in the interstitial space across the kidney, their long cellular processes are wrapped around tubules, vessels and also other interstitial cells; interstitial cells in direct contact with blood vessels are classically viewed as pericytes

By the classical definition, only cells in direct contact to blood vessels are labeled as pericytes[1,12,13]. Other, non-classical pericytes, located in the interstitial space of the kidney, share many characteristics and cellular markers with classical pericytes and are called interstitial fibroblast-like cells. These cells show the same morphology as pericytes with elongated cell processes and close contact to tubules, but are not inflammatory or endothelial cells (Figure 2). Functionally these cells produce collagen, fibronectin and include the population of native EPO producing cells in the kidney[1,14].

Due to the similarities between classical pericytes and interstitial fibroblast-like cells a clear distinction is difficult. Additionally, the above-mentioned overlap in markers, such as the platelet derived growth factor receptor β (PDGFR-β) in the whole kidney and ecto-5'-nucleotidase (CD73) in the cortex gives no clear identifier[1]. This overlap is probably caused by their common origin from forkhead box D1 positive ($FoxD1^{+}$) stromal progenitor cells (Figure 3)[3,15,16]. Due to the close relation of these cell types, the terms pericytes and interstitial cells are used synonymously in this work.

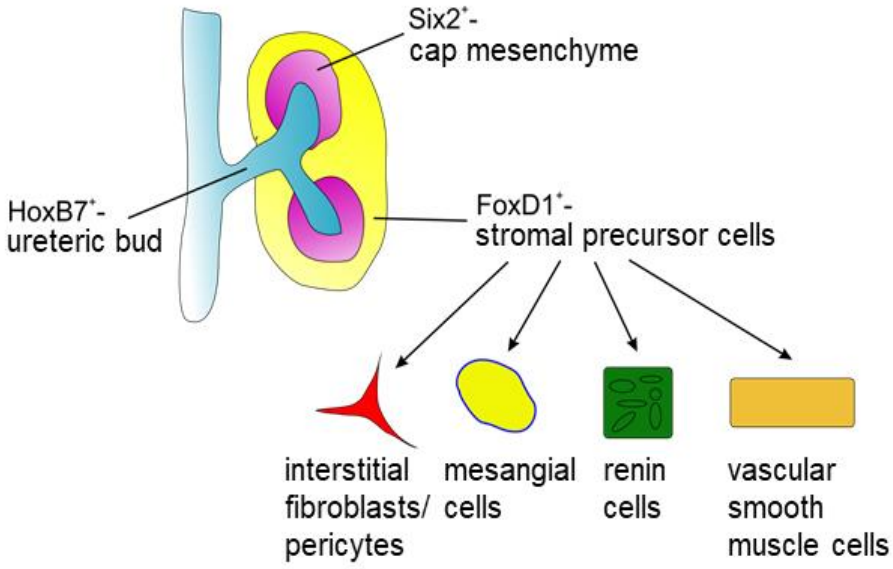

Figure 3: Cells deriving from the FoxD1⁺ stromal progenitor compartment of the kidney include interstitial pericytes, mesangial cells, renin producing cells and vascular smooth muscle cells; cells of HoxB7⁺ decent differentiate into the collecting ducts while cells of the Six2⁺ mesenchyme become the tubular system; figure modified from Gerl 2018

Other cells from the compartment of stromal progenitors are the mesangial cells, renin producing and vascular smooth muscle cells[11,17].

1.2 Cyclooxygenase

1.2.1 Structure and Subtypes, Prostaglandin production and regulation

The first enzyme described to catalyze the reaction of arachidonic acid (AA) to prostaglandin G and H (PG), was discovered in 1971, called prostaglandin-endoperoxide synthase (PTGS)[18] and cloned in 1988[19]. The later discovery of a second isoform of this enzyme led to the distinction into Cyclooxygenase (Cox) 1 and 2[20,21]. More recently a third isoform of Cox, Cox-3, has been reported in the central nervous system and heart of mice. This Cox-3 is a splicing variant of Cox-1[19,22]. Splicing variants of Cox-2 have also been reported, but none showed an enzymatic activity[19].

Cox-1 and Cox-2 share about 66% of their amino acid sequence, but are located on different chromosomes[19,23–27]. The two enzymes differ in a number of important key factors. In Cox-2 the catalytic center is larger than in Cox-1, but the speed for the reaction of arachidonic acid to prostaglandin H_2 (PGH_2) is similar[19,28]. The speed of Cox-3 on the other hand is markedly lower[19,22]. Intracellular Cox-1 and Cox-2 both can be found in the endoplasmic reticulum and on the nuclear envelope. But two isoforms

differ in the source of AA used in the catalyzed reaction, which for Cox-1 is mostly exogenous while Cox-2 uses both endo- and exogenous sources of AA. The intrinsic intracellular mobilization of AA from phospholipids of the nuclear membrane is most relevant for the function of Cox-2 and can be affected by a number of different phospholipases (PL) for example the cytosolic or secreted form of PLA_2 (cPLA2, $sPLA_2$)[19,28].

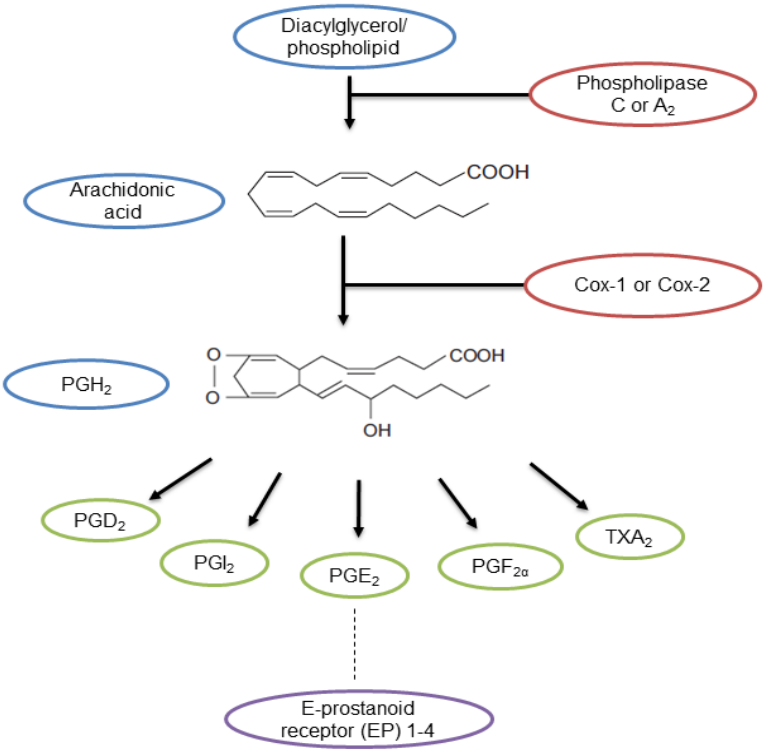

Figure 4: Pathway of prostaglandin synthesis from AA to the different biologically active prostaglandins; AA is converted to prostaglandin PGH_2 by either Cox-1 or Cox-2, depending on cell and tissue type; from PGH_2 specialized synthases are responsible for the formation of the effector PGs; figure modified after Hao et. al 2008

Cox catalyzes the reaction of AA to PGH_2 in two sequential reactions. In the initial step AA is cyclized by Cox-1 or Cox-2 through the formation of a 15-hydroperoxy group, resulting in PGG_2. This cyclizing step gave the Cyclooxygenase enzymes their name. In the following step, performed by the same enzyme, PGG_2 is reduced at the hydroperoxy group to PGH_2[19]. Once arachidonic acid has been transformed to prostaglandin H_2, specialized and locally restricted synthases catalyze the reactions to the biologically active compounds such as PGE_2, PGI_2, $PGF_{2\alpha}$ and TXA_2 (Figure 4)[29]. In the kidney, the most abundant prostaglandin is PGE_2. It is formed mostly by the microsomal (also called membrane associated) prostaglandin E synthase (mPGES1 or 2)[19,30,31]. Other PGES have been described for the formation of PGE_2 but are not predominant in the kidney.

Through the multidrug resistance protein 4 (MRP4) PGE_2 is transported out of the cells and can affect the surrounding tissue[32]. Receptors for prostaglandins formed by Cox-1 and Cox-2 are G-protein coupled E-prostanoid receptors (EP) of different subtypes, locations and functions[31,33–35].

A further difference between the two Cox genes is their translational regulation, so that the production of PGs is in part controlled through the degree of Cox gene expression. Cox-1 has been labeled as a "housekeeping"-gene with a stable constitutive expression in many tissues, it lacks inducible promotor regions in the 5´- region of the gene[19,28]. For Cox-2 a number of distinct promotor regions in the 5´ sequence have been identified[4,28,36,37] (Figure 5).

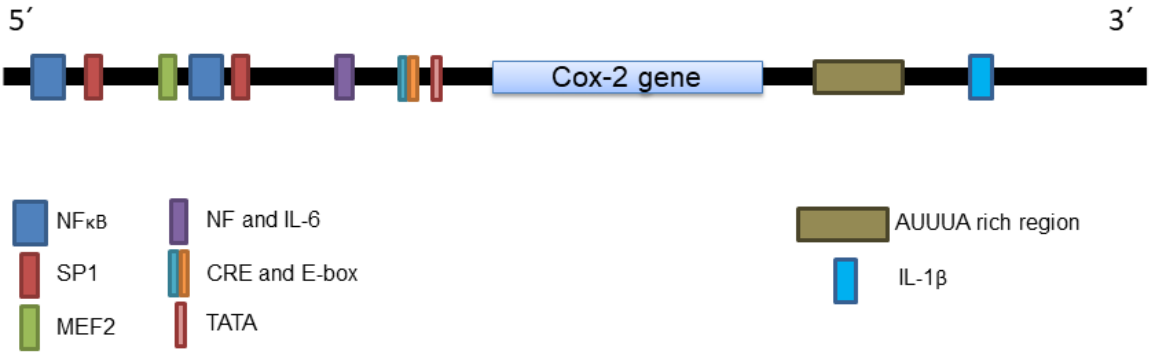

Figure 5: Stylized overview of the different promotor sites associated with the Cox-2 gene; in the 5´-region various inflammatory as well as growth factors are able to bind and then induce transcription of the Cox-2 gene; among these are Nuclear factor-kappa-B (NFκB), transcription factor Sp1(SP1), myocyte enhancer factor-2 (MEF2), nuclear factor (NF), interleukin 6 (IL-6), a cAMP-responsive element (CRE) and a TATA motive; in the 3´-untranslated region of the Cox-2 gene, regulator regions for the stability of the mRNA could be identified; figure modified from Harris et. al 2001

Among the transcriptional factors enhancing the Cox-2 gene expression many growth factors such as NF and PDGF as well as inflammatory stimulants such as IL-6 and NFκB can be found[4,37–40]. The numerous promoters of the Cox-2 gene also explain its designation as "the inducible" Cox isoform. In the 3´-untranslated region of the Cox-2 gene two different binding sites influencing the stability of Cox-2 mRNA could be sequenced[4,41]. A region with a 22 times repeat of the mRNA destabilizing AUUUA motive was found, but a binding site for IL-1β stabilizing the mRNA could also be identified[42]. It has been postulated that the AUUUA rich regions are responsible for the Cox-2 suppressing effects exerted by glucocorticoids, as these regions are missing in the Cox-1 gene[41].

1.2.2 Localization of Cox in the kidney

In the human and murine kidney, the two Cox isoforms and their respective prostaglandin receptors have been located in diverse compartments[4,23,29,43,44].

Cox-1 is thought to be expressed in the loop of Henle, smooth muscle cells, collecting ducts, endothelial cells and interstitial cells[23,28]. The expression of Cox-2 is more contested. Controversial locations for the expression of Cox-2 have been published over the years for humans and different laboratory animals[43–45]. The most commonly postulated expression sites for Cox-2 in mammals are the cells of the macula densa in the renal cortex and medullary interstitial cells[43,44,46,47]. But the low expression of Cox-2 in mice and humans, when compared to other laboratory animals such as rats, has made the investigation of this enzyme difficult[43].

As mentioned above the cells of the macula densa are specialized cells of the cTAL and part of the JGA. Due to the involvement of the macula densa cells in the regulation of renin release, this Cox-2 expression site has been studied extensively [4,5,7,23,28,43]. While some functions for the interstitial medullary Cox-2 expression have been postulated (see 1.2.3) the nature of these cells and their origin has not been investigated in detail[48].

1.2.3 Function and regulation of Cyclooxygenase-2 in the kidney

In the kidneys of mice PGE_2 is the most abundant prostaglandin in the cortex and medulla, but PGI_2 and $PGF_{2\alpha}$ can also be detected in substantial concentrations[30,49]. In principal Cox-1 and Cox-2 are able to produce these prostaglandins. A number of physiological functions have been postulated for these prostaglandins based on different models. More functions of Cox in the kidney became apparent with the widespread use of Cox inhibitors to treat pain and inflammation.

The cells of the macula densa sense the ion concentration in the lumen of the cTAL through the transport rate of the Na^+-K^+-$2Cl^-$ (NKCC2) cotransporter[4,6,10]. It has been postulated that a lower luminal salt concentration or the pharmacological inhibition of NKCC2 leads to an activation of intracellular kinases such as p38 mitogen-activated protein kinase (p38), mitogen-activated protein MAP kinases ERK1 and 2 which in turn activate Cox-2[4,6]. This same pathway also induces the microsomal prostaglandin E synthase (mPGES)[50] in the macula densa cells that processes PGH_2 into PGE_2, which

then effects the release of renin. But the degree to which renin release is dependent on Cox-2 is still unclear[10].

In the renal medulla, the postulated functions and mechanisms for Cox-2 are more diffuse. PGE_2 has been repeatedly linked to cell survival under hypertonic stress such as during dehydration[24,51] and to the salt handling ability of the kidney[30,52–54]. The cellular expression site and Cox-isoform involved in these functions and the underlying mechanism have not yet been defined.

Besides dehydration, other conditions have been reported to induce medullary PGE_2 formation. For example an increased dietary salt intake leads to increased PGE_2 in the medulla[48,53]. Additionally, PGE_2 has also been reported to play a protective role in states of renal tissue hypoxia and during times of high medullary oxygen consumption[55–57].

1.2.4 Pharmacological inhibition of Cyclooxygenase

Blocking cyclooxygenase activity has been one of the first ways of pain management[19,58]. But the inhibition of both isoforms, Cox-1 and Cox-2, with non steroidal anti-inflammatory drugs (NSAIDs) is associated with a predisposition for hypertension, gastro-intestinal lesions and increased renal and cardiovascular risks[31,59–67]. Furthermore the application of Cox-inhibitors during pregnancy can cause severe renal developmental defects[68,69]. These side effects were long attributed to the unspecific block of Cox-1, the “housekeeper” isoform, by NSAIDs.

The larger binding pocket for AA in the Cox-2 enzyme made it possible to design drug molecules inhibiting only Cox-2 activity[28]. Unfortunately, the introduction of these Cox-2 specific inhibitors did not eliminate all side effects. On the contrary, as Cox-2 selective inhibitors gained widespread use as chronic pain mediators with less gastro-intestinal side effects, it became clear that these drugs had severe side effects unique to their class[44,68,70].

Cox-2 selective inhibitors are associated with an increased risk of hypertension[71] and decreasing the efficiency of antihypertensive drugs[44,62,72,73]. A link between dietary salt intake, Cox-2 selective inhibitors and blood pressure dysregulation in otherwise normotensive patients has also been published[10,48,54,59,74]. In some patients treated with Cox-2 selective inhibitors, incident of papillary necrosis, water and sodium retention with edema and tubulo-interstitial nephropathy were reported[31,44,45,66,67,70].

These effects showed that Cox-2, which had been labeled as the inflammatory induced isoform at its discovery, must also have important basal functions besides inflammation and pain. But the detailed origin and mechanism for the heightened incidence of cardiovascular events, renal injury and the salt sensitive hypertension have not yet been described completely[44,70,75]. It is also not clear yet where inhibition of Cox-2 expression is causative for these side effects.

1.2.5 Models for the functional investigation of Cox-2 in the kidney

To date most of the functional data for Cox-2 in the kidney has been gathered either in rat or dog models[43,44,46,54,74,76–79], in cultivated cells[24,53,80] or global deletion models for mice[49,61,81,82].

An inherent problem with isolated cells are the phenotypic and genetic shifts that can occur by taking the cells out of their *in-vivo* environment. It is to be expected that the generation of a stable cell line from primary cells also leads to a change in the expression of a number of genes[83]. The Cox-2 expressing cells in the medulla are just described as interstitial cells in the literature[4,28,46,53]. It is conceivable that the function of these cells is influenced by their close contact to other cells, vessels and tubules around them[84]. This cell-cell interaction is lost in a cultured environment. Further complicating the investigation of Cox-2 besides the low basal expression in mice is the lack of a reliable antibody to locate Cox-2 in different tissues of mice or other laboratory animals.

The difficulty with the use of rats or other species for the investigation of Cox-2 is the lack of information about the comparability of Cox-2 expression between mice, rats and humans concerning the expression pattern and strength as well as the regulation[43–45]. Furthermore, the lack of genetically modified rats only allows for either a systemic inhibition of Cox-2 or very complicated experimental approaches for the medullary infusion of pharmacological compounds[46].

Even in mice, only global knock-out models for the key components of the prostaglandin pathway were available until recently. Dinchuk et.al[81] generated a mouse model with a global deletion of Cox-2 in all cells (Cox-2$^{-/-}$ mice). This model provided insights into the function of Cox-2 but the global deletion complicates the distinction between the different expression sites for Cox-2[61,81,85,86]. However, these mice showed good parallels to human pathologies after NSAID application. Cox-2$^{-/-}$

mice presented with problems in postnatal kidney development as seen in human fetuses with NSAID application during pregnancy, culminating in a severe kidney phenotype[44,61].

This phenotype consists of a reduced number of sclerotic glomeruli with a subcapsular location, interstitial fibrosis and papillary atrophy (Figure 23)[61,81]. The subcapsular glomeruli have a low renin expression in their JGA region and are most likely not functional[87]. Another study showed that the severity of this phenotype was dependent on the genetic background of the mice used[61]. Cox-1 knock-out mice show no renal phenotype[61].

Despite the novel insights provided by this model it is not very suitable for the separate investigation of different Cox-2 functions, because the deletion affects all cells. Furthermore, the severe renal phenotype that develops during nephrogenesis and leads to the malformation in the kidneys of Cox-$2^{-/-}$ mice, prohibits a direct transfer of the findings in this mouse model to normally developed murine kidneys and humans.

Ishikawa et. al established a new mouse model with floxed Cox-2 alleles, allowing for the first time the targeted deletion of Cox-2 from specific tissues with the Cre/loxP system[88]. But the poor characterization of Cox-2 expressing cells has stalled a cell specific approach to the investigation of Cox-2 in the kidney to date.

1.3 Aims of this study

The first aim of this study was to clearly identify and characterize Cox-2 expressing cells in the kidney. Specific emphasize was placed on finding markers for the medullary Cox-2 expressing cells. This task was in part performed to establish a selective mouse model in the course of this work. To this end it was necessary to ensure all Cox-2 expressing cells of the inner medulla were included in the potential mouse model. Therefore, I wanted to determine which cells express Cox-2 in a stimulated setting and how it is regulated in adult wildtype animals. Three conditions were to be evaluated: a high salt diet, water deprivation for 24h and genetically induced hypoxia signaling. The number, cell type markers and distribution of Cox-2 expressing cells across the kidney was characterized in detail under these conditions with the novel RNAscope® *in-situ* hybridization technique.

Secondly, after establishing a suitable mouse model, the role of Cox-2 in the adult kidney and the involvement of Cox-2 during nephrogenesis were to be investigated. In the global knockout model of Cox-2 as well as human fetuses exposed to NSAIDS in the third trimester a severe renal phenotype was reported. The phenotype presents with tubular hyperplasia, a large number of sclerotic glomeruli in the subcapsular region and interstitial fibrosis. Due to the contribution of these cells to the phenotype, I investigated whether Cox-2 expression during nephrogenesis in the cells of the FoxD1^{+} stromal progenitor compartment is necessary for normal kidney development and function. These stromal progenitor cells differentiate into interstitial cells, renin and mesangial cells as well as vascular smooth muscle cells. The role of this cell population was investigated with the help of a targeted deletion of floxed Cox-2 alleles combined with a cell specific Cre-recombinase for the FoxD1 compartment (FoxD1$^{+/Cre}$ Cox2$^{fl/fl}$ mice).

The third part of this study was to distinguish and clarify the functional relevance of Cox-2 expression in medullary interstitial cells from the previously described function of Cox-2 in the macula densa of adult kidneys. To evaluate the function of Cox-2 in medullary interstitial cells I used a selective deletion of the Cox-2 gene in interstitial cells of the kidney with an inducible Cre-recombinase under control of the PDGFR-β promotor (PDGFR-β$^{+/iCre}$ Cox2$^{fl/fl}$ mice). As parameters for kidney function systolic blood pressure, GFR, water intake, urinary ion concentrations, -volume and key mRNA targets were determined and analyzed.

The concluding part of this study was concerned with investigating the role of resident Cox-2 expression in the kidney as an inflammatory mediator in the model of adenine induced fibrosis and unilateral ureter obstruction. Contradicting reports for the role of Cox-2 in pathological settings have been published to date[89–92]. But the source for the potentially disease progression relevant Cox-2 expression has not been identified due to the lack of an appropriate animal model[91]. Using a cell specific deletion, I investigated whether the absence of Cox-2 in PDGFR-β^{+} cells has any effect on the progression of renal fibrosis. The evaluation of disease progression was investigated through functional parameters, mRNA expression of fibrotic markers with qPCR and RNAscope® *in-situ* hybridization.

2 Material and Methods

2.1 Material

2.1.1 Instruments

Instrument	Manufacturer
Anthos 2010 Microplate reader	anthos Mikrosysteme GmbH, Friesoythe, Germany
Cameras	AxioCam MRm, Zeiss, Jena AxioCam 105 color, Zeiss, Jena
Centrifuges	Haematokrit 210, Hettich, Tuttlingen Tischzentrifuge, neoLab, Heidelberg Z300, Hermle, Wehingen Zentrifuge 5417R, Eppendorf, Hamburg
Chemidoc™ Touch Imaging System	Biorad, München, Germany
Filter sets for microscopy: TRITC-Filter Cy2-Filter Cy3-Filter DAPI-Filter	 Filter set 43 DsRed, Zeiss, Jena Filter set 38 HE, Zeiss, Jena Filter set 50, Zeiss, Jena Filter set 49, Zeiss, Jena
Fluorescent lamp	Colibri.2, Zeiss Jena
Gel Electrophorese System	Compact M. Biometra, Göttingen
Heating blocks	Thermomixer, Eppendorf, Hamburg Thermomixer 5436, Eppendorf, Hamburg
Heating plate	HI 1220, Leica, Wetzlar
Homogenizer	Ultra-Turrax T25, Janke &Kunkel, Staufen
Ice machine	Ziegra Eismaschinen, Isernhagen
Incubator	Memmert, Schwabach
Inhalation Device UniVet	Groppler, Deggendorf, Germany
Invitrogen™Qubit™3.0 Fluorometer	Thermo Fisher Scientific, UK
Magnetic mixer	MR 80, Heidolph, Schwabach MR 3001 K, Heidolph, Schwabach
Metabolic cages	Tecniplast, Hohenpeißenberg, Germany
Microscope	Axio Observer.Z1, Zeiss, Jena
Microtome	Rotationsmikrotom RM2165, Leica, Wetzlar Rotationsmikrotom RM2265, Leica, Wetzlar
Microwave	Sharp, Osaka
Osmomat 030	Gonotec, Germany
PCR machine	Labcycler, SensoQuest, Göttingen Lightcycler LC480, Roche, Mannheim
Peristaltic pump	323, Watson Marlow, Wilmington, USA

Personal Computer	Dell, Intel Core i7, NVIDIA GeForce GTX1080 8 GB
PH meter	Hanna Instruments, Vöhringen
Photometer	NanoDrop 1000, Peqlab, Erlangen
Pipettes	Pipetman P2, P10, P20, P100, P200, P1000, Gilson, Middleton, USA
RNAscope® oven	HybEZ Oven, Advanced Cell Diagnostics, Hayward, USA
Scales	Feinwaage ABT 120-5DM, Kern, Balingen-Frommern EMS, Kern, Balingen-Frommern
Shaker	GFL, Burgwedel Rotamax, Heidolph, Schwabach
Tail cuff BP measurement system	Non-Invasive Blood Pressure Monitoring System, TSE Systems, Bad Homburg
Vortex	USA REAX1, Heidolph, Schwabach
Water bath	Aqualine AL12, Lauda, Lauda-Königshofen 1083, GFL, Burgwedel
Water purification	MilliQ Plus PF, Millipore, Schwalbach
XP flame photometer	BWB Technologies, UK

2.1.2 Consumables

Product	**Manufacturer**
FINE-JECT 12mm, gauge 30mm	VWR International, Ismaning
Cannula 27G for hematocrit	Becton Dickinson, Franklin Lakes, USA
Minicaps end to end, na-heparinized, 5µl	Hirschmann Laborgeräte GmbH & Co. KG, Eberstadt
Minicaps end to end, na-heparinized, 0,5µl	Hirschmann Laborgeräte GmbH & Co. KG, Eberstadt
Cover for Pasteur pipettes	Roth, Karlsruhe
Cover slip	Roth, Karlsruhe
Dissecting tools	Fine Science Tools, Heidelberg
Filter paper	Schleicher & Schuell, Dassel
Glassware	Roth, Karlsruhe Schott, Mainz
Gloves	Roth, Karlsruhe
Hematocrit capillaries	Sanguis Counting, Nümbrecht
Hematocrit sealing kit	Brand, Wertheim
ImmEdge Pen	Vector Laboratories, Burlingame, USA
Microscope slides, SuperFrost® Plus	Menzel, Braunschweig

Parafilm	Bemis, Neenah, USA
Pasteur pipettes	VWR, Darmstadt
Pipette controller accu-jet pro	Brand, Wertheim
Pipette tips with and without filter	Nerbe, Winsen Sarstedt, Nümbrecht Biozym Scientific, Hessisch Oldendorf
Plates, 96 well for qPCR	Sarstedt, Nümbrecht
Serological pipettes 5ml, 10ml, 25 ml	Sarstedt, Nümbrecht
Silicon forms for embedding	Roth, Karlsruhe
Syringes	Becton Dickinson, Franklin Lakes, USA
Tissue embedding cassettes	Roth, Karlsruhe
Tubes 0.5ml, 1ml, 2ml	Sarstedt, Nümbrecht
Tubes 15ml, 50ml	Sarstedt, Nümbrecht
Aspiration tube assemblies for calibrated microcapillary pipettes	Sigma-Aldrich, München
Multipurpose container 30ml	Greiner Bio-One GmbH, Frickenhausen
surgical suture Vicryl	Ethicon, Norderstedt, Germany

2.1.3 Commercial kits, enzymes and chemicals

Product	**Manufacturer**
Adenine Chow (0,2%)	Altromin Spezialfutter GmbH & Co. KG, Lage, Germany
Agarose	Sigma-Aldrich, München
Bovine Serum Albumin (BSA)	Sigma-Aldrich, München
Chloroform	Merck, Darmstadt
Dulbecco´s PBS	Sigma-Aldrich, München
Elisa kit ANG I	IBL International, Hamburg
Enalapril maleate	Sigma-Aldrich, München
Ethanol p.a	Honeywell, Morris Plains, USA
Ethylenediaminetetraacetic acid	Merck, Darmstadt
First Strand Buffer, 5x	Invitrogen, Karlsruhe
FITC-Sinistrin	Fresenius Kabi, Bad Homburg
Formaldehyde solution (min. 37%)	Merck, Darmstadt
Gene Ruler™ 100bp plus DNA ladder	Thermo Scientific, Waltham, USA
Glycergel mounting medium (IF)	Dako Cytomation, Glostrup, Dänemark
Glycerin 87%	Merck, Darmstadt
Glycogen	Invitrogen, Karlsruhe

GoTaq DNA Polymerase, 5 U/µl	Promega, Mannheim
GoTaq Reaction Buffer Green	Promega, Mannheim
Hematoxylin solution, Gill Nr. 1	Sigma-Aldrich, München
HCl 1N	Merck, Darmstadt
HCl fuming	Merck, Darmstadt
HEPES(4-(2-hydroxyethyl)-1-piperazineethanesulfonic acid)	Sigma-Aldrich, München
High Salt chow (4% NaCl)	Ssniff, Soest, Germany
Horse Serum (HS)	Gibco, Life technologies, Grand Island, USA
Isoflurane	Baxter, Unterschleißheim
Isopropanol	Merck, Darmstadt
Isopropanol p.a	AnalaR Normapur, VWR, Radnor, USA
Isotonic NaCl Solution, sterile 0,9%	B. Braun, Melsungen
K_2HPO_4 x 3 H_2O	Merck, Darmstadt
Ketamine, 10%	bela-pharm, Vechta
KH_2PO_4	Merck, Darmstadt
Lightcycler480®SYBR-Green-Master-PCR Kit	Roche, Mannheim
Low Salt chow (0,03% NaCl)	Ssniff, Soest, Germany
Methanol	Merck, Darmstadt
M-MLV Reverse Transcriptase, 200 U/µl	Invitrogen, Karlsruhe
Na_2HPO_4	Sigma-Aldrich, München
NaCl	Merck, Darmstadt
NaH_2PO_4	Sigma-Aldrich, München
NaOH 1N	Merck, Darmstadt
Oligo(dT)$_{15}$ Primer, 0,5µg/µl	Thermo Scientific, Waltham, USA
Paraformaldehyde	Roth, Karlsruhe
Paraplast-Plus Paraffin	Roth, Karlsruhe
PCR Nucleotide Mix (dATP, dCTP, dGTP, dTTP, 10 mM each)	Promega, Mannheim
RNAscope® 2.5 HD Detectionreagents – brown	Advanced Cell Diagnostics, Hayward, USA
RNAscope® 2.5 HD Detectionreagents – duplex	Advanced Cell Diagnostics, Hayward, USA
RNAscope® H_2O_2 & Protease Plus Reagents	Advanced Cell Diagnostics, Hayward, USA
RNAscope® Target Retrieval Reagent	Advanced Cell Diagnostics, Hayward, USA
RNAscope® Wash Buffer	Advanced Cell Diagnostics, Hayward, USA
RNAscope® Multiplex Fluorescent Assay	Advanced Cell Diagnostics, Hayward, USA
Roti®-Safe GelStain	Roth, Karlsruhe

Tamoxifen Chow (400mg tamoxifen citrate/kg)	Harlan Laboratories, NM Horst, Niederlande
Tris(hydroxymethyl)-aminomethan (Tris)	Affymetrix, Cleveland, USA
TRIsure®-Reagent	Bioline, Luckenwalde
VectaMount™ mounting medium (ISH)	Vector Laboratories, Burlingame, USA
Xylazine, 2%	Serumwerk, Bernburg
Xylol	Merck, Darmstadt
Xylol (for RNAscope®)	AppliChem, Darmstadt
Acidic acid 100%	Sigma-Aldrich, München
TSA Plus Cyanine 3 and Cyanine 5 System	Perkin Elmer, Rehbach, Germany
Maleic acid	Sigma-Aldrich, München

2.1.4 Buffers and Solutions

Unless stated otherwise, all Buffers and Solutions were prepared with purified water (MilliQ-Water).

PBS (Phosphate Buffered Saline)-Otto-Buffer, pH 7,4	
NaCl	140 mM
K_2HPO_4 x 3 H_2O	10 mM
KH_2PO_4	2,5 mM

Paraformaldehyde fixation solution for immunofluorescence (IF), pH 7,4	
Dulbecco´s PBS	
Paraformaldehyde	3%

Tris-EDTA Buffer, (epitope unmasking) pH 8,5	
Tris	9,9 mM
EDTA	1,3 mM

Stock-Solution for IF	
PBS-Otto	
BSA	1%

Blocking-Solution for IF	
PBS-Otto	
BSA	1%
Horse Serum	10%

NBF fixation solution for ISH, pH 7,0	
Formalin (37-40% stock solution)	10%
NaH_2PO_4	33,3 mM
Na_2HPO_4	45,8 mM

TAE (Tris-Acetate-EDTA) Buffer, pH 8,5	
Tris	40 mM
Acidic acid	20 mM
EDTA	1 mM

Agarose Gel for genotyping	
TAE	
Agarose	2%
Roti®-GelStain	0,02%

HEPES Buffer for GFR, pH 7,4	
HEPES	0,5 M

FITC injection solution for GFR	
NaCl solution 0,9%, sterile	
FITC	1%

NaOH for genotyping	
NaOH	25 mM

Tris-HCl, pH 8,0, for genotyping	
Tris	1 M

Maleate Buffer, pH 6,0	
Tris	33,5 mM
maleic acid	50 mM
EDTA	10,0 mM

2.1.5 Primer for genotyping and real time pcr

All primers were produced by Eurofins Genomics GmbH (Ebersberg) according to the sequences provided by us. Primers were shipped as lyophilized powder and dissolved in purified water to a final concentration of 100pmol/µl for all uses.

Primer for genotyping of mice

Construct	Sequence (5´-3´)	product size (bp)
Cox-2^{del}	s AATTACTGCTGAAGCCCACC as GAATCTCCTAGAACTGACTGG	1054 = del
Cox-2^{flox}	s AATTACTGCTGAAGCCCACC as AGAAGGCTTCCCAGCTTTTGTAACC	1058 = flox 823 = wt
FoxD1$^{+/Cre}$	s1 CTCCTCCGTGTCCTCGTC s2 TCTGGTCCAAGAATCCGAAG as GGGAGGATTGGGAAGACAAT	450 = Cre 237 = wt
PDGFR-β$^{+/iCre}$	s1 GAA CTG TCA CCG GCA GGA as AGG CAA ATT TTG GTG TAC GG c1 CAA ATG TTG CTT GTC TGG TG c2 CTC AGT CGA GTG CAC AGT TT	400 = Cre 200 = internal conrtol
CAG$^{+/iCre}$	s CAGAACCTGAAGATGTTC as CCAGATTACGTATATCC	286 = Cre
Vhl^{flox}	s CTAGGCACCGAGCTTAGAGGTTTGCG as CTGACTTCCACTGATGCTTGTCACAG	450 = flox 270 = wt

Primer for quantitative Real-Time-PCR

Gene	Sequence (5´-3´)	product size (bp)
AQ2	s CTGGCTGTCAATGCTCTCCAC as TTGTCACTGCGGCGCTCATC	122
AR	s GCAATTGCAGCCAAGTACAA as ATGGTGTCACCGACTTGG	97
BGT1	s GGTCCTTTTGGTCACAGAG as GCTGGAGGCGTAGTAGTCAAA	65

Col1a1	s CTGACGCATGGCCAAGAAGA as ATACCTCGGGTTTCCACGTC	91
Cox-2	s AGC CAT TTC CTT CTC TCC TG as ACA ACA ACT CCA TCC TCC TG	894
Cx3CR1	s CCTGCCTCTGAGAAATGGAG as ATCTCTCCAGCCCCTGAAAT	332
ENACα	s TACGCGACAACAATCCCCAAGTGG as ATGGAAGACATCCAGAGATTGGAG	334
GAPDH	s CACCAGGGCTGCCATTTGCA as GCTCCACCCTTCAAGTGG	294
HSP70.1	s ACCATGAAGAAGACTTTAAATAACCTTGAC as CCCGGTGTGGTCTAGAAAACA	90
PDGFR-β	s GAG GCT TAT CCG ATG CCT TCT as AAA CTA ACT CGC CAG CGC C	79
Renin	s ATGAAGGGGGTGTCTGTGGGGTC as ATGTCGGGGAGGGTGGGCACCTG	194
RPL32	s TTA AGC GAA ACT GGC GGA AAC as TTG TTG CTC CCA TAA CCG ATG	100
SMIT1	s AGTGGCTTCCATGGGTCAT as TGCCCATTGGAATAAGCATC	60
UTA-1	s TGAGACGCAGTGAAGAGGAGAA as ATGACCACTCGATGTGGAACAC	141
α-SMA	s ACTGGGACGACATGGAAAAG as CATCTCCAGAGTCCAGCACA	240

2.1.6 Probes for *in-situ* hybridization and antibodies

Primary antibodies

Antibody	Manufacturer	Dilution
Chicken-anti-Renin	Davids Biotech., Regensburg	1 : 400
Mouse-anti-α-SMA	Abcam, Cambridge, UK	1 : 600

Secondary antibodies

Antibody	Conjugation	Manufacturer	Dilution
Donkey-anti-chicken	Cy 2	Dianova, Hamburg	1 : 400
Donkey-anti-mouse	Cy 5	Dianova, Hamburg	1 : 400

Probes for *in-situ* hybridization with RNAscope®

All probes were manufactured by Advanced Cell Diagnostics (Hayward, USA).

Probe
RNAscope® Negative Control Probe – DapB
RNAscope® Positive Control Probe – mM-PPIB
RNAscope® Probe – mM-Col1a1 C1
RNAscope® Probe – mM-CSPG4 C1 & C2
RNAscope® Probe – mM-Cx3CR1 C1
RNAscope® Probe – mM-EPO C1& C2
RNAscope® Probe – mM-PDGFRb C1 & C2
RNAscope® Probe – mM-Ptgs1-O1 C1
RNAscope® Probe – mM-Ptgs2-O1 C1& C2
RNAscope® Probe – mM-Ren C1 & C2
RNAscope® Probe – mM-TNC C1 & C2
RNAscope® Probe – Rn –Ptgs2 C1

2.1.7 Software and internet services

This work was written with *Microsoft Office 2016*. Graphs were prepared using GraphPad prism 5. For microscopy, the *Zen Blue* software was used. Pictures were edited using *Zen Blue* and *Adobe Photoshop CS5.* The PubMeb site of the NCBI (The National Center for Biotechnology; Information: http://www.ncbi.nlm.nih.gov/pubmed/) was used for literature research. Citations were cataloged and organized with the *Zotero* software (version 5.0.59).

2.2 Methods

2.2.1 Animals

2.2.1.1 Mouse strains and animal breeding

All animal experiments were conducted according to the “National Institutes of Health guidelines for the care and use of animals in research” and were approved by the local ethics committee. All mice were kept under optimal conditions, consisting of constant 23°C room temperature, relative humidity of 55 ± 5% and a constant 12h dark/light cycle. Standard rodent chow (0,6% NaCl, Ssniff, Deutschland) and tab water were provided ad libitum unless stated otherwise. All mice were bred in a C57/Bl6 background.

For this work, several genetically modified mouse lines were used:

- PDGFR-β-CreER^{T2} (PDGFR-β$^{+/iCre}$) transgenic mice expressing a tamoxifen inducible Cre-recombinase under control of the PDGFR-β promoter. The PDGFR-β-CreER^{T2} is a fusion protein consisting of the Cre-recombinase and a modified estrogen binding site (CreER^{T2})[14,93]. Mice were kindly provided by Ralf H Adams, Max-Planck-Institut.
- FoxD1$^{tm1(GFP/cre)Amc}$ (FoxD1$^{+/Cre}$) knock-in mice express a fusion protein of Cre-recombinase and eGFP under the endogenous FoxD1 promotor. Mice were purchased from Jackson Laboratories, Bar Harbor, ME, USA (Stock No: 012463)[94,95]
- CAGG-CreER^{T2} (CAG$^{+/iCre}$) mice express a tamoxifen inducible Cre-recombinase under control of the beta actin promoter/enhancer coupled with the cytomegalovirus (CMV) immediate-early enhancer. Mice were kindly provided by Andreas Ludwig, Pharmacology, Universität Erlangen.[96]
- B6;129S4-Ptgs2^{tm1Hahe}/J (Cox2^{flox}) mice have loxP sites targeting exon 4 and 5 of the Cox-2 gene. After Cre-recombination a stop codon is created in exon 6, disrupting gene transcription[88]. Mice were purchased from Jackson Laboratories, Bar Harbor, ME, USA (Stock No: 030785)
- Vhl^{flox} mice contain loxP sites, targeting the sequence coding for the promotor and exon 1 of von-Hippel-Lindau protein (Vhl)[14,97]. After Cre-recombination a null allele is created and transcription does not take place. Deletion of Vhl inhibits the proteasomal degradation of hypoxia inducible factors, stably inducing hypoxia signaling in the affected cells. Mice were provided by Volker H. Haase, Vanderbilt University, Nashville, USA.

For the comparison between the newly generated genotypes and Cox-2$^{-/-}$ mice, paraffin section generated in the course of previous work at the institute for physiology at Regensburg, were used[87]. No live Cox-2$^{-/-}$ mice were used for this work. Tissue of young non-albuminuric MWF rats was kindly provided by AG Castrop, institute for physiology, Regensburg.

For experiments mice of both genders were used, except for the model of adenine-induced fibrosis, where only males were used[98]. Animals had an average age of 15 weeks at the time of the experiments. All newly generated genotypes were born in mendelian rations.

2.2.1.2 Genotyping of mice

Routine genotyping of mice was performed according to our laboratory standard protocol as follows by extracting genomic DNA and performing PCR.

At the age of 4 weeks mice were labeled with ear tags and ear punch out tissue of approximately 3mm diameter was taken in the same step. Ear tissue was digested in 50µl NaOH (25mM) at 96°C for 45 minutes in a heating block. After vortexing and adding 10µl Tris-HCl (1M, pH 8,0), samples were centrifuged 6 min at 10000 rpm. For PCR 0,5µl of the supernatant was used.

25 µl PCR mixture	
5 µl	GoTaq Buffer
0,75 µl for each	Primer (10pmol/µl)
2 µl	dNTPs (2,5mM)
0,2 µl	GoTaq
0,5 µl	gDNA
ad 25 µl	MilliQ-H_2O

PCR-running-programm

number of cycles	Duration	Temperature	Phase
1	5 min	94 °C	activation
⌐	30-60 s	94 °C	denaturation
36	30-60 s	x °C	annealing
⌙	30-50 s	72 °C	elongation
1	10 min	72 °C	elongation
1	∞	4 °C	storage

Primer specific annealing temperatures

PCR	Temperature
$Cox2^{del}$	56 °C
$Cox2^{flox}$	61 °C
$FoxD1^{+/Cre}$	58 °C
$CAG^{+/iCre}$	54 °C
$PDGFR\text{-}\beta^{+/iCre}$	56 °C
Vhl^{flox}	62 °C

For separation of the resulting products, 10µl PCR mixture were applied to a 2% Agarose gel and separated by horizontal electrophoresis with 130V in TAE running buffer.

2.2.1.3 Induction of Cre-Recombinase activity with tamoxifen

To activate the inducible Cre-recombinases used in this work, namely $PDGFR\text{-}\beta^{+/iCre}$ and $CAG^{+/iCre}$, mice aged 8 weeks, were fed a tamoxifen containing diet (400mg/kg tamoxifen citrate) for 4 weeks. This was followed by a 3 week rest period on normal rodent diet (0,6% NaCl) to ensure that any observed effects were not caused by tamoxifen.

2.2.1.4 High salt diet

To test the reaction of the generated mouse strain to a salt stimulus, after induction of Cre-recombinase activity and the following rest period, mice were fed a diet containing 4% NaCl for 14 days. Experiments were performed on day 14 unless stated otherwise.

2.2.1.5 Treatment with low salt diet and Enalapril

In order to stimulate the RAAS, animals were treated with a low salt diet containing 0,03% NaCl for 10 days. Additionally 50 mg/L of the ACE-inhibitor enalapril was added to the drinking water for the same period. Experiments were performed on day 10 unless stated otherwise.

2.2.1.6 Adenine-induced kidney fibrosis

For studying the effects of the targeted deletion of Cox-2 in the kidney on the progression of fibrosis, the model of adenine-induced fibrosis was used[98–100]. After tamoxifen induction of Cre-recombinase and the following rest period, male mice were fed adenine containing diet (0,2%) for 3 weeks. Experiments were performed after exactly 3 weeks (3wks adenine) or after an additional 3 weeks in which the mice were again feed a normal diet (3wks adenine + 3wks).

2.2.1.7 Water deprivation for 24h

To induce Cox-2 expression in the inner medulla and evaluate the osmotic stress response of the mice, they were deprived of drinking water for 24h and killed immediately after this time period.

2.2.1.8 Unilateral ureteral obstruction

Mice were anesthetized with 2% isoflurane inhalation and placed on a 37°C warming plate. An anesthetic mask was placed over the nose of the mouse to ensure a continuous application of isoflurane for the duration of the procedure.

To ligate the right ureter a small incision was made over the approximate location of the ureter. The skin was carefully retracted and the ureter located with a soft Q-tip to avoid internal damage. A double knotted ligature was placed on the ureter and the skin was sewed up twice to prevent an opening of the wound. Mice were kept under observation for 2h after the operation and then daily checked to ensure wellbeing.

2.2.1.9 GFR measurement

To measure the glomerular filtration rate (GFR) in conscious mice, a slightly modified protocol utilizing the clearance of FITC-Sinistrin by the kidney[101] was used. This

technique makes it possible to repeatedly measure the GFR of the same mouse. Thus changes in GFR in the same mouse between different treatments could be evaluated.

Briefly, mice were immobilized for two minutes in 4% isoflurane inhalation anesthesia. While the mice were unconscious a single bolus injection of FITC-Sinistrin, adjusted to the bodyweight (BW), was given in the tail vein. Mice were then placed in a heated chamber, leaving access to the tail. Mice were awake and active within one minute after the bolus injection. Blood samples were collected 3,7,10,15,35,55 and 75 min after the injection into 5µl capillaries from the tail vein. After collection, blood samples were centrifuged at 12000 rpm for 7min. 0,5µl of the resulting plasma were diluted in HEPES-Buffer and the FITC-Sinistrin fluorescence in the samples was measured with a Qubit™ 3.0 Fluorometer. GFR of mice was calculated by applying the two-compartment model. To get a better comparison between mice, especially when of different gender, GFR/BW was calculated and used for analysis.

2.2.2 Retrograde arterial perfusion of mice

To fix kidney tissue for histological evaluation, mice were perfused with either 3% paraformaldehyde (pH 7,4) for immunofluorescence, or with 10% NBF solution (pH 7,0) if the tissue was used for *in-situ* hybridization with the RNAscope® technology. Mice were first anesthetized with an i.p injection of Ketamine (80mg/kg BW) and Xylazine (16mg/kg BW). After opening the abdominal cavity and exposing the abdominal aorta the left kidney was ligated to preserve the tissue for mRNA extraction. A clamp was placed on the aorta just below the branching of the kidney arteries (Arteriae renales) to preserve the kidney perfusion. The aorta abdominalis was carefully opened below the clamp with scissors and a perfusion catheter was inserted into the aorta with the help of a vessel dilator and fixed with a clamp. After removing the upper clamp the vena cava inferior is opened below the catheter to equilibrate the pressure. Continous perfusion of the kidney with a steady flow of 13ml/min and a total volume of 40ml fixation solution was started. After the perfusion the ligated left kidney was removed, cut in half and snap frozen with liquid nitrogen. Tissue was stored at -80°C until used. The perfused kidney was removed, cut in half and stored either in 70% Methanol (for IF) at 4°C or in NBF (ISH) at RT for 16-24h before embedding in paraffin.

2.2.3 Zonal dissection of kidneys

To determine the zonal distribution of different mRNA targets, kidneys were dissected into three zones after removal from the mouse. The kidneys were halved and thin slices were prepared with a razorblade and immediately transferred into petri dish containing 10ml ice-cold sterile NaCl 0,9% solution. Under a microscope, the thin kidney slices were then separated with a razorblade into cortex, outer medulla and inner medulla. At least four slices per kidney were dissected, the tissue was then pooled by zone into a cup and snap frozen in liquid nitrogen. Tissue was stored the same as complete kidneys at -80°C for mRNA extraction.

2.2.4 Tail cuff blood pressure measurement

Blood pressure measurements were performed on conscious mice with tail cuff manometry. Briefly, mice were placed in a restraining chamber, giving free access to the tail, the measurement probe and inflatable pressure cuff were placed over the tail and the mouse was left for 5 min to rest. Performing this procedure at the same time each day the mice were acclimatized to the measurement procedure for five days. Then on each day for the duration stated in the experiments, five measurements were performed per mouse and a mean of these measurements was used for evaluation of the results.

2.2.5 Metabolic cages

For determination of 24h urine volume and the corresponding water intake, mice were housed in individual metabolic cages. Each cage was pre-treated with a thin silicon film in the lower part to facilitate a better separation of urine and fecal matter into separate containers. The mice were given a house for better acclimatization and feed sufficient for one day along with a weighted water bottle. Each morning mice were transferred to a fresh cage, urine was collected and water intake calculated by weighing the water bottle again. Mice were placed in the cages for two days before the measurement period, undergoing the entire procedure to get them acclimatized. Unless stated otherwise, 5 days of urine collection and water intake were measured for each mouse per condition.

2.2.6 Spot urine collection and analysis

Mice were placed in a clean plastic box with a lid each day for 3 consecutive days to collect urine samples. If the mice did not urinate spontaneously (spot urine) after 15min in the box, they were placed back into the cage and the procedure was repeated the next day. Samples were frozen at -80°C until analysis.

2.2.6.1 Osmolality measurement

Urine osmolality was determined by freezing point depression. 5µl urine were diluted in 45µl Millipore-H_2O, vortexed and measured in the Osmomat 030. Resulting values were multiplied with the dilution and converted to mOsmol/l for evaluation.

2.2.6.2 Sodium and potassium measurement in urine

The concentration of sodium and potassium in urine was determined simultaneously by flame photometry. Before the measurement, the instrument was calibrated with standard dilutions (5 point, linear dilution) made from commercial stocks for both ions. 10µl urine were diluted in 10ml MilliQ-H_2O, vortexed and then measured in duplicates. The mean values were multiplied with the dilution and converted to mMol/l for evaluation of the results.

2.2.7 Histological methods

2.2.7.1 Embedding of tissue in paraffin

For embedding the perfused tissue in paraffin, the halved kidneys were transferred to embedding cassettes and dehydrated in an ascending alcohol series.

Time, temperature	***in-situ* hybridization**	**immunofluorescence**
1 x 30 min, RT	70% Ethanol p.a.	70% Methanol
2 x 30 min, RT	80% Ethanol p.a.	80% Methanol
2 x 30 min, RT	90% Ethanol p.a.	90% Methanol
2 x 30 min, RT	100% Ethanol p.a.	100% Methanol
2 x 30 min, RT	100% Isopropanol p.a.	100% Isopropanol
1 x 30 min, 45 °C	100% Isopropanol p.a.	100% Isopropanol
1 x 30 min, 60 °C	1 : 1 Isopropanol/paraffin	1 : 1 Isopropanol/paraffin
2 x 24h, 60 °C	Paraffin	Paraffin

Kidneys were then placed in silicon forms with liquid paraffin, the cut surface facing down. Paraffin was left to solidify overnight, blocks were then removed from the silicon forms and stored at RT.

2.2.7.2 Section of paraffin embedded tissue

Tissue blocks were roughly trimmed with a razorblade before placing them in the microtome holder and firmly screwed into place. Sections of 5µm thickness were prepared from the tissue and carefully placed in a 41°C water bath to stretch out wrinkles in the tissue. Sections were then placed on SuperFrost® Plus slides with a brush and dried overnight at room temperature.

2.2.7.3 Immunofluorescence staining

Immunofluorescence staining was used to visualize protein structures in the kidney tissue studied. For this aim indirect immunofluorescence with two antibodies (AB) was used, the primary antibody binding to the target epitope in the tissue and the secondary antibody reacting specifically with the primary AB. To make the target visible for microscopy the secondary AB is conjugated to a fluorescent dye to show a strong fluorescence when exited with light at distinct wavelengths. Before the incubation of the primary AB the paraffin was removed and the tissue rehydrated by a decreasing alcohol series.

Time	**Solution**
2 x 10 min	100% Xylol
2 x 5 min	100% Isopropanol
1 x 5 min	90% Isopropanol
1 x 5 min	80% Isopropanol
1 x 5 min	70% Isopropanol
1 x 5 min	MilliQ-H_2O

Staining was then performed according to a standard protocol:

- 3 x 10 min washing in PBS-Otto Buffer
- Creating a hydrophobic barrier around the tissue
- Blocking unspecific binding sites for 30 min with the IF blocking solution (10% HS, 1% BSA in PBS-Otto) at RT
- Incubation of the primary AB diluted in blocking solution overnight at 4°C
- Remove the primary AB by washing 3 x 5 min in Stock solution (1% BSA in PBS-Otto)
- Incubation of the secondary AB, diluted in stock solution, for 1,5h in the dark at RT
- Remove the secondary AB by 3 x 5 min washing in PBS-Otto Buffer in the dark

- Mount slides with pre-warmed mounting medium and dry overnight at 4°C

2.2.7.4 Sirius Red staining

For the visualization of collagens, Picro-Sirius-Red staining (SR) was performed. Tissue sections of 5µm thickness were deparaffinized as described above for immunofluorescence staining. Slides were placed in the SR-solution for 1h at room temperature. After the incubation two short wash steps in 0,5% acidic acid were performed, followed by two wash steps in isopropanol (p.a). To remove residual water slides were placed in xylol and then immediately mounted with cover slides and left to dry under a fume hood.

2.2.8 *In-situ* hybridization utilizing the RNAscope® technique

With the RNAscope® *in-situ* hybridization method, mRNA for different targets was made visible on kidney tissue. This technique was used to localize and co-localize the expression of different mRNA throughout the kidney tissue. This form of *in-situ* hybridization was performed according the manufacturer´s protocol with minor changes[102]. Probes for *in-situ* hybridization were mixed and diluted according to the manufacturer´s protocol and are described in the individual experiments. Negative controls routinely did not show any positive signal.

2.2.8.1 Chromogenic and duplex RNAscope

For *in-situ* hybridization using the RNAscope® 2.5 HD Reagent Kit (brown or red) RNAscope® 2.5 HD Reagent Kit (Duplex Assay) or Multiplex Fluorescent Assay slides received the same pre-treatment:

- Slides were incubated for 60 min at 60°C in dry heat
- To remove paraffin slides were washed 2 x 10 min in Xylol (RT) then 2 x 2 min in 100% Ethanol p.a.
- Sections were air-dried for 5 min
- All sections were covered with RNAscope® Hydrogenperoxide (RT) for 10 min
- Slides were washed twice in MilliQ-H_2O
- Placed in a holding cassette the slides were submerged and boiled (98-102°C) in RNAscope® 1x Target Retrieval-Solution for 15 min
- After briefly washing in MilliQ-H_2O and 100% Ethanol p.a., sections were air-dried
- Single tissue sections were surrounded by a hydrophobic barrier

- Directly, or on the next day the sections were incubated for 30 min with RNAscope® Protease Plus (40°C)
- Slides were washed in MilliQ-H_2O
- After application of the probe (red or brown kit) or the probe mixture (for duplex assay and Fluorescent Assay) the slides were incubated for 2h in the hybridization oven
- Each step was then followed by 2 x 2 min washing in 1 x RNAscope® Washing Buffer
    - AMP 1: 30 min (40°C)
    - AMP 2: 15 min (40°C)
    - AMP 3: 30 min (40°C)
    - AMP 4: 15 min (40°C)
    - AMP 5: 45 min (RT)
    - AMP 6: 15 min (RT)

Slides treated for the brown/red single color kit underwent signal detection at this point by applying the DAB-Substrate solution (30µl per section) for 10 min and then counterstaining the slides as in the duplex assay

- Slides treated with the duplex assay kit underwent detection of the channel 2 (C2) red signal at this point by applying the Fast Red mixture (30µl per section) for 10 min
- After washing for 2 x 2 min in 1 x RNAscope® Washing Buffer, the green signal was amplified by the following steps, each was again followed by a washing step
    - AMP 7: 15 min (40°C)
    - AMP 8: 30 min (40°C)
    - AMP 9: 30 min (RT)
    - AMP 10: 15 min (RT)
- Incubation of the Fast Green detection mixture (30µl per section) on the slides for 10 min visualized the channel 1 green signal
- Slides were placed in 50% Hematoxylin solution for 30s then washed very fast 3 times in MilliQ-H_2O and counterstained in 0,02% NH_4OH solution for 10s
- After drying for 20 min at 60°C in dry heat, the slides were mounted with VectaMount™ mounting medium and dried at RT overnight

2.2.8.2 RNAscope® Multiplex Fluorescent Assay

Slides for the RNAscope® Multiplex Fluorescent Assay were pre-treated in the same manner as described above, with the exception that here protease IV used instead of protease plus. After 2h incubation of the probes the amplification, blocking and detection steps were performed per the manufacturer´s protocol. Detection of the probes was performed with the PerkinElmer fluorophores according to the protocol. For these slides, no counterstaining with hematoxylin was performed, but nuclei were visualized by staining with the DAPI solution included in the RNAscope® Multiplex Fluorescent Assay.

2.2.9 Microscopy

2.2.9.1 Microscopy for fluorescent dyes

All tissue treated with fluorescent dyes was viewed with a Axio Observer.Z1-Mikroscope fitted with a motorized slide table and a black-white-CCD-Camera (AxioCam MRm), using the *ZEN blue* (2012) Software. Using different filters the different fluorophores were excited at their optimal wavelength and the resulting emissions captured. In the case of multiple fluorophores being used on the same tissue, the different channels were captured separately, merged and then converted to a RGB-Color scheme.

Fluorophore	**Excitation (nm)**	**Emmission (nm)**
Cy 2	450 – 490	500 – 550
TRITC	533 – 558	570 – 640
Cy 5	625 – 655	665 – 715
DAPI	335 – 383	420 – 470

2.2.9.2 Microscopy for RNAscope® 2.5 HD Reagent Kit (brow/duplex)

Tissue with a chromogenic *in-situ* hybridization was viewed with the same microscope as described above, but an Axiocam 105 color camera was used to capture the images. All overviews showing whole kidney sections were made by stitching tiles with a 200x magnification together using the tile function in *ZEN blue* (2012).

2.2.10 Molecular biology methods

2.2.10.1 Measurement of mRNA expression levels and cDNA synthesis

The protocol for the isolation of the whole RNA content of kidneys is based on the guanidine thiocyanate-Phenol-Chloroform-Method that has been previously described[103] with some modifications.

First the still frozen tissue was homogenized in TRIsure®-reagent (1ml), a single phase mixture of Phenol and guanidine thiocyanate. All steps were performed on ice, unless stated otherwise. After the addition of chloroform (200µl) a centrifugation step (30min, 13000rpm) was performed to separate the solution into three phases. DNA and hydrophobic proteins remain in the green phenol phase at the bottom, followed by a white interphase consisting of hydrophilic proteins and a aqueous phase containing RNA. The aqueous phase was removed and added to 500µl Isopropanol and 2µl Glycogen to precipitate the RNA. After centrifugation of the RNA (30min, 13000rpm) and washing (1ml 75% Ethanol p.a.), repeated centrifugation (30min, 13000rpm), Ethanol was removed and RNA pellets were air-dried and dissolved in MilliQ-H_2O. RNA was stored at -80°C for further use.

Total isolated RNA content was quantified with a nanodrop photometer. To this end the optical density of the RNA solution was measured at 260 nm and 280 nm. Optimal concentration of the RNA for accurate pipetting in the following experiments was set to 1µg/µl. To evaluate the quality of the obtained RNA the absorption ratio between 260 nm and 280 nm was used. Only RNA with a ratio between 1,5 to 2,0 was used for the experiments in this work.

To ensure only mRNA was transcribed into the complimentary cDNA by reveres transcriptase, Oligo$(dT)_{15}$-Primer were used to selectively amplify the 3´-poly(A)-tail of the isolated mRNA. The cDNA was synthesized using a 10µl reaction mixture containing RNA (1µg), Oligo$(dT)_{15}$-Primer (1µl) and MilliQ-H_2O (ad 10µl). This mixture was placed in a thermocycler for 5 min at 65°C to bind the primer. After short centrifugation, the samples were placed on ice and 10µl master mix (4µl FSB, 1µl 10mmol dNTP-mix, 1µl reverse transcriptase, 4µl MilliQ-H_2O) was added to each sample. Synthesis of cDNA was performed for 1h at 37°C followed by inactivation of the reverse transcriptase through heating the samples for 2 min to 94°C. The resulting cDNA was diluted with 35µl MilliQ-H_2O and stored at -20°C.

2.2.10.2 Quantitative real time PCR

For quantitative real time PCR the LightCycler® 480 SYBR Green I Master Kit was used in this work. To quantify the exponential increase in DNA content of the samples with each cycle in real time, the DNA content is assessed with photometry. This is possible through the high affinity intercalation of the SYBR Green Dye with the small furrow of double strand DNA. The fluorescence of SYBR Green bound to DNA is 1000x increased compared to unbound SYBR Green. Thus the intensity of the fluorescent signal is proportional to the DNA content in the sample. Real time PCR was performed with specific primers for each target in a Roche LightCycler LC480® Instrument, following a standard protocol.

Real time PCR reaction mixture per sample

- 5µl LightCycler® 480 SYBR Green I Master
- 0,5µl sense-Primer (10 pmol)
- 0,5µl antisense-Primer (10 pmol)
- 3µl MilliQ-H_2O
- 1 µl cDNA

Amplification protocol

Cycle	Temperature	Duration	Phase
1	95 °C	5 min	activation
50	95 °C	15 s	denaturation
	62 °C	20 s	annealing
	72 °C	20 s	elongation

After the end of the amplification protocol, a melting curve was run on the samples to check for product purity. The amplified DNA was slowly heated in 0,1 °C/s steps from 60 °C to 95 °C with continuous measurement of the fluorescence in the sample.

2.2.11 Measurement of plasma parameters

2.2.11.1 Blood sample collection

Blood samples for evaluation of hematocrit values and plasma collection were taken from adult mice at predetermined times. Blood was collected into EDTA coated capillaries from the tail vein. Capillaries were firmly capped with sealing kit on one side and centrifuged at 12000rpm for 4 min to separate plasma and solid blood cells.

Hematocrit values were taken as the ratio between total volume and solid blood cells. Plasma was removed from the capillaries and stored in cups at –80°C until further use.

2.2.11.2 Renin-ELISA

The Renin concentration in plasma samples was measured indirectly by quantifying the amount of ANG I produced by a plasma sample in the presence of excess substrate. ANG I content was determined by ELISA. For ANG I production, plasma was diluted in maleate buffer and PMSF and incubated with renin-substrate and generation buffer. Renin-substrate was isolated from plasma of double nephrectomized male rats. Two reaction mixtures were prepared for each sample. One was incubated at 37°C for 90min and the other was left on ice for the same time. Of each samples, both cold and warm, 45µl were used in the ELISA for the quantification of ANG I, according to the manufacturer´s protocol. Calculation of renin concentration in the plasma samples, stated as $ng_{ANG\ I}/min*h^{-1}$, was done as described in the manual.

2.2.12 Statistics

For each experiment the single values for each mouse were used to calculate a mean value and standard deviation of the mean per genotype, unless stated otherwise. Student's t-test was used to determine significance between experimental groups. Significant difference between groups was defined at $p<0,05$ and labeled with (*) in graphs.

3 Results

3.1 Localization of Cox-2 in the kidney and characterization of Cox-2 expressing cells

In the murine kidney different expression sites for Cox-2 have been described[4,23,104]. One location for Cox-2 expression in the kidney are the macula densa cells of the JGA in the cortex[3,4,18,21]. Various studies have also described the expression of Cox-2 in medullary interstitial cells[4,23,46,58] or collecting ducts[53,80,105] but no systematic investigation into the characteristics of the cells expressing Cox-2 in the inner medulla or their origin has been performed to date.

To clarify the nature and characteristics of Cox-2 expressing cells in the inner medulla, I utilized the novel RNAscope® technique to study these cells regarding the co-expression of other markers. Furthermore I used this technique to compare the two most used rodent laboratory animals, concerning differences in Cox-2 expression.

In the kidneys of adult wildtype mice Cox-2 expression could only be detected in the macula densa cells of the cortex (Figure 6,D) and in interstitial cells in the inner medulla (Figure 6,A). By using the RNAscope® 2.5 HD Duplex and Mulitplex Assay to detect two target mRNA at the same time, I found that these interstitial cells are not only double positive for Cox-2 and PDGFR-β, but that they also express the glycoprotein tenascin-C (TNC) (Figure 6,B and C). In Cox-2$^+$ macula densa cells no co-expression with PDGFR-β or TNC could be detected.

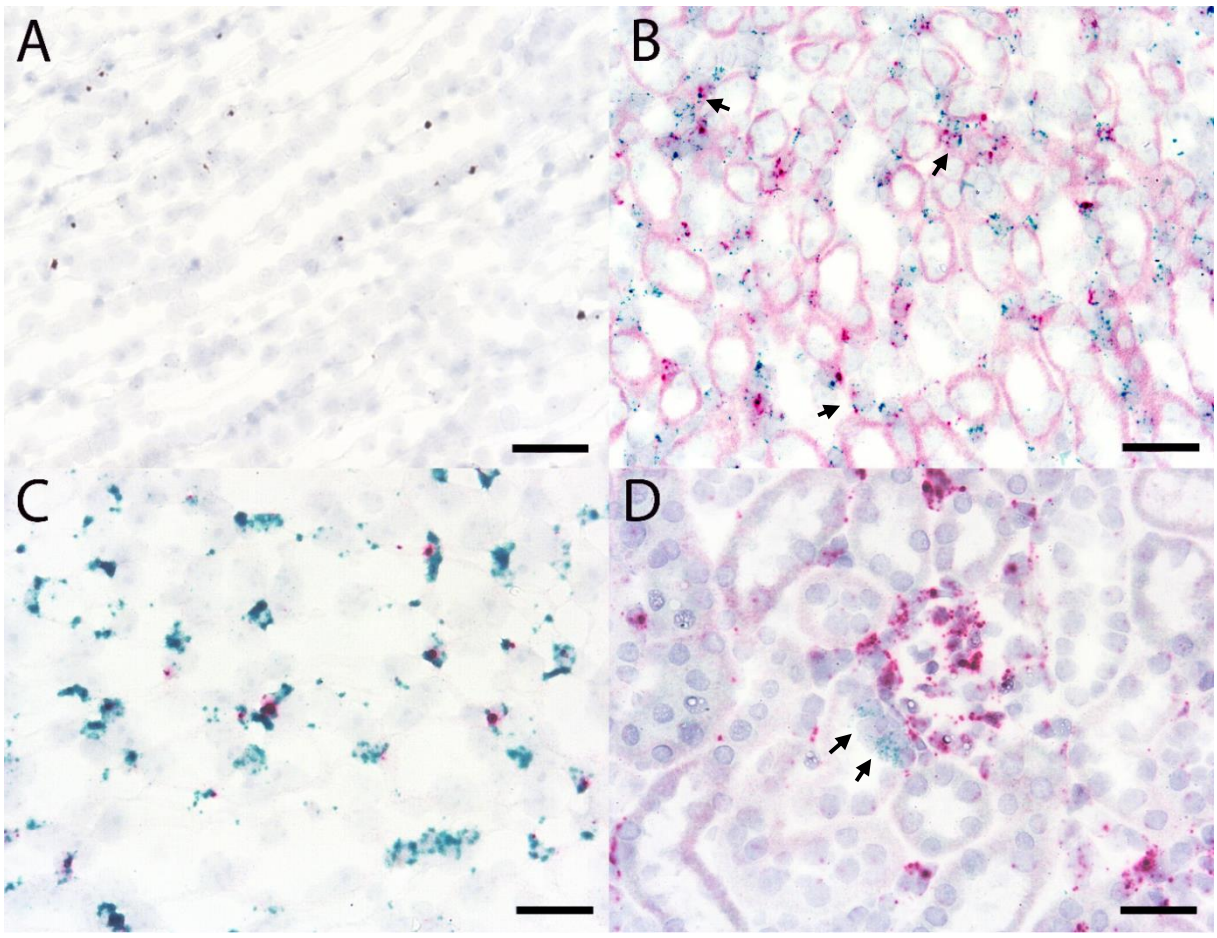

Figure 6: Localization of Cox-2 in medullary interstitial cells of the mouse kidney, brown signal denotes Cox-2 mRNA location (A); co-localization of Cox-2 (red) and PDGFR-β (green) mRNA marked with arrows in interstitial cells at the border between inner and outer medulla (B); TNC (green) and Cox-2 (red) mRNA can be detected in the same interstitial cells of the inner medulla (C); in cells of the macula densa no co-localization between Cox-2 (green, arrows) and PDGFR-β (red) could be detected (D); scale bar 50µm

Quantitative analysis of the co-localization images showed that about 90% of Cox-2 expressing cells of the inner medulla also express PDGFR-β (Figure 7).

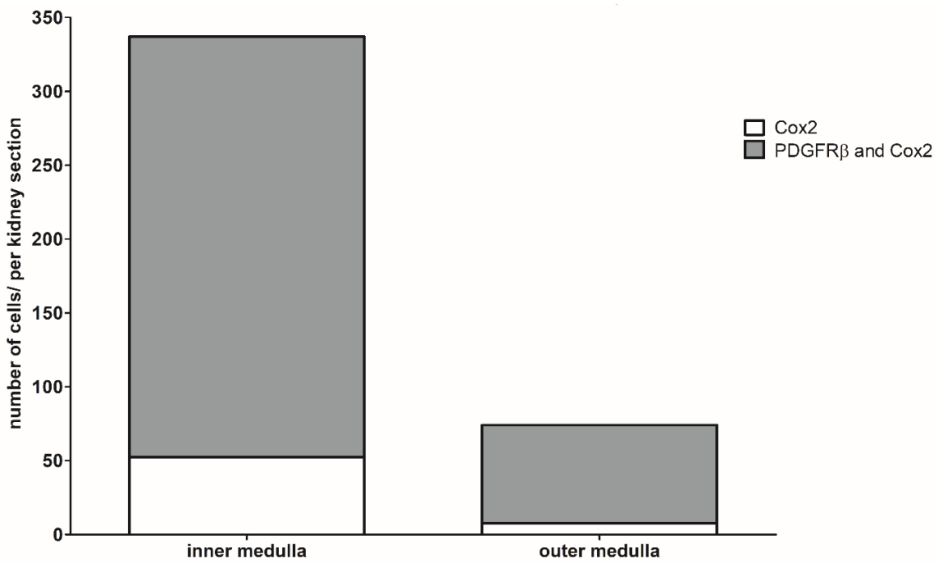

Figure 7: Quantitative co-localization of Cox-2 and PDGFR-β showed that the vast majority of Cox-2 expressing cells in the inner medulla also express PDGFR-β (left; 337 cells with PDGFR-β vs. 52,5 without; n = 3); in the outer medulla co-localization between PDGFR-β and Cox-2 is even more pronounced (right; 74 cells with PDGFR-β vs. 7,5 without; n = 3)

Further investigation into these interstitial cells showed a 98% overlap between PDGFR-β and TNC (Figure 8;left side) in the inner medulla and the inner stripe of the outer medulla. TNC is only expressed by interstitial cells in these areas, but not by interstitial PDGFR-β^+ cell of the cortex. Therefore, I conclude that there is no subpopulation that expresses PDGFR-β and Cox-2, but not TNC among the interstitial cells of the inner medulla.

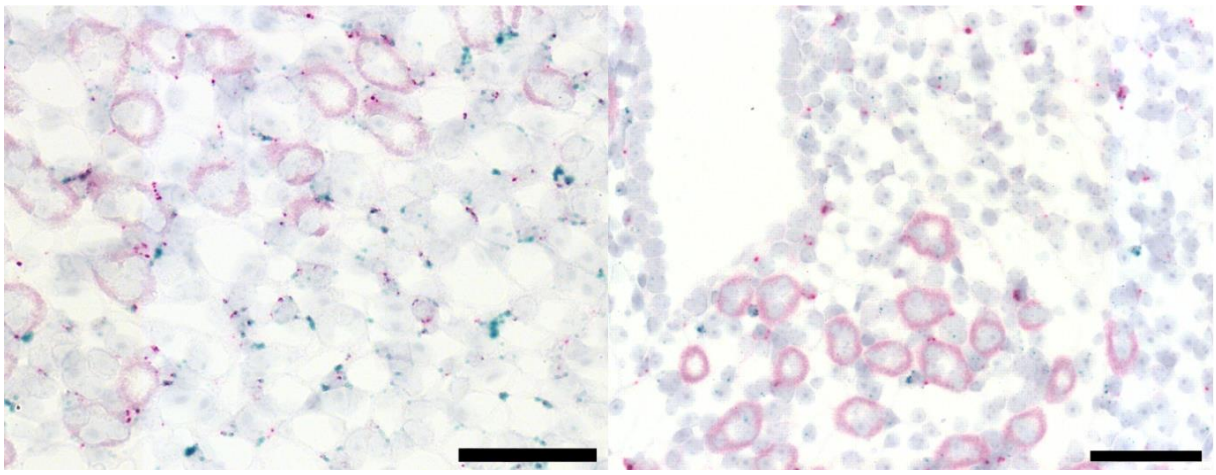

Figure 8: Between PDGFR-β (red) and TNC (green) a co-localization of 98% could be detected in the inner and outer medulla (left); in the interstitial Cox-2 expressing cells (red) of the inner medulla only an occasional co-expression with NG2 (green) could be observed (right); scale bar 50µm

The Cox-2^+ interstitial cells showed only occasional co-expression of NG2, which has been described as a marker of interstitial cells[12,106] besides PDGFR-β (Figure 8;right side). No Cox-2 mRNA was detected in collecting duct cells or other non-interstitial cells of the medulla.

Co-*in-situ* hybridization for Cox-1 and Cox-2 mRNA showed that, although Cox-1 is expressed much more abundantly than Cox-2, the intracellular overlap for the two isoforms is minimal (Figure 9). Cox-1 expression in the collecting duct of the inner medulla was accompanied by Cox-2 in the surrounding interstitial cells. Only few Cox-1 signals could be detected in the Cox-2^+ cells. In the cortex, interstitial cells showed a weak Cox-1 signal. But in all co-localization experiments no Cox-2 mRNA was detected in interstitial cells outside the area of the inner and outer medulla or the macula densa cells in the cortex (Figure 10).

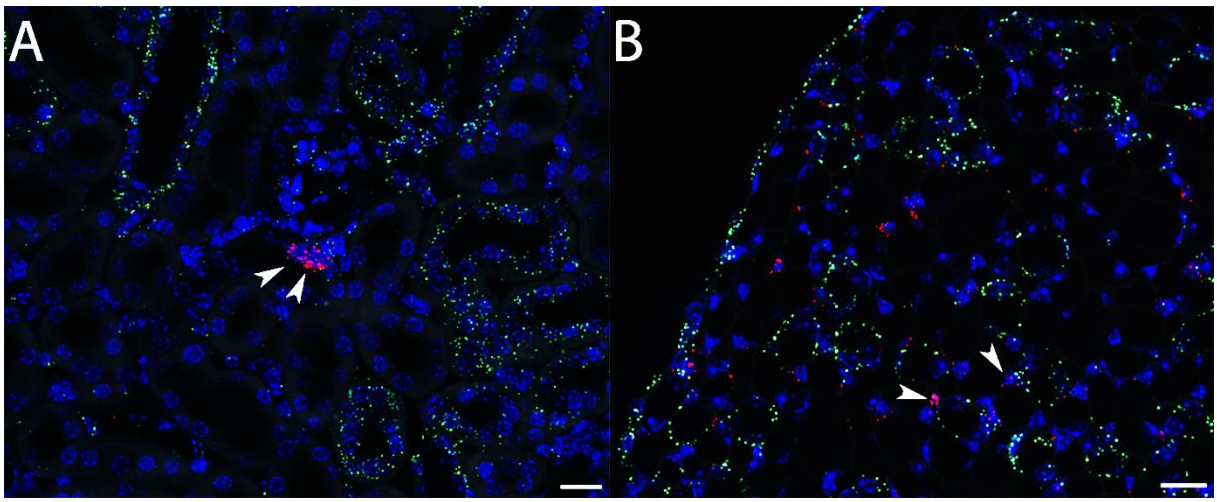

Figure 9: Co-localization of Cox-1 (green) and Cox-2 (red) mRNA; in the kidney cortex (A) Cox-1 expression was detected in distinct tubular compartments, intraglomerular and to a lesser degree in interstitial cells. In cells of the macula densa no overlap between Cox-1 and Cox-2 occurred (arrows); the inner medulla of wildtype mice (B) showed a strong Cox-1 expression in the collecting duct, Cox-2 positive interstitial cells (arrows) were located around the tubules and showed only weak Cox-1 expression; scale bar 20µm

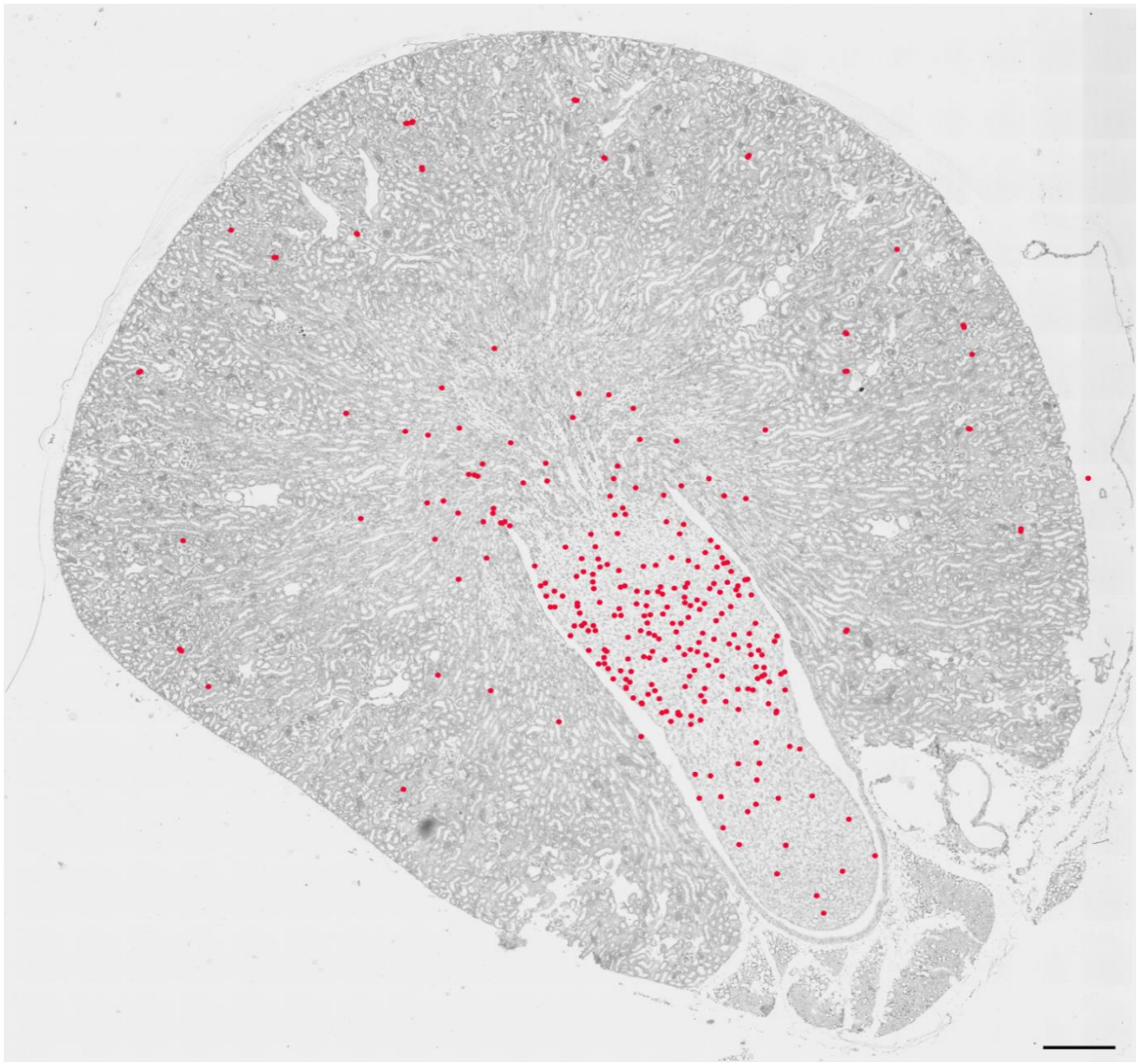

Figure 10: Whole kidney section of an adult wildtype mouse with a normal salt diet; red markings emphasize Cox-2 mRNA expressing cells and were placed over the original signal after imaging; Cox-2 mRNA was only detected in the interstitial cells of the inner and outer medulla and in cells of the macula densa in the kidney cortex; scale bar 500µm

Due to the locally restricted interstitial expression of Cox-2 no co-localization between Cox-2 expressing cells and interstitial fibroblast like cells expressing PDGFR-β and CD73 in the cortex could be detected (data not shown).

These findings support my definition of medullary Cox-2 expressing cells as interstitial pericytes or fibroblast like cells expressing PDGFR-β and TNC, but not CD73.

To gain a better perspective of the results obtained for mice in this study I performed an exploratory *in-situ* hybridization, comparing the Cox-2 expression in mice with the expression in rats. Rats have been used for numerous studies concerning Cox-2 to date, but no expression comparison between the two animal models has been conducted to my knowledge.

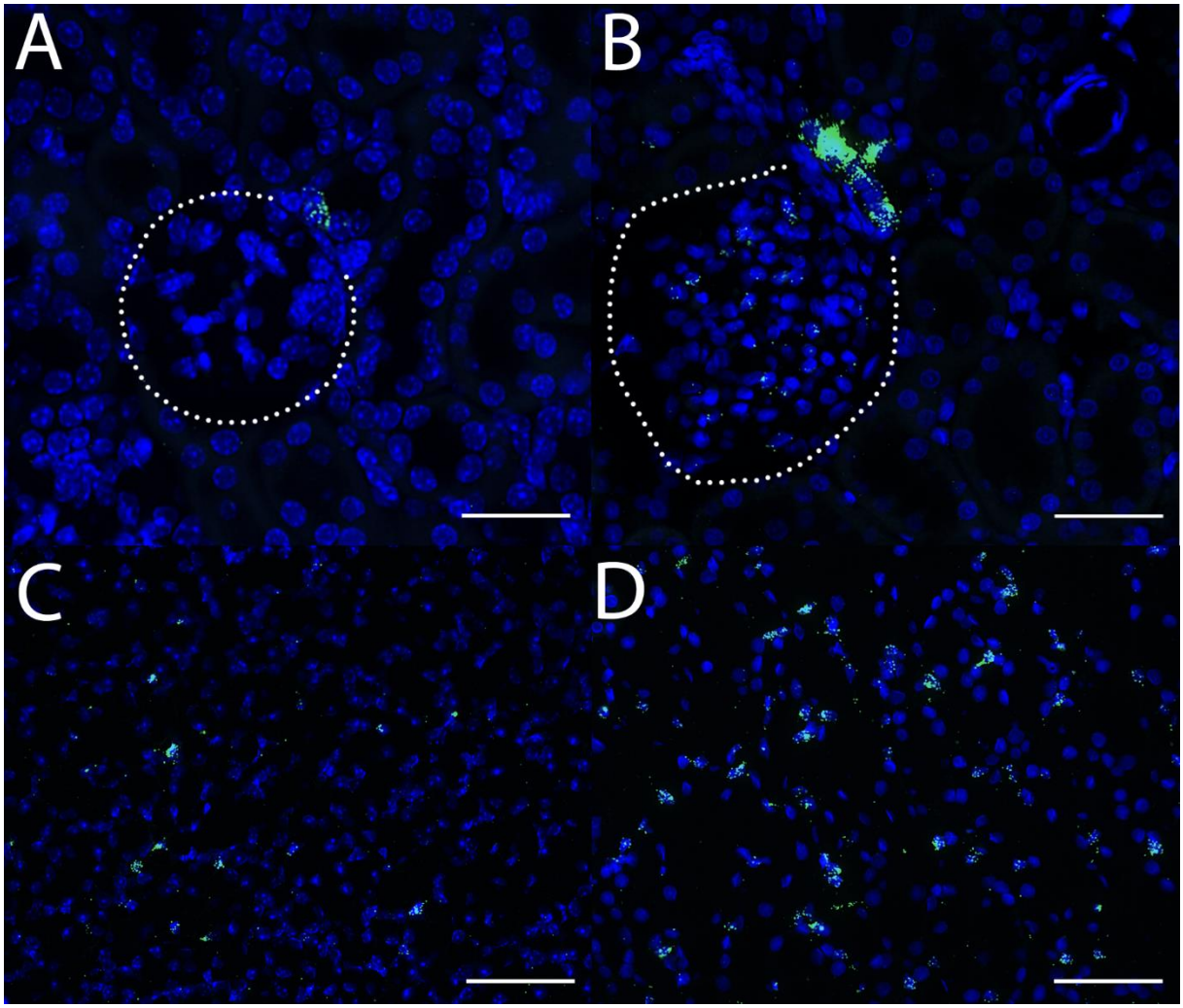

Figure 11: For comparison of different laboratory animal models, Cox-2 mRNA (green) was located on mouse (A and C) and rat (B and D) tissue; in rat kidneys Cox-2 expression in the macula densa was much stronger (B) than in mice (A); glomeruli are marked by dotted lines; additionally rat kidneys show a weak Cox-2 expression in the glomerulus, that is completely absent in mice; in the inner medulla Cox-2 expression in rat kidneys (D) is also much stronger under basal conditions than in mice (C) while the localization of Cox-2 is also restricted to interstitial cells; scale bar 50µm

The amount of Cox-2 expressed in rat kidney's is much higher under basal conditions for both expression sites, macula densa and medullary, than in mice (Figure 11). Additionally Cox-2 is expressed intraglomerular in rats, which is not the case for mice. But the collecting duct cells of rats were also free of any Cox-2 signal.

3.2 Regulation of Cox-2 expression in the kidney

A number of factors tightly modulate the renal Cox-2 expression. In the macula densa cells a salt deficient diet has been reported to increase Cox-2 expression[4,6,23]. Conversely, a high salt diet lowers the expression of Cox-2 in the cortex. The expression of Cox-2 in the kidney medulla seems to be regulated in a reverse fashion[44,104]. Stabilization of the hypoxia inducible factors (HIF) has been shown to induce the expression of Cox-2 in the kidney[17,53] and other tissues[55]. No localization for the hypoxia induced Cox-2 expression in the kidney was known to date.

It was an aim of this study to investigate in which cells a recruitment or regulation of Cox-2 takes place under certain challenges. Focus has been placed on the type, number and location of Cox-2$^+$ cells in each condition. It was evaluated whether an increase in Cox-2 mRNA is caused by more Cox-2 expression per cell or the recruitment of additional Cox-2 expressing cells.

Using *in-situ* hybridization, I analyzed the expression pattern of Cox-2 on whole kidney sections of wildtype mice with a normal or high salt diet, after 24h water restriction and of mice with a genetically activated hypoxia signaling pathway.

The strongly increased expression of Cox-2 mRNA in the medulla of mice fed a high salt diet or after 24h water restriction was caused by a recruitment of additional cells producing Cox-2 as well as an increased mRNA production per cell (Figure 12).

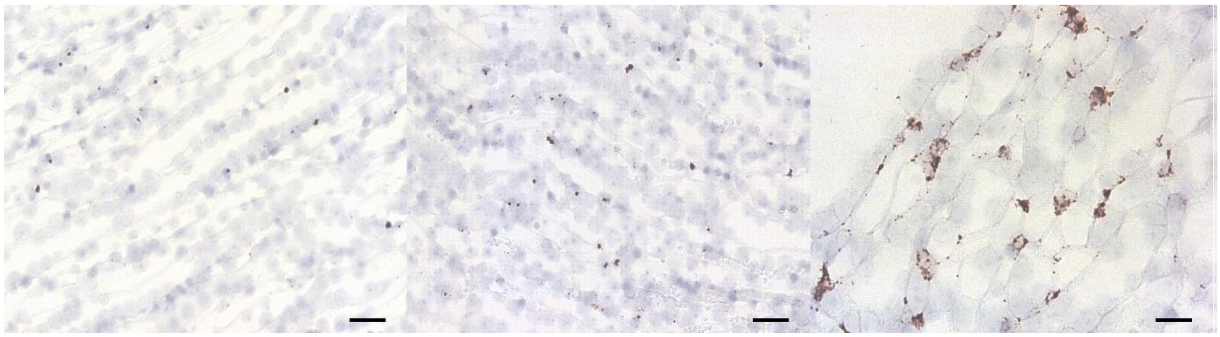

Figure 12: Basal expression of low levels of Cox-2 (brown signal) in the inner medulla (left), recruitment of additional Cox-2 expressing cells after water deprivation and increased Cox-2 production per cell (middle), maximal physiological recruitment and Cox-2 production under a high salt diet (right); scale bar 50µm

Additionally recruited Cox-2 expressing cells were localized in the inner medulla and the inner stripe of the outer medulla (Figure 13, B-D). After 24h water deprivation a marked increase in the number of Cox-2^{+} cells could be detected, but the maximal physiological induction of Cox-2 expression in the medulla was observed after 14d high salt diet (Figure 13,B and C, Figure 15).

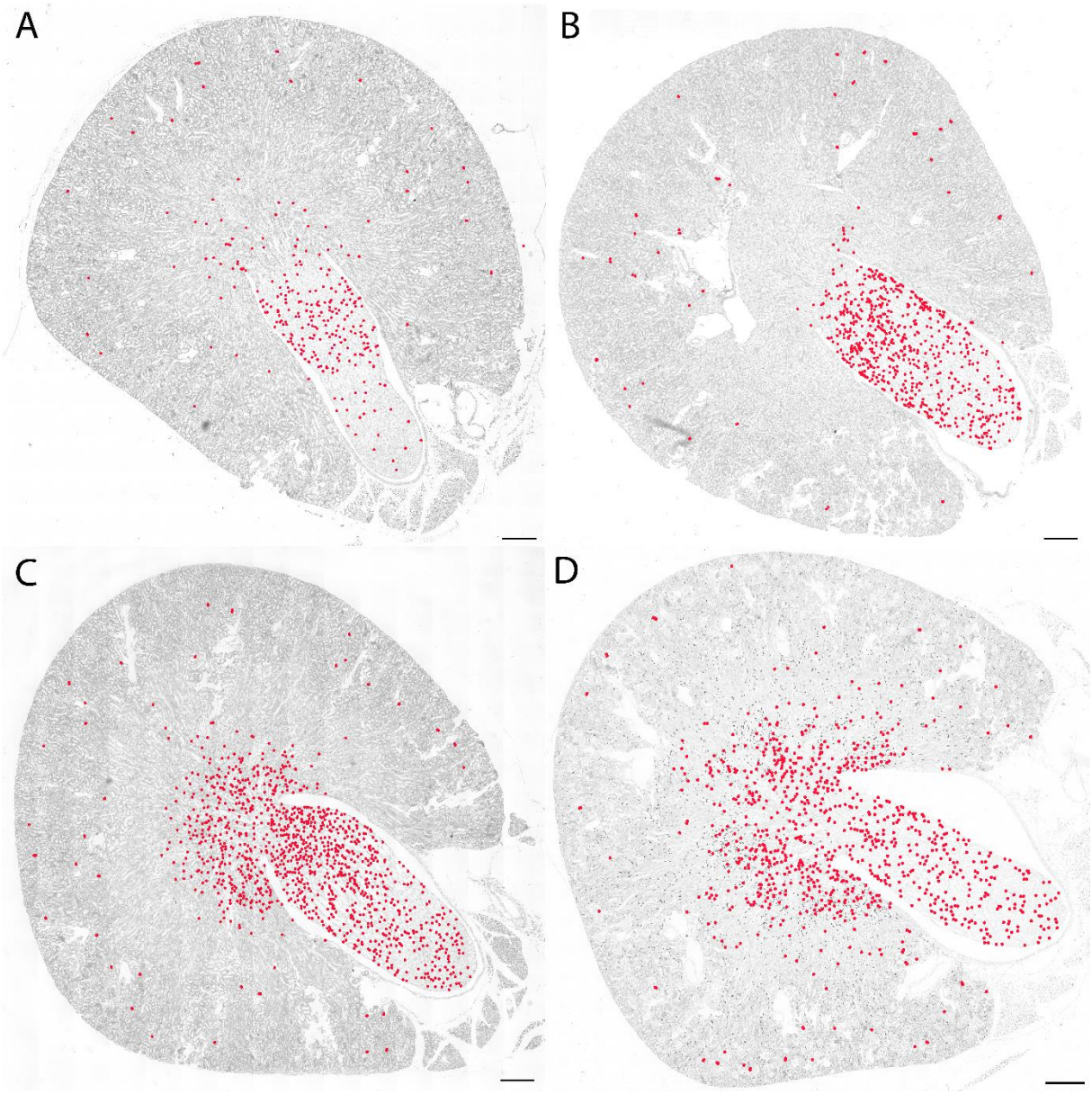

Figure 13: Kidney section of a wildtype mouse fed a normal salt diet, Cox-2 mRNA was marked in red (A); recruitment of additional Cox-2 expressing cells can be observed especially in the inner medulla after 24h water deprivation (B); maximal recruitment of Cox-2 expressing cells in mice fed a high salt diet (C); Cox-2 expression in mice with genetically activated hypoxia signaling pathway after deletion of Vhl in PDGFR-β^{+} cells (D); scale bar 500µm

The additional expression of Cox-2 was present only in PDGFR-β and TNC positive cells, no further subset of inducible Cox-2 expressing cells could be detected under any of these conditions (Figure 14).

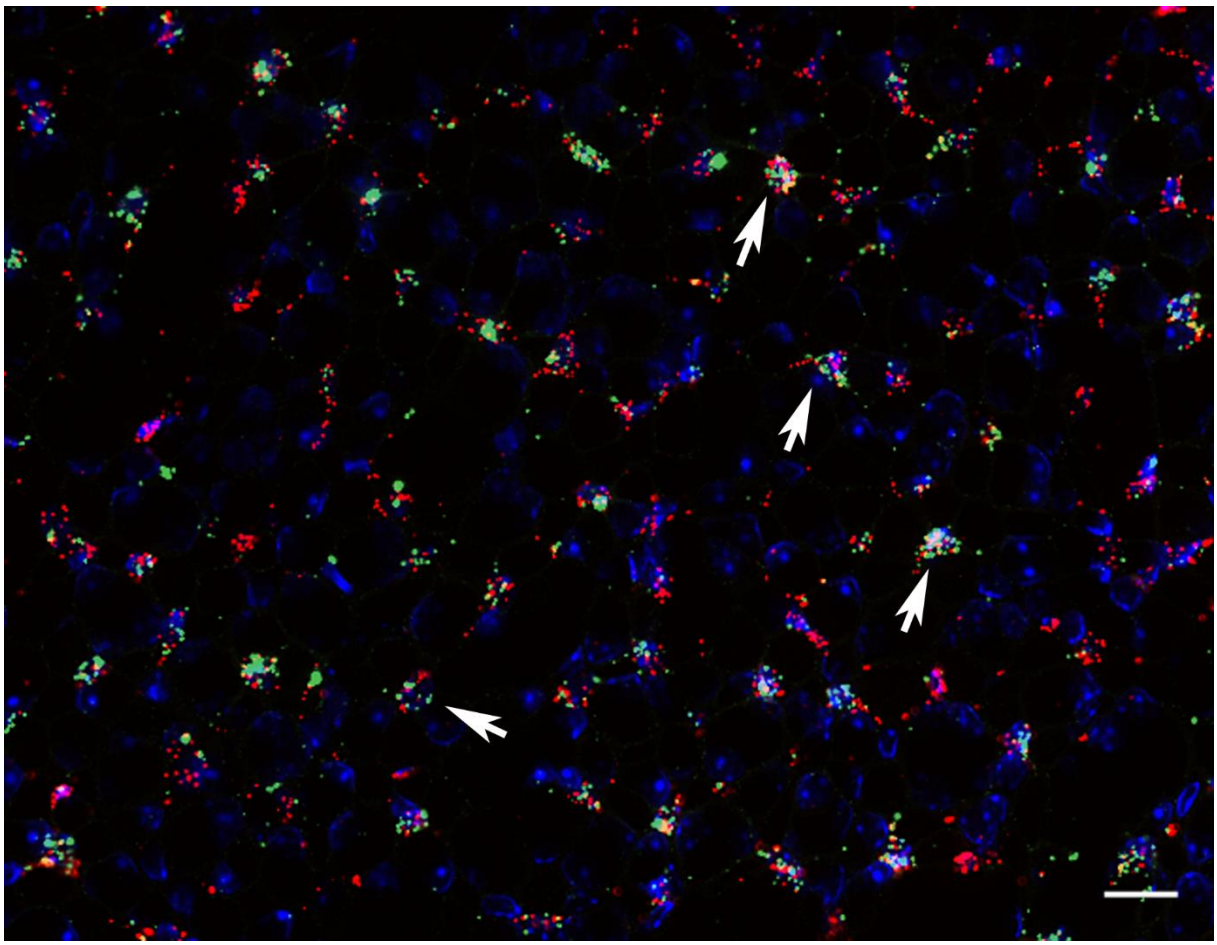

Figure 14: Recruitment of additional Cox-2 expressing cells (green) in the inner medulla after high salt diet was observed only in cells also positive for PDGFR-β (red) examples are marked with arrows, but not in tubular cells or other kidney structures; nuclei were counterstained with DAPI (blue); scale bar 20µm

Deletion of the Vhl gene leads to stabilization of hypoxia inducible factors (HIFs)[1,55]. These HIFs control the expression of numerous hypoxia inducible gene-targets such as EPO and Cox-2[17,55]. Under the genetically induced hypoxia in PDGFR-β^+ cells (PDGFR-$\beta^{+/iCre}$ $Vhl^{fl/fl}$ mice), an increase in medullary Cox-2 expression was observed (Figure 13, Figure 15). Besides an increase in Cox-2 expression these mice were severely polycythemic[1] due to heightened EPO production in newly recruited EPO producing PDGFR-β^+ cells.

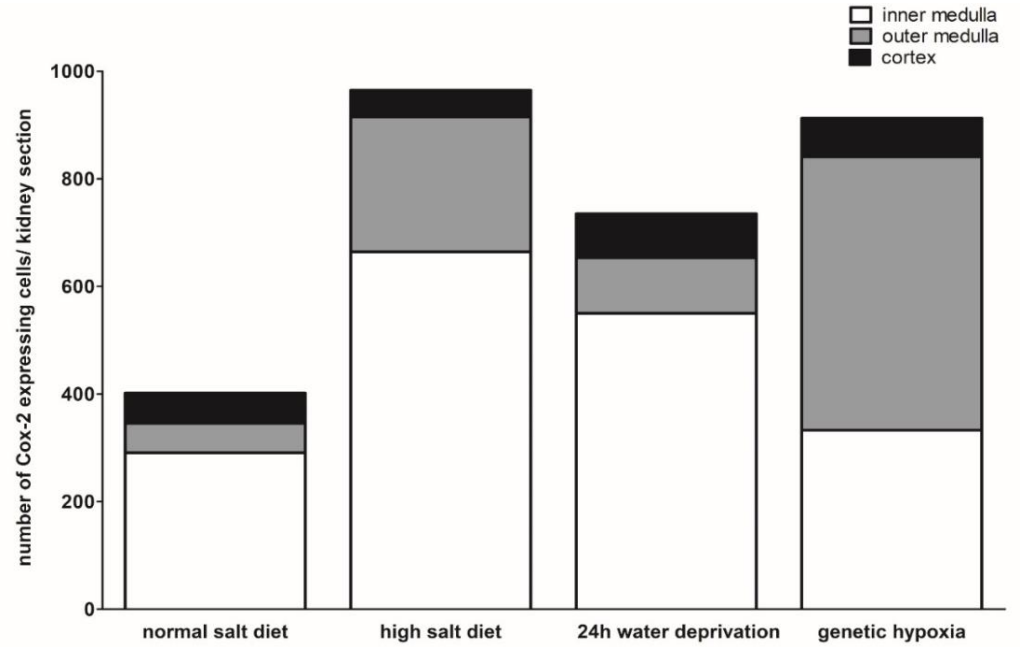

Figure 15: Number and location of recruited Cox-2 expressing cells; the maximal induction of Cox-2 expression can be observed after feeding mice a high salt diet; chronic hypoxia signaling by deletion of the Vhl gene leads to a recruitment of Cox-2 cells mainly in the outer medulla; n = 3 for each condition

Closer investigation of the EPO producing cells that are located in the inner and outer medulla of PDGFR-$\beta^{+/iCre}$ $Vhl^{fl/fl}$ mice showed a substantial number of PDGFR-β^{+} cells that are able to express EPO and Cox-2 at the same time. These were located mostly in the outer medulla (Figure 16).

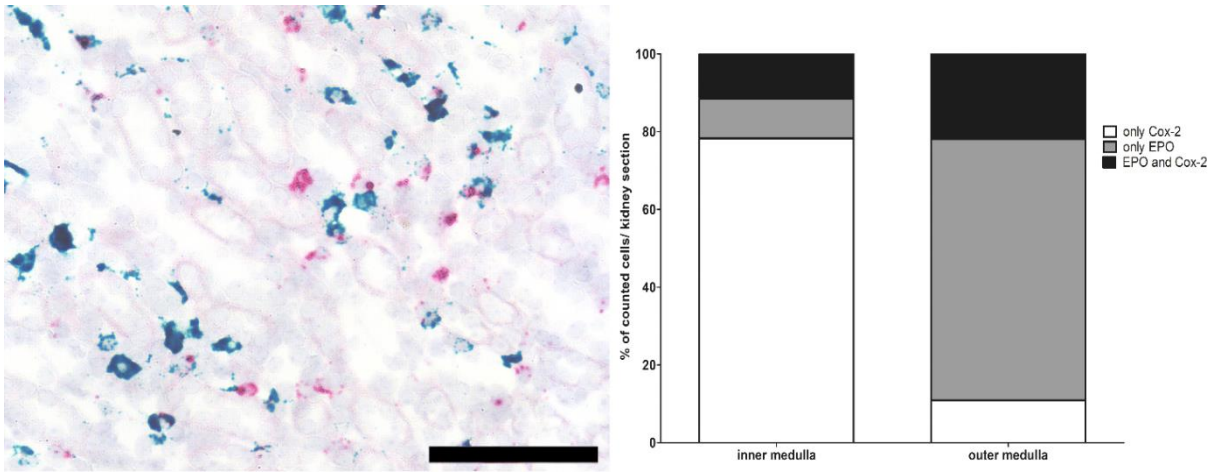

Figure 16: Expression of EPO (green) and Cox-2 (red) mRNA in cells of the outer medulla of PDGFR-$\beta^{+/iCre}$ $Vhl^{fl/fl}$ mice (left); percentage of counted cells with EPO and Cox-2 mRNA in the inner and outer medulla of PDGFR-$\beta^{+/iCre}$ $Vhl^{fl/fl}$ mice; cells expressing both mRNAs at the same time were mostly located in the outer medulla (right); n = 4; scale bar 50µm

From these findings I conclude that PDGFR-β^{+} interstitial cells are the only cell type able to express Cox-2 in the inner and outer medulla of the murine kidney under the four conditions mentioned above. Recruitment of additional Cox-2 expressing cells is only possible in other PDGFR-β^{+} cells and is locally restricted to the inner and outer

medulla. Interstitial cells of the kidney cortex that express CD73 besides PDGFR-β, but not TNC, seem incapable to express Cox-2 regardless of the stimulus.

Furthermore, there seems to be a subset of PDGFR-β^{+} cells that is in principal able to produce EPO and Cox-2 at the same time, but these are distinct from the majority of EPO producing cells in PDGFR-$\beta^{+/iCre}$ $Vhl^{fl/fl}$ mice by their location in the medulla and lack of CD73 expression.

3.3 Importance of Cox-2 for kidney development and function

3.3.1 Function of Cox-2 investigated by conditional gene deletion in specific compartments

The two distinct expression compartments for Cox-2 identified in the first part of this work, macula densa cells and medullary interstitial cells, give rise to the theory that they serve different functions.

It was the second aim of this study to find a suitable mouse model, allowing the separate investigation of the Cox-2 function in its two expression sites. Through the targeted deletion of the Cox-2 expression in distinct cell types the different functions of Cox-2 were investigated more closely.

3.3.1.1 Conditional deletion of Cox-2 in all cells of the adult kidney

For the conditional deletion of Cox-2 a mouse model with floxed Cox-2 alleles was used as first described by Ishikawa et al[88]. In this model exon 4 and 5 of the Cox-2 gene can be excised by a Cre-recombinase, leading to a frameshift and a stop codon in exon 6.

To evaluate the efficiency of the deletion of the Cox-2 gene, I first crossed these mice with mice bearing $CAG^{+/iCre}$, an ubiquitously expressed tamoxifen inducible Cre-recombinase ($CAG^{+/iCre}$ $Cox2^{fl/fl}$ mice). After induction of Cre-activity, Cox-2 mRNA abundance was drastically reduced across all kidney zones (Figure 17).

A specific RNAscope® probe was generated to bind in the mRNA section after exon 6, so a positive Cox-2 signal is only achieved in cells expressing functional Cox-2 mRNA (Figure 17).

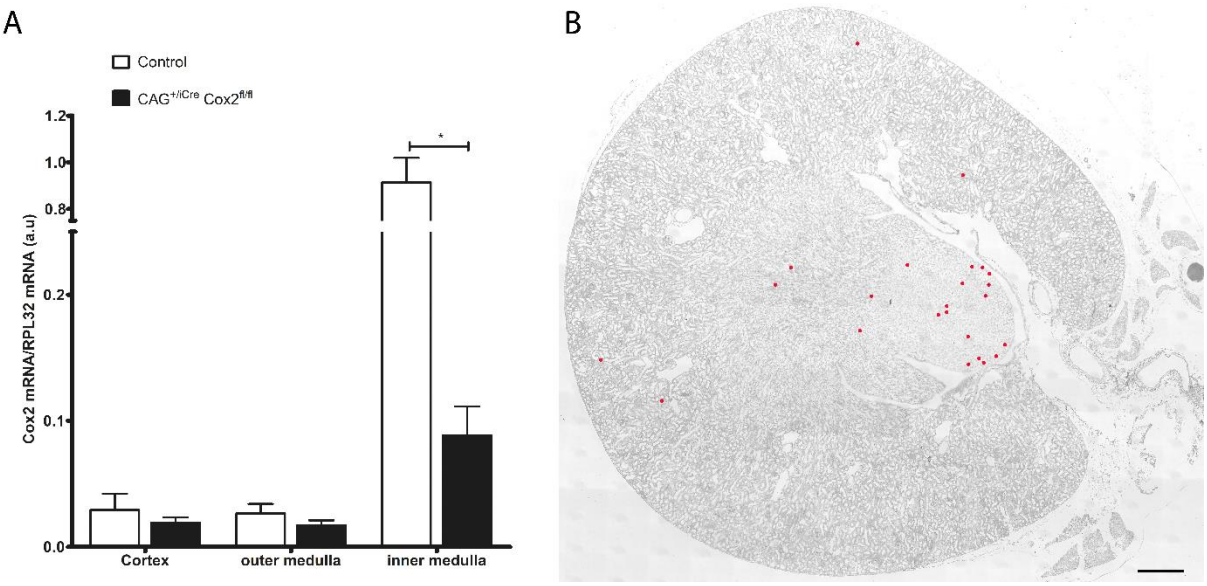

*Figure 17: Cox-2 mRNA abundance was greatly reduced in the inner medulla of CAG$^{+/iCre}$ Cox2$^{fl/fl}$ mice (0,91 vs 0,08 a.u; * is p<0,05; n = 4 for each group (A); in-situ hybridization for Cox-2 showed only very few remaining Cox-2^{+} cells (red; B); scale bar 500µm*

To further verify the successful excision of the Cox-2 gene, genotyping for the gene sequence newly created after recombination, as described previously[88], was performed for all experimental animals (Figure 18).

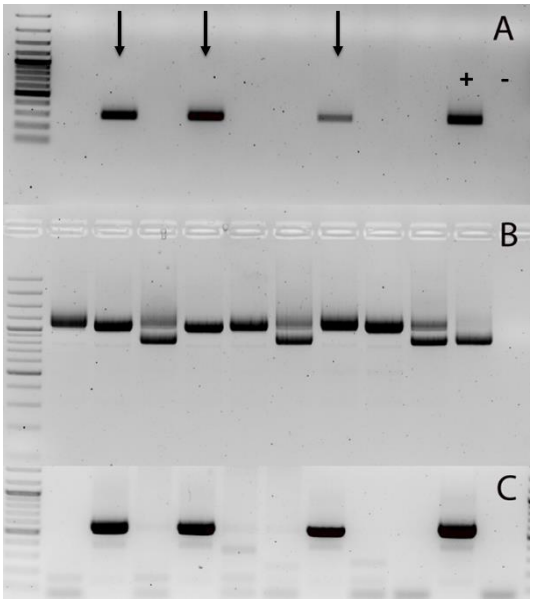

Figure 18: Genotyping gel for a representative litter of CAG$^{+/iCre}$ Cox2$^{fl/fl}$ mice; product for cre-recombinase at 286bp (A); genotyping for the floxed Cox-2 alleles with a band at 1058bp for the floxed and at 823bp for the wildtype allele (B); test for recombination after tamoxifen induction yielded a product with 651 bp, arrows mark mice with successful recombination (C); last two columns show positive and negative control for each pcr reaction.

With these data I conclude that the mouse models made up of a Cre-recombinase and floxed Cox-2 alleles yield a sufficient reduction of Cox-2 expression to study the function of Cox-2 in the so targeted cells.

3.3.1.2 Functional consequences of Cox-2 deletion in normally developed kidneys

Analysis of the histological morphology of CAG$^{+/iCre}$ Cox2$^{fl/fl}$ mice showed none of the anomalies that are present in Cox-2 $^{-/-}$ mice[61] (Figure 17). Under basal conditions these animals appeared healthy and had a normal kidney function (Figure 19).

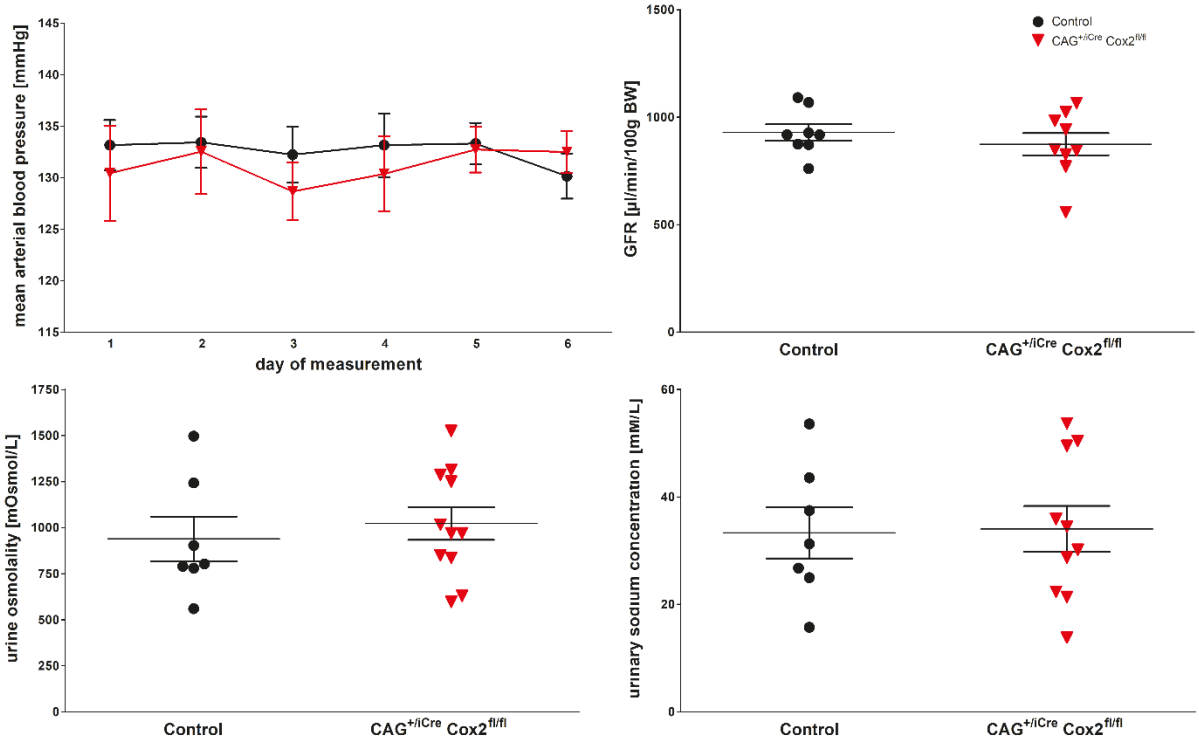

Figure 19: Basal kidney function of CAG$^{+/iCre}$ Cox2$^{fl/fl}$ mice; the mice showed normal blood pressure (upper left; mean was 130,2 in CAG$^{+/iCre}$ Cox2$^{fl/fl}$ mice vs. 132,5mmHg in controls; n = 5), unchanged GFR (upper right; 874,1 vs. 928,7µl/min/100gBW; n = 8); the urinary concentrating ability in these mice was normal (lower left; 1022,3 vs. 939,5mOsmol/L); these mice showed a normal sodium excretion (lower right; 34,1 vs. 33,3mMol/L)

In Cox-2$^{-/-}$ mice a lower expression of renin has been reported under basal conditions[52,87]. This was not observed in the CAG$^{+/iCre}$ Cox2$^{fl/fl}$ mice where renin mRNA abundance and plasma renin concentration (PRC) was not significantly different from control mice (Figure 20) under basal conditions.

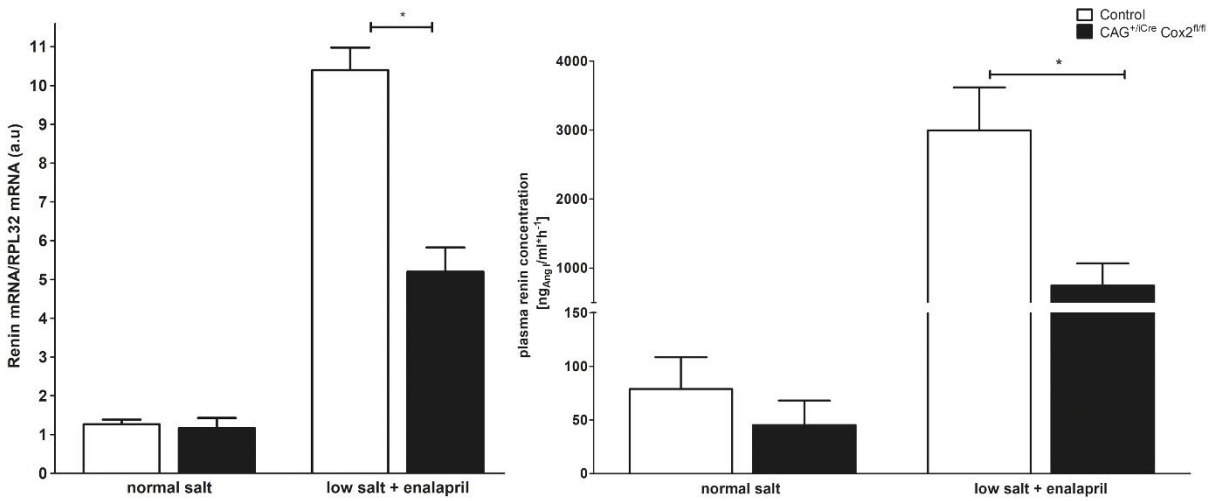

Figure 20: Renin expression and plasma concentration in CAG$^{+/iCre}$ Cox2$^{fl/fl}$ mice with a normal and low salt diet plus enalapril; under a basal conditions the CAG$^{+/iCre}$ Cox2$^{fl/fl}$ mice showed an unchanged renin mRNA abundance (1,16 vs.1,26a.u in controls; n = 4; left); renin mRNA recruitment during low salt plus enalapril was significantly impaired in CAG$^{+/iCre}$ Cox2$^{fl/fl}$ mice (5,2 vs.10,4a.u in controls; n = 5; is p< 0,05); plasma renin concentration was parallel to mRNA unchanged under basal conditions, but with an impeded recruitment under LSE (745,6 vs. 2995,83ng$_{ANGI}$/ml*h^{-1} in control; n = 6)*

If fed a low salt diet with the additional application of the ACE-inhibitor enalapril (LSE) for 10 days, control mice reacted with a heightened production and release of renin[23]. In mice with disrupted Cox-2 function in all cells of the kidney, however, a marked reduction in the recruitment of renin cells and decreased release of renin could be observed compared to control mice of the same treatment (Figure 20, Figure 21).

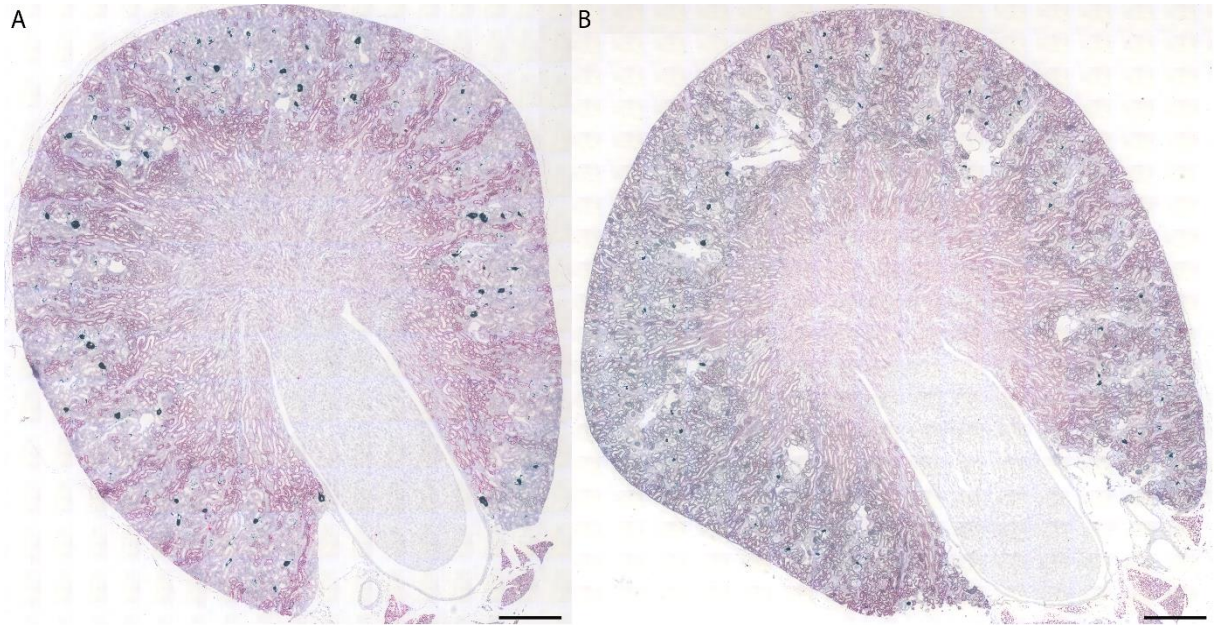

Figure 21: mRNA abundance of renin (green) visualized with RNAscope® on kidney sections of mice treated with a low salt diet and Enalapril for 10d; in wildtype mice large renin producing fields could be observed (A), these fields were absent in CAG$^{+/iCre}$ Cox2$^{fl/fl}$ mice (B); scale bar 500µm

In the reverse case, if these CAG$^{+/iCre}$ Cox2$^{fl/fl}$ mice were fed a high salt diet, the recruitment of Cox-2 in the medullary region of the kidney was absent. Blood pressure measurement in these mice, showed that mice with a Cox-2 deficiency in all cells had

a slightly higher rise in blood pressure but do not develop significant hypertension compared to their littermate controls (data not shown).

3.3.2 Importance of Cox-2 in the FoxD1 compartment during nephrogenesis

After identifying the medullary Cox-2 expressing cells as PDGFR-β^+ interstitial fibroblast-like cells, I wanted to investigate their importance for kidney development.

Interstitial fibroblast-like PDGFR-β^+ cells derive from the FoxD1 compartment during nephrogenesis along with mesangial, vascular smooth muscle cells and renin producing cells[11,107] (Figure 3). These cells are also strongly involved in the phenotype of Cox-$2^{-/-}$ mice.

FoxD1 is expressed during nephrogenesis from embryonic day 11,5 on[16]. The expression of FoxD1 is limited to the embryonic phase and up to 3 days after birth in mice[17]. To evaluate the relevance of Cox-2 during this time and the immediate post-natal period, I therefore generated FoxD1$^{+/Cre}$ Cox2$^{fl/fl}$ mice to delete Cox-2 already during nephrogenesis.

Cox-2 was successfully deleted in the interstitial cells of the inner medulla, but Cox-2 expression in the macula densa was conserved (Figure 22).

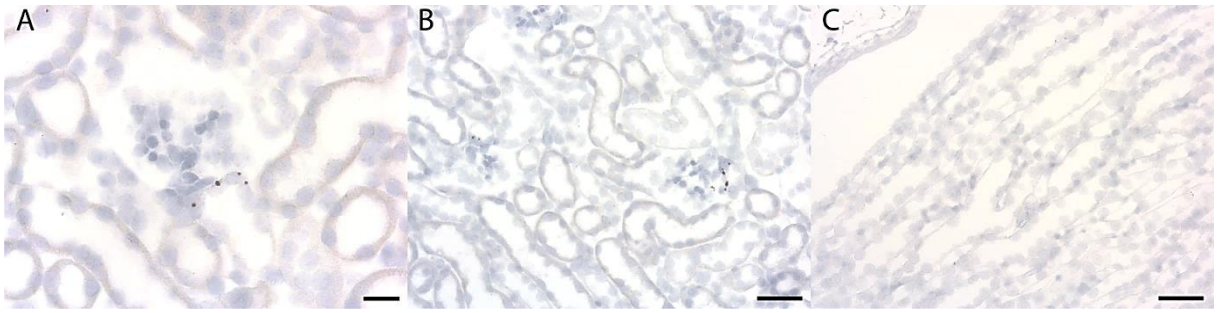

Figure 22: In-situ hybridization for Cox-2 mRNA (brown signal) on a kidney section of a FoxD1$^{+/Cre}$ Cox2$^{fl/fl}$ mouse; Cox-2 mRNA signal is conserved in the cells of the macula densa (A and B); no Cox-2 signal could be detected in the kidney cortex outside of the macula densa (B); basal Cox-2 mRNA expression was absent in interstitial cells of the inner medulla (C); scale bar 20µm in A; scale bar 50µm in B and C

FoxD1$^{+/Cre}$ Cox2$^{fl/fl}$ mice were born in mendelian ratios and both genders were fertile. Histological analysis of the FoxD1$^{+/Cre}$ Cox2$^{fl/fl}$ mice showed that the kidneys were developed normally. Glomeruli were distributed across the cortex and shaped normally, the subcapsular glomeruli found in Cox-$2^{-/-}$ mice were entirely absent (Figure 23).

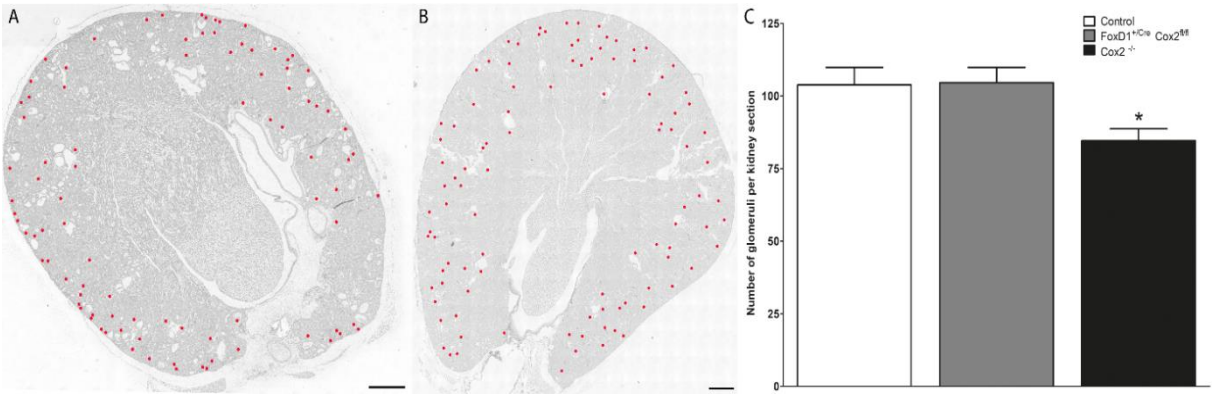

Figure 23: Whole kidney section of a Cox-2 $^{-/-}$ mouse, position of the glomeruli is marked in red (A); kidney section of a FoxD1$^{+/Cre}$ Cox2$^{fl/fl}$ mouse (B) showing a normal structure and normal distribution of glomeruli across the cortex and no subcapsular glomeruli; in addition to the subcapsular position of the glomeruli, Cox-2 $^{-/-}$ mice also showed a reduced number of glomeruli per section, this was not the case for FoxD1$^{+/Cre}$ Cox2$^{fl/fl}$ mice (C, n = 4); scale bar 500µm

Animals with deletion of Cox-2 in stromal progenitors were normal in size and showed no abnormal kidney function (Figure 24). In all analyzed parameters, GFR, urine and sodium concentration as well as bodyweight no difference between FoxD1$^{+/Cre}$ Cox2$^{fl/fl}$ mice and their littermate controls could be measured.

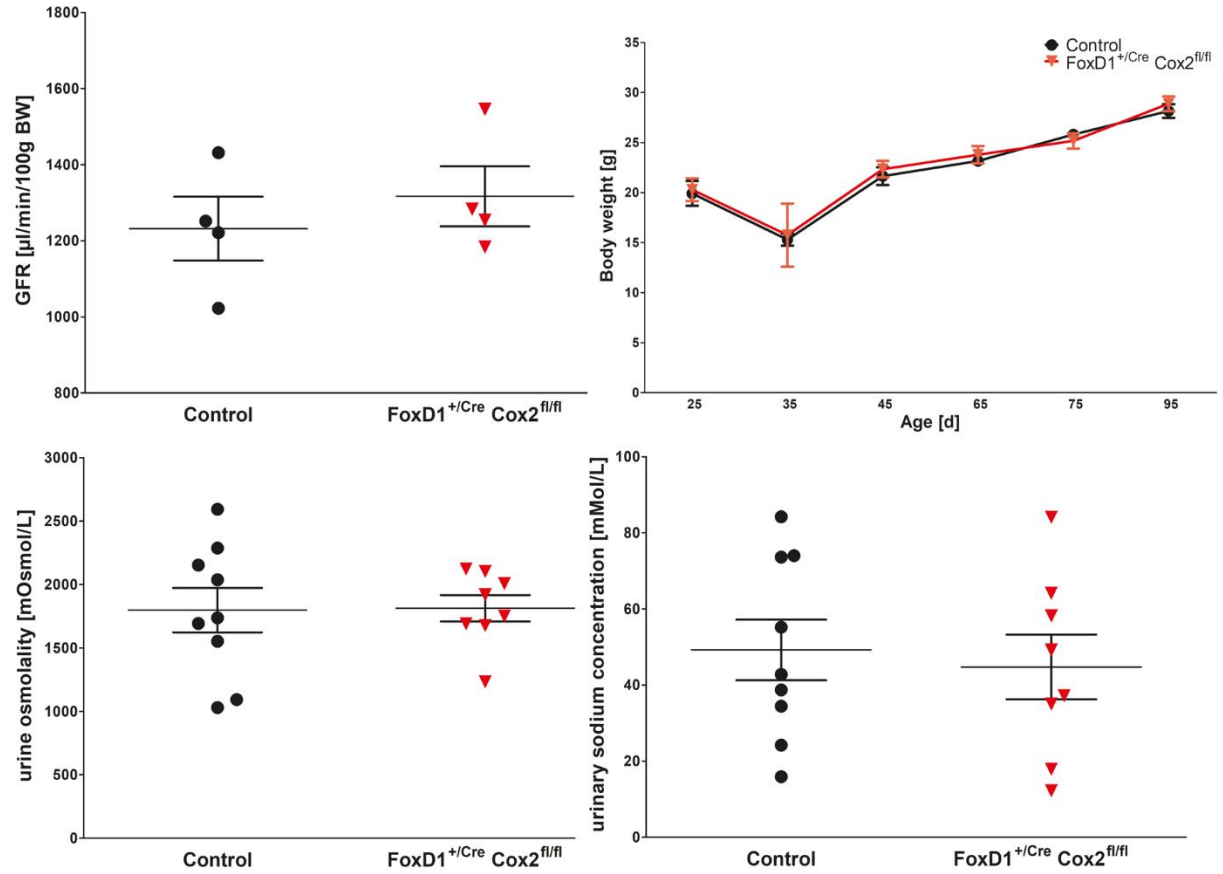

Figure 24: FoxD1$^{+/Cre}$ Cox2$^{fl/fl}$ mice showed normal GFR (1316,6 vs. 1221,4µl/min/100gBW; upper left); normal weight (upper right); the ability to concentrate urine was unchanged (1812,8 vs. 1797,3mOsml/L in controls; lower left) and a normal sodium excretion (44,7 vs. 49,2mMol/L lower right) was measured; n ≥ 4 for each group

In these mice Cox-2 in macula densa cells was not deleted. Renin cell number and distribution was normal (Figure 25).

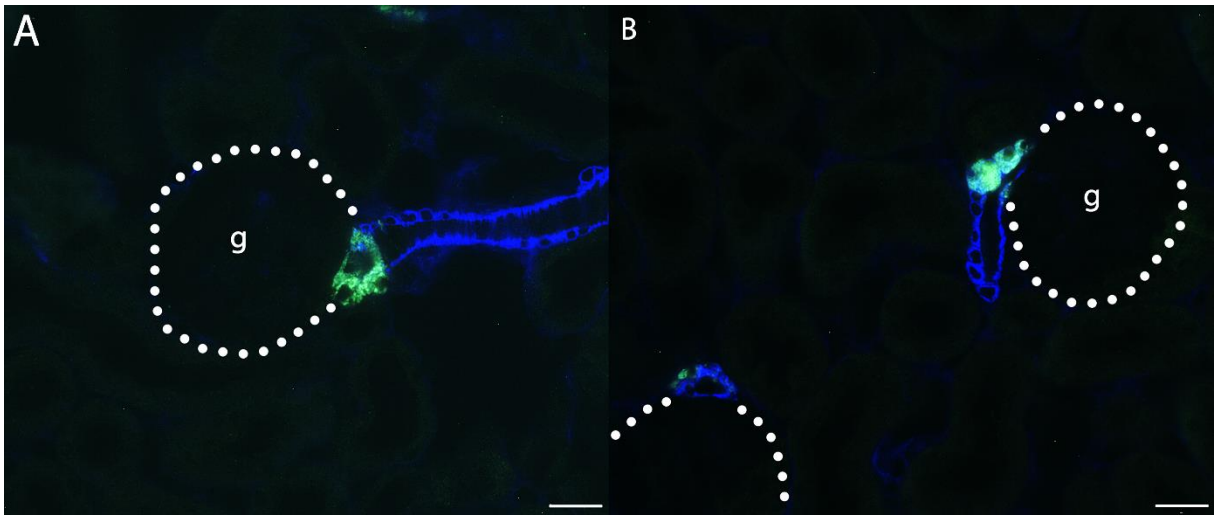

Figure 25: Representative glomeruli (g) with immunohistochemical staining for α-SMA (blue) and renin (green) on a control (A) kidney section and the kidney section of a FoxD1$^{+/Cre}$ Cox2$^{fl/fl}$ mouse (B); no difference in the number or location of the renin cells could be observed, n = 4; scale bar 20µm

qPCR measurement of Col1a1 mRNA in kidney tissue and Sirius red staining was performed to check for interstitial fibrosis seen in Cox2$^{-/-}$ mice[61]. Results did not show any pathological changes in adult FoxD1$^{+/Cre}$ Cox2$^{fl/fl}$ mice (Figure 26).

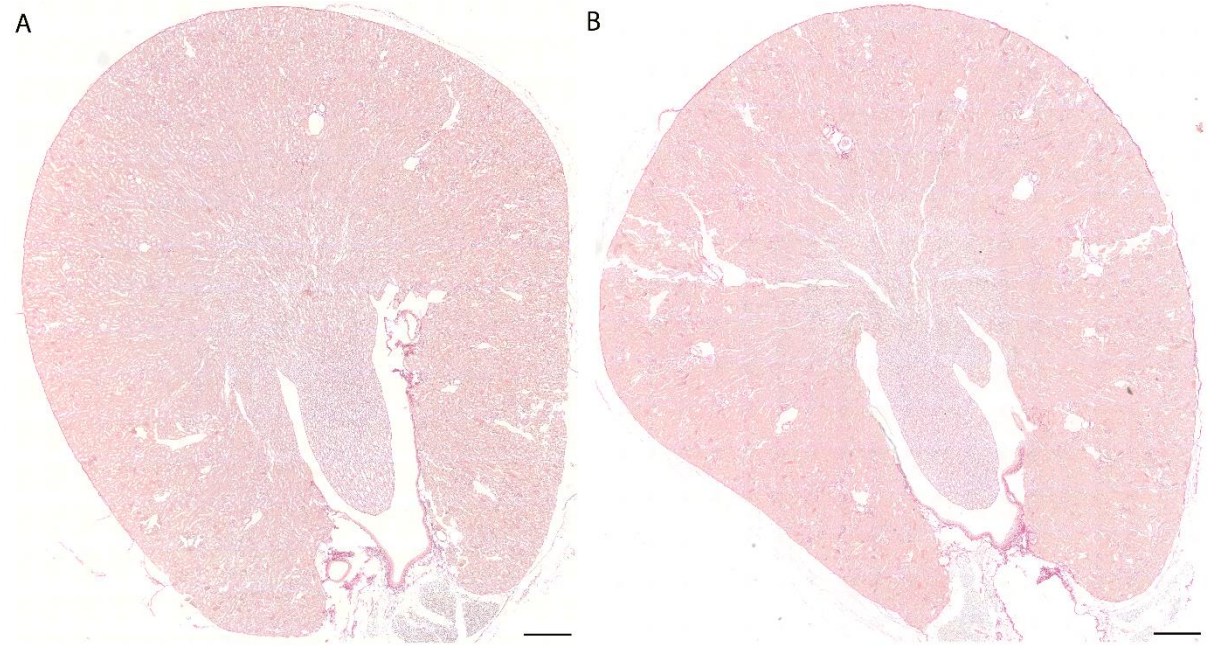

Figure 26: Sirius red staining to visualize collagen deposits in the kidney tissue of an adult wildtype mouse (A) and an age matched FoxD1$^{+/Cre}$ Cox2$^{fl/fl}$ mouse (B); no difference in collagen disposition could be detected between groups; scale bar 500µm

3.3.2.1 Renin cell recruitment in FoxD1$^{+/Cre}$ Cox2$^{fl/fl}$ mice

With the intact function of Cox-2 in cells of the macula densa (Figure 22) the recruitment of renin cells was unimpeded in FoxD1$^{+/Cre}$ Cox2$^{fl/fl}$ mice, when the RAAS was challenged. Plasma renin concentrations were unchanged under basal conditions and increased to similar levels when the mice were fed a low salt diet and treated with the ACE-Inhibitor enalapril (Figure 27) for 10 days. Renal renin mRNA levels also showed no difference between genotypes at any time.

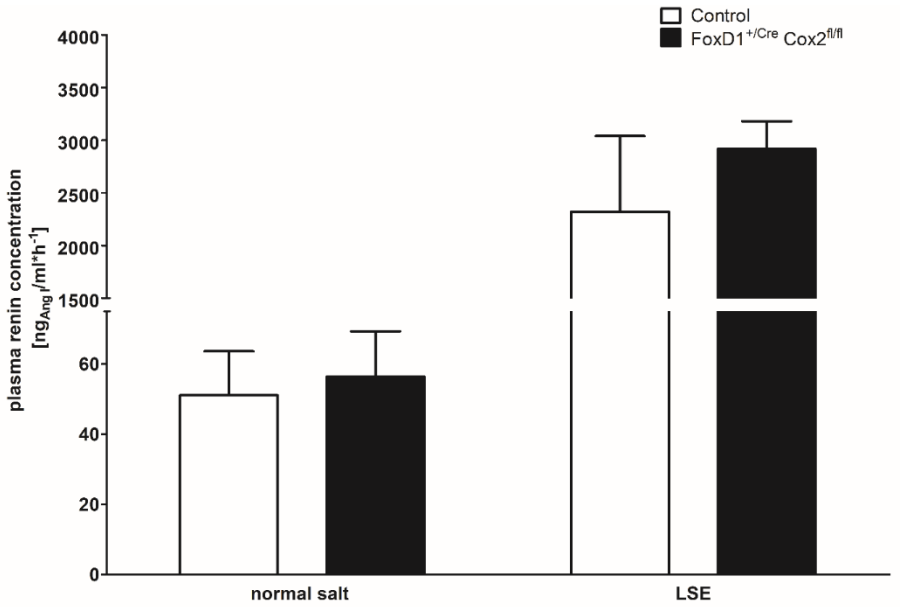

Figure 27: Plasma renin concentration of FoxD1$^{+/Cre}$ Cox2$^{fl/fl}$ mice and littermate controls with a normal salt diet and with a low salt diet plus enalapril (LSE) in the drinking water; under normal conditions the plasma renin concentration was not different between FoxD1$^{+/Cre}$ Cox2$^{fl/fl}$ mice and their controls; when challenged with LSE both groups showed a strong increase in plasma renin concentration; n = 5 for each group

3.3.3 Function of Cox-2 in PDGFR-β^{+} interstitial medullary cells

For the evaluation of the distinct function of Cox-2 in the medullary interstitial cells of the kidney, mice with a selective deletion of Cox-2 in only PDGFR-β^{+} cells were used (PDGFR-β$^{+/iCre}$ Cox2$^{fl/fl}$ mice). The function of Cox-2 in the macula densa of these mice was unchanged, allowing the attribution of any observed effects to the lack of medullary interstitial Cox-2 function.

Deletion of Cox-2 was induced with a tamoxifen containing diet at an age of two month for four weeks and the mice were fed a normal diet for three weeks after the tamoxifen period before any experiments were performed. *In-situ* hybridization and quantification of the remaining Cox-2^{+} cells showed only few signals in the inner and outer medulla, but an unchanged expression in the macula densa cells of the cortex (Figure 28).

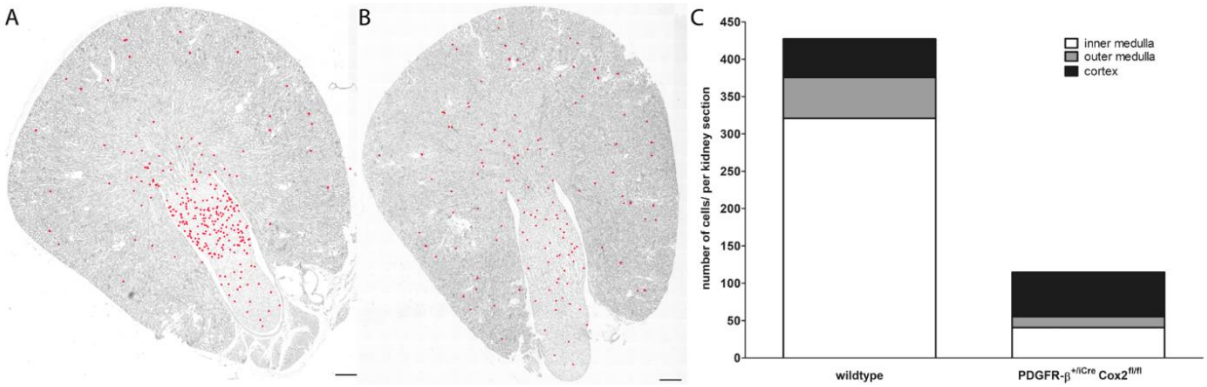

Figure 28: In-situ hybridization for Cox-2 on a kidney section of a wildtype (A) and a PDGFR-β$^{+/iCre}$ Cox2$^{fl/fl}$ mouse (B), Cox-2^{+} cells were emphasized in red; few cells expressing Cox-2 could be found in the inner medulla of PDGFR-β$^{+/iCre}$ Cox2$^{fl/fl}$ mice, most were located in the cortex; quantitative analysis of Cox-2^{+} cells per kidney zone (C) showed a strong reduction in the number of cells in PDGFR-β$^{+/iCre}$ Cox2$^{fl/fl}$ mice in the inner medulla (40,6 vs. 321 cells in controls) and outer medulla (14,5 vs. 60,8 cells), while the cortical expression was unchanged (59,5 vs. 51,4 cells); n = 4; scale bar 500µm

3.3.3.1 Functional relevance of interstitial Cox-2 expression under normal conditions

After deletion of Cox-2 in interstitial PDGFR-β^{+} cells of adult mice, their basic kidney functions were evaluated to see whether the lack of Cox-2 in these cells produced a phenotype.

Under basal conditions PDGFR-β$^{+/iCre}$ Cox2$^{fl/fl}$ mice showed no aberrations in their basic kidney functions. GFR in these mice was unchanged and no abnormalities in the urinary concentrating ability or the excretion of sodium and potassium could be measured (Figure 29).

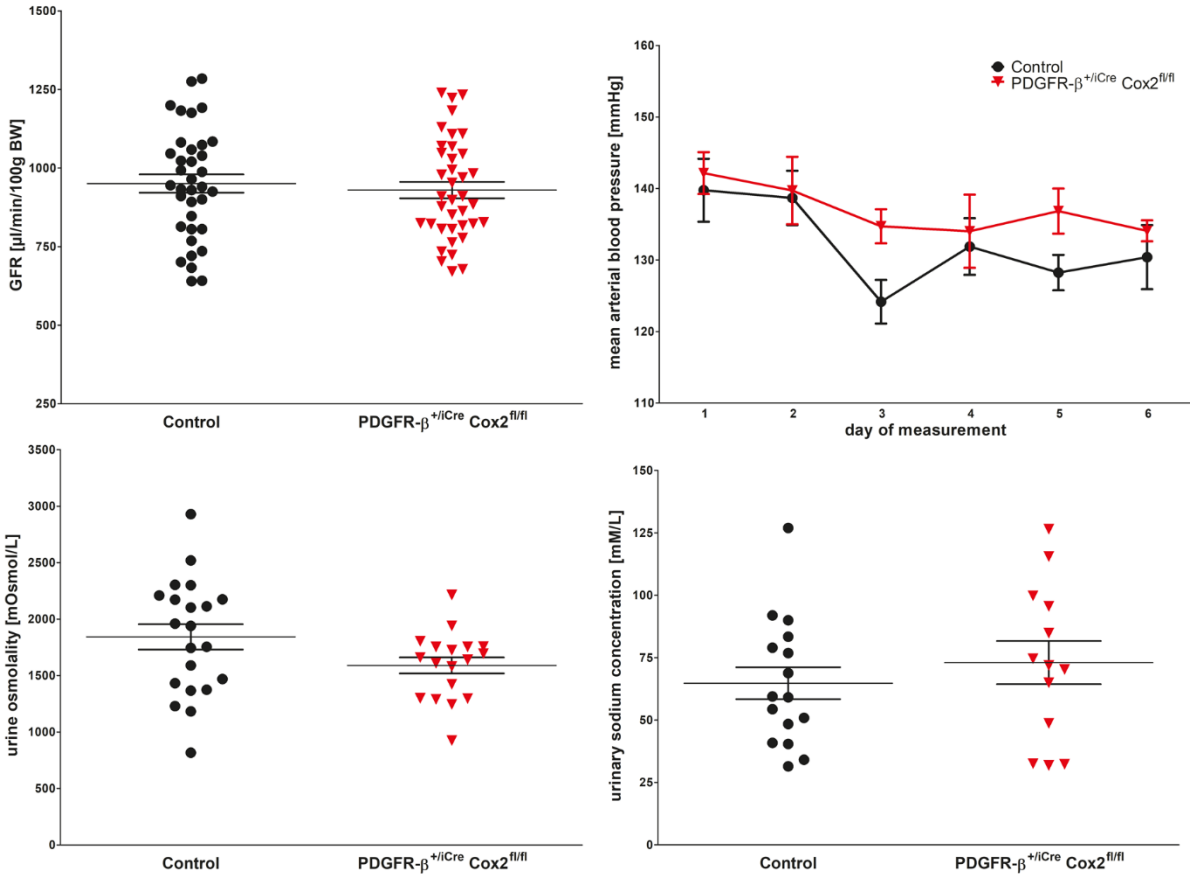

Figure 29: Basal kidney function of PDGFR-β$^{+/iCre}$ Cox2$^{fl/fl}$ mice with a normal salt diet; GFR was unchanged in these mice 4 weeks after Cox-2 deletion (929,7 vs. 950,4µl/min/100gBW in controls; upper left); in line the urinary osmolality (1590 vs. 1843 mOsmol/L; lower left) and sodium excretion (73,1 vs. 64,7mMol/L; lower right) were also unchanged, n ≥ 10; the PDGFR-β$^{+/iCre}$ Cox2$^{fl/fl}$ mice showed no persistent change in mean arterial blood pressure (136,1 vs. 132,2mmHg; n = 4; upper right)

The deletion of Cox-2 in interstitial medullary PDGFR-β^{+} cells led to no persistent change in the mean arterial pressure. Furthermore, the excreted urine volume and correlating water intake, as measured over 24h in metabolic cages, was unchanged (Figure 33).

On the level of mRNA abundance a significant reduction of medullary Cox-2 mRNA (Figure 30) was observed. Selected mRNA targets associated with salt and water handling in the inner medulla were measured. While a trend toward downregulation was conceivable for most targets, only the change in the sodium and chloride dependent betain/GABA transpoter 1 (BGT1) and Urea transporter A1 (UTA1) reached significance. Renin expression was unchanged in PDGFR-β$^{+/iCre}$ Cox2$^{fl/fl}$ mice.

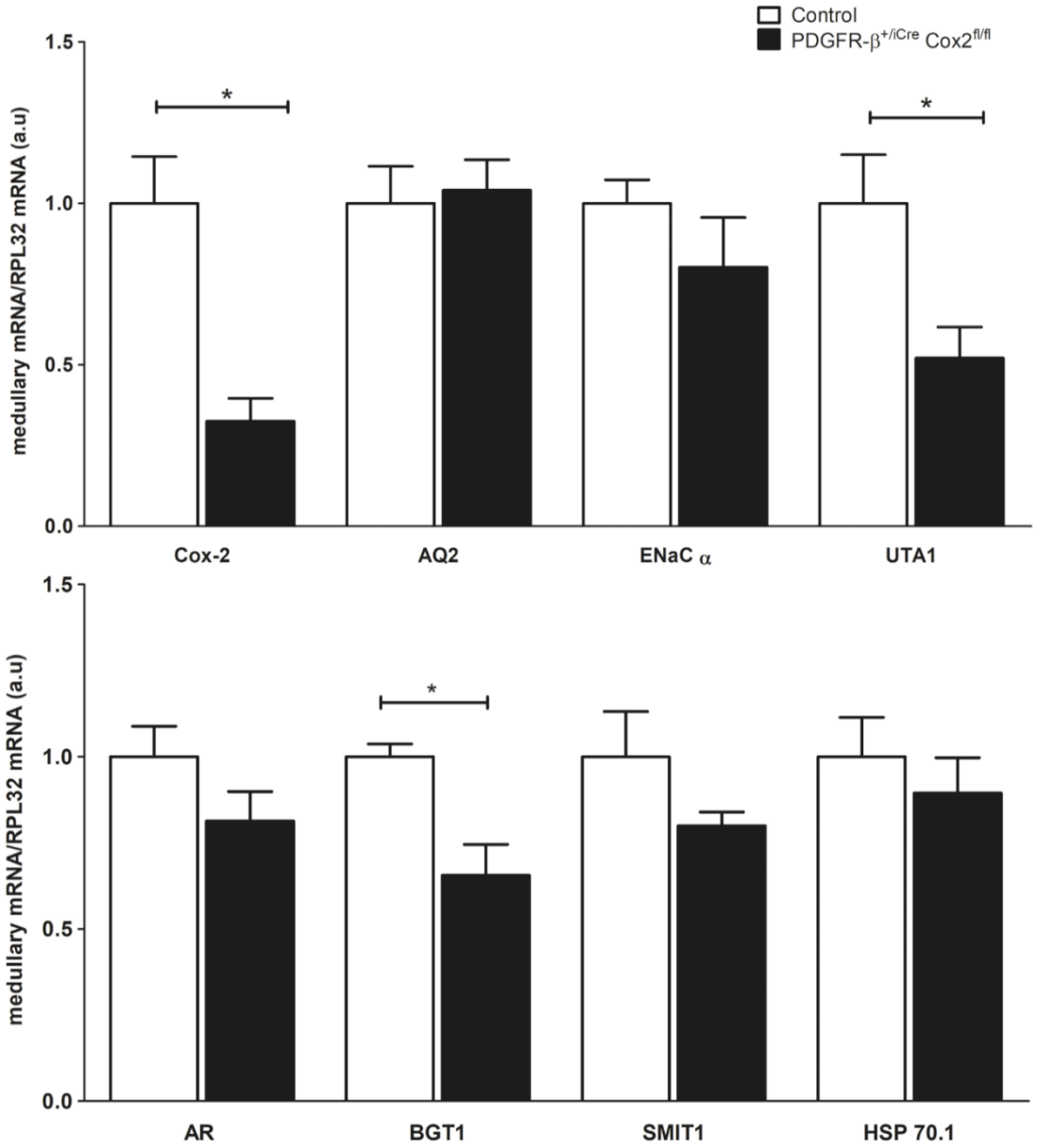

*Figure 30: mRNA abundance in the inner medulla of wildtype and PDGFR-β$^{+/iCre}$ Cox2$^{fl/fl}$ mice with a normal salt diet; expression of Cox-2 is significantly reduced in PDGFR-β$^{+/iCre}$ Cox2$^{fl/fl}$ mice along with UTA-1 and BGT1; other targets connected to osmolyte handling showed a trend to be downregulated but did not reach significance; n = 7 for each group; * is p < 0,05*

3.3.3.2 Handling of high dietary sodium in mice deficient for Cox-2 in PDGFR-β^{+} cells

After evaluating the basic kidney function of PDGFR-β$^{+/iCre}$ Cox2$^{fl/fl}$ mice, I wanted to investigate the ability of these mice to handle a high dietary sodium intake, as the recruitment of Cox-2 expression in this condition takes place only in medullary interstitial cells.

Using *in-situ* hybridization I evaluated the recruitment pattern of Cox-2 after 14d high salt diet in PDGFR-β$^{+/iCre}$ Cox2$^{fl/fl}$ mice (Figure 31).

Here only few additional cells could be recruited to express Cox-2 in the inner and outer medulla even under the high salt stimulus.

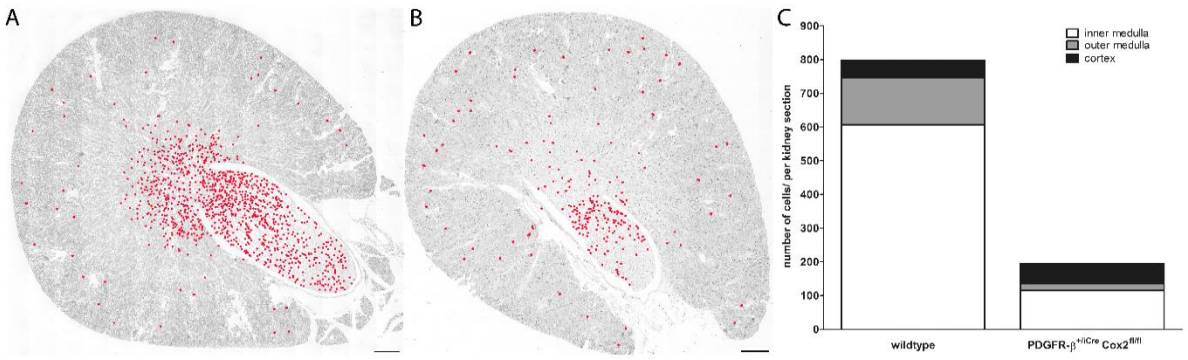

Figure 31: Recruitment of Cox-2 mRNA expressing cells (red signals) after a high salt diet in a wildtype mouse (A) and a PDGFR-β$^{+/iCre}$ Cox2$^{fl/fl}$ mouse (B); scale bar 500µm; number of Cox-2 expressing cells per kidney section and their zonal distribution in wildtype and PDGFR-β$^{+/iCre}$ Cox2$^{fl/fl}$ mice with a high salt diet (C; n = 4)

In line with the *in-situ* hybridization results, only a slight increase in Cox-2 mRNA could be measured in the inner medulla of PDGFR-β$^{+/iCre}$ Cox2$^{fl/fl}$ mice compared to their littermate controls (Figure 32) when fed a high salt diet.

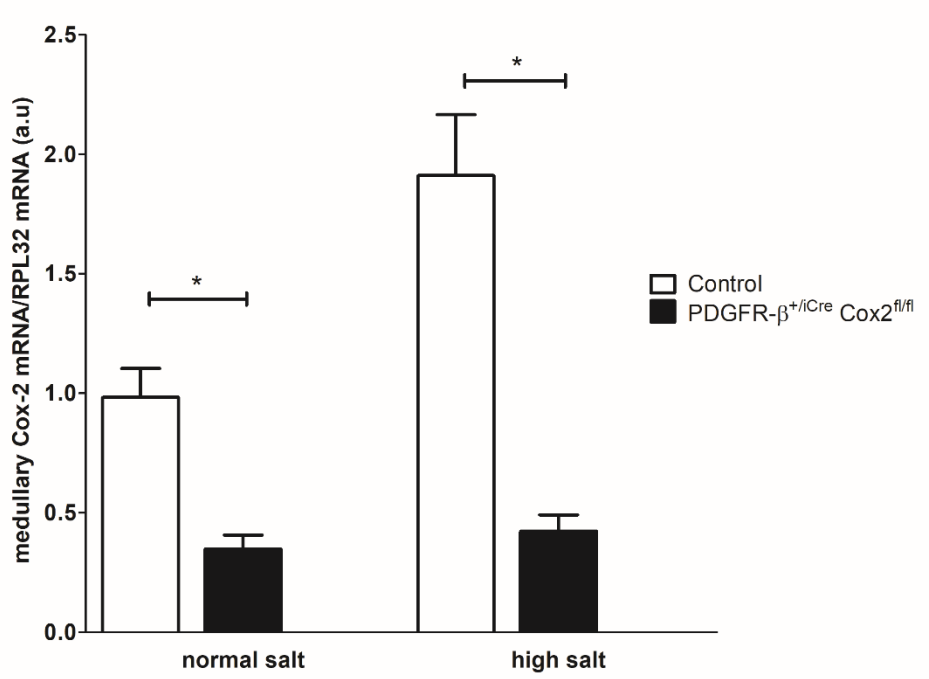

*Figure 32: Relative Cox-2 mRNA expression in the inner medulla of control mice or PDGFR-β$^{+/iCre}$ Cox2$^{fl/fl}$ mice on a normal salt diet (left pair) or a high salt diet (right pair); in control mice a clear induction of Cox-2 expression could be observed after 14d high salt diet, in the PDGFR-β$^{+/iCre}$ Cox2$^{fl/fl}$ mice this heightened Cox-2 expression was absent (n = 7 animals in each group); * is p < 0,05*

For analysis of the kidney function in PDGFR-β$^{+/iCre}$ Cox2$^{fl/fl}$ mice, the high salt diet was fed for 14 days and then urine was collected, urine volume, water intake as well as GFR were measured (Figure 33).

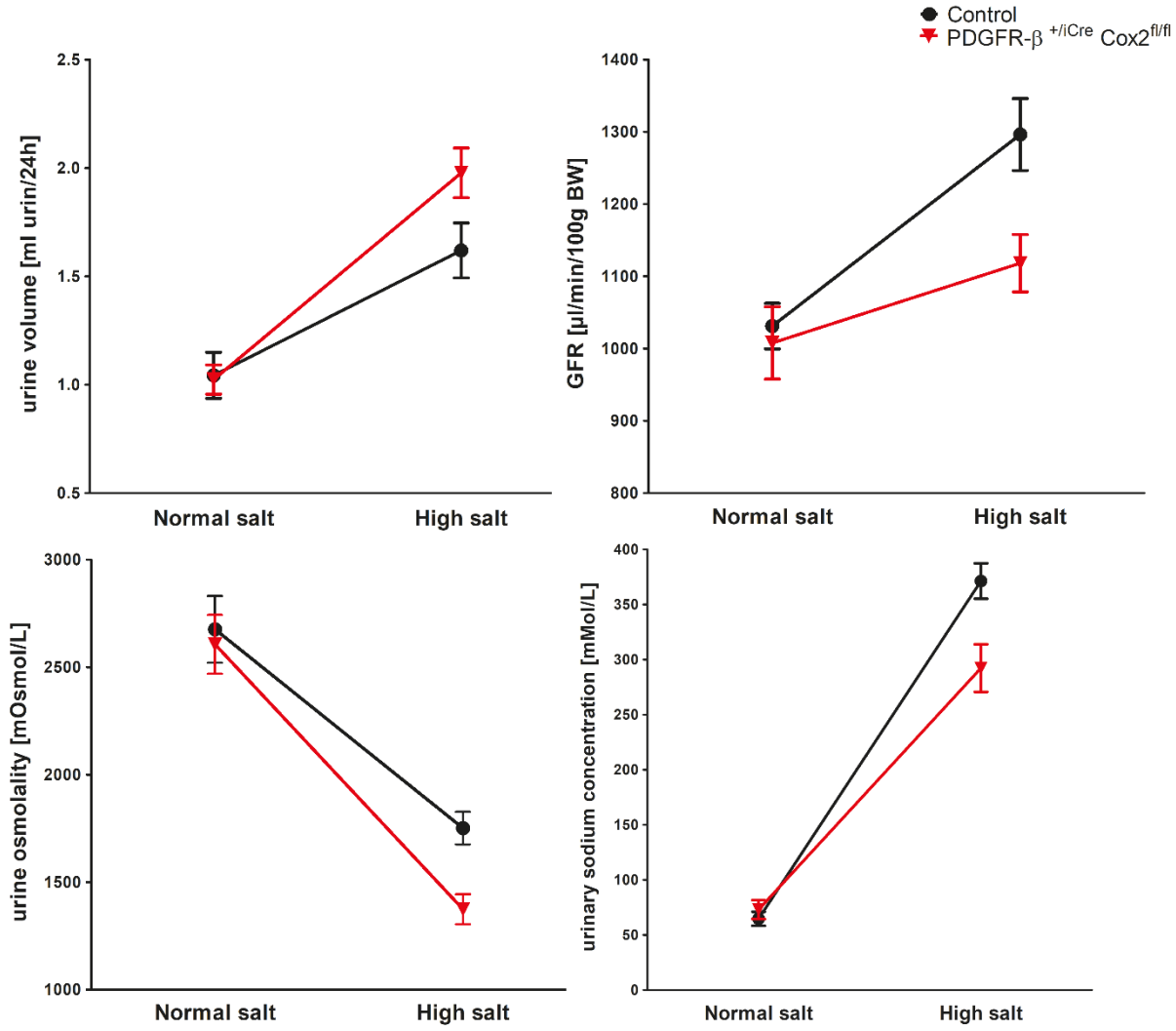

Figure 33: Changes in kidney function of control and PDGFR-β$^{+/iCre}$ Cox2$^{fl/fl}$ mice fed a normal salt diet or a high salt diet; in the mice lacking Cox-2 a significant increase in urine volume (1,97 vs. 1,59ml/24h in controls; p<0,05; n = 4; upper left) with a corresponding lowering of the urinary sodium concentration (305,5 vs. 371,3mMol/L; p<0,05; lower right) and urine osmolality (1363 vs. 1680 mOsmol/L; p<0,05; lower left) was observed compared to control mice; in addition the increase in GFR that was observed in control mice was blunted in PDGFR-β$^{+/iCre}$ Cox2$^{fl/fl}$ mice (1118 vs. 1296µl/min/100gBW; p<0,05)

Control mice fed a high salt diet showed a strong increase in urinary sodium excretion, GFR and urine volume when compared to a normal salt diet. In PDGFR-β$^{+/iCre}$ Cox2$^{fl/fl}$ mice the urinary concentration of sodium was significantly lower under the high salt diet than in control animals. To compensate this, the urine volume in PDGFR-β$^{+/iCre}$ Cox2$^{fl/fl}$ mice with high salt was increased to such a degree that the overall excretion of sodium was comparable to the control mice (601,8 in PDGFR-β$^{+/iCre}$ Cox2$^{fl/fl}$ vs. 590,4µMol/24h sodium in controls). The increase in GFR observed in control mice was significantly lower in the mice without Cox-2 in PDGFR-β^{+} interstitial cells. In line with this, the PDGFR-β$^{+/iCre}$ Cox2$^{fl/fl}$ mice did not gain an inappropriate amount of weight during the treatment and showed no sign of edema or water retention.

To gain a better understanding of the importance of Cox-2 in PDGFR-β^{+} interstitial cells for the regulation of blood pressure, the switch from a normal to a high salt diet was monitored by tail cuff measurement of arterial blood pressure. This allowed a direct observation of a rise in blood pressure in PDGFR-β$^{+/iCre}$ Cox2$^{fl/fl}$ mice and showed that this change was already significant within 48h after the start of a high salt diet and was persistent over several days (Mean of 142,3 vs 131,7mmHg in controls during high salt (Figure 34).

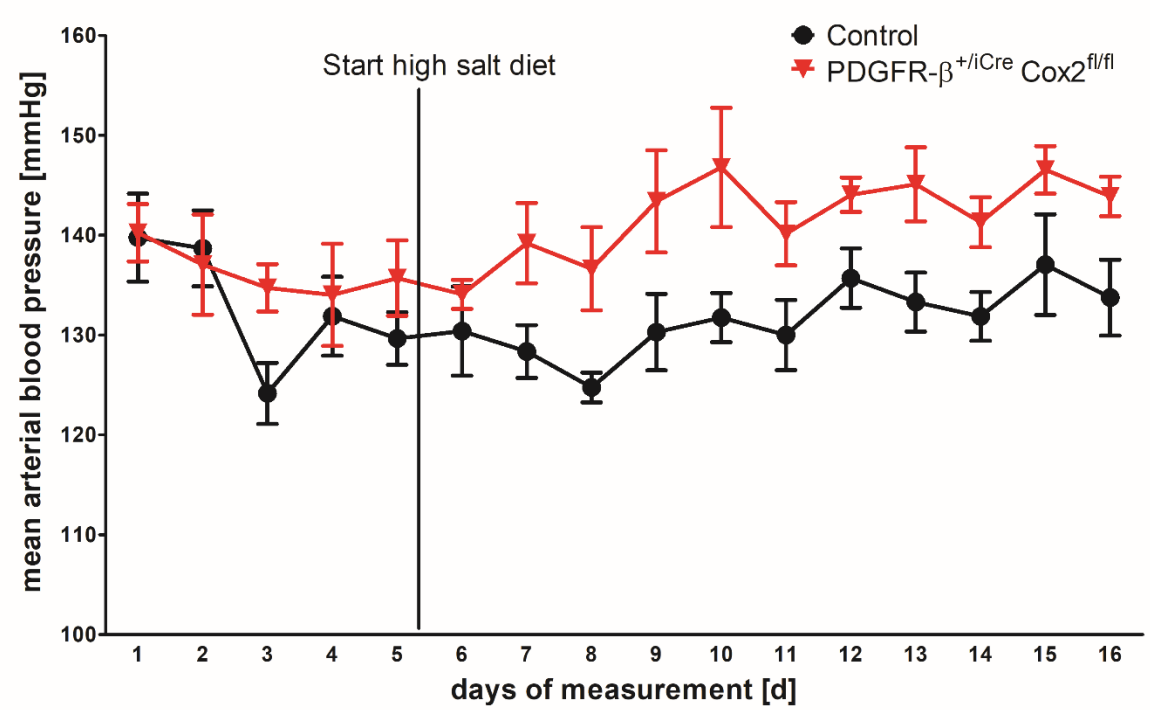

Figure 34: Change in mean arterial blood pressure of wildtype and PDGFR-β$^{+/iCre}$ Cox2$^{fl/fl}$ mice, when switched from a normal salt to a high salt diet; the change in blood pressure was significant within 48h and persisted over several days in PDGFR-β$^{+/iCre}$ Cox2$^{fl/fl}$ mice while wildtype mice showed no significant increase in blood pressure (mean of 142,3 vs 131,7mmHg in controls) in response to the heightened salt intake; n = 4 for each group

To analyze the reason for the reduced concentrating ability in the kidney and permanently increased blood pressure in PDGFR-β$^{+/iCre}$ Cox2$^{fl/fl}$ mice a study of different transporters and channels in the inner medulla associated with salt handling was undertaken. Targets associated with Cox-2 were chosen to evaluate this maladaptation. The mRNA abundance for AQ2 and ENACα was unchanged between genotypes. Only UTA-1 and BGT1 showed a significantly reduced mRNA expression in PDGFR-β$^{+/iCre}$ Cox2$^{fl/fl}$. Other osmolality-activated genes such as SMIT1, AR and HSP70.1 showed a downward trend, but failed to reach significance (Figure 35).

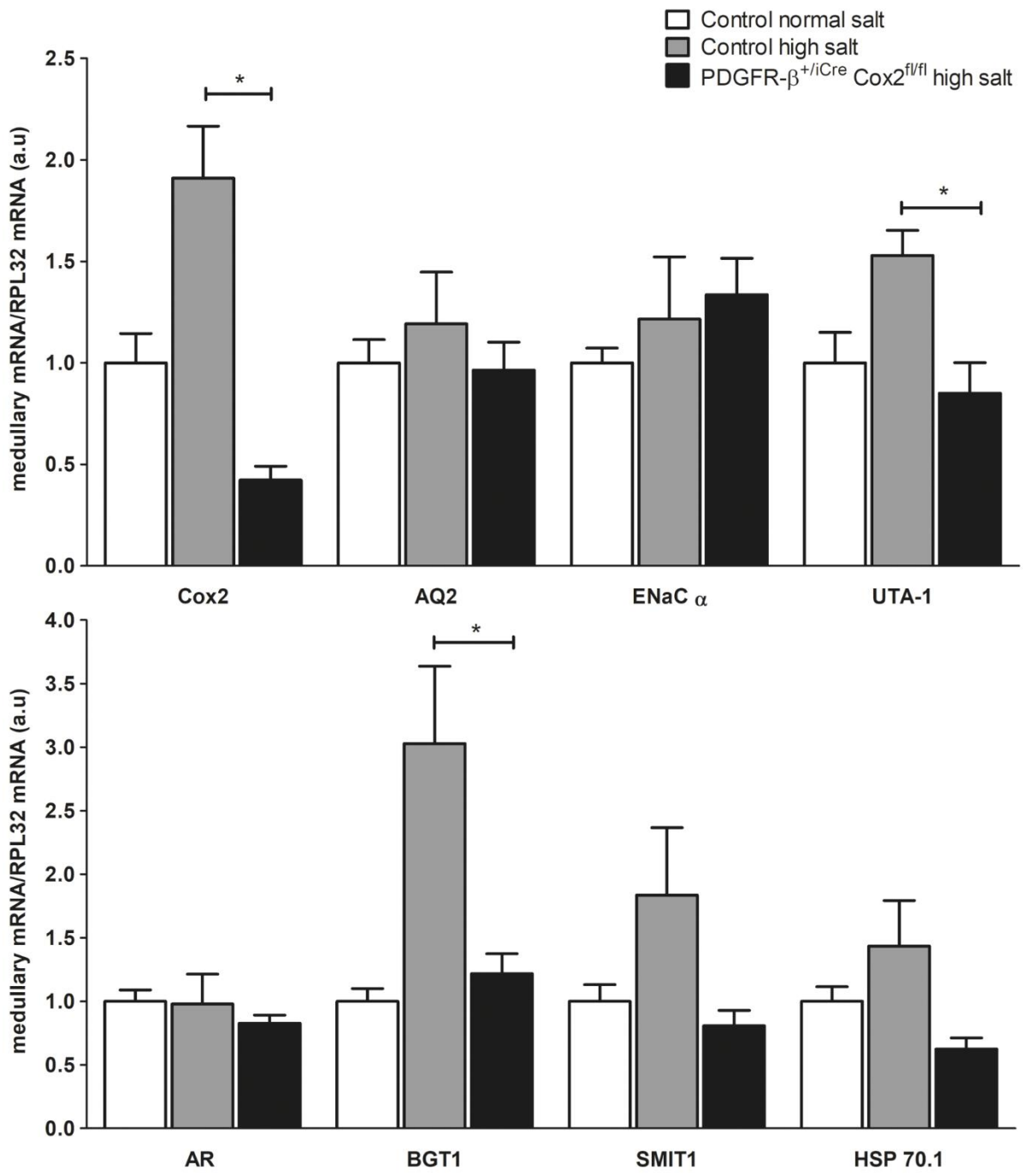

*Figure 35: Selected mRNA targets in the inner medulla of control and PDGFR-β$^{+/iCre}$ Cox2$^{fl/fl}$ mice after 14d high salt diet, mRNA abundance for control mice on a normal salt diet was set as reference expression; as shown above no recruitment of Cox-2 took place in PDGFR-β$^{+/iCre}$ Cox2$^{fl/fl}$ mice; mRNA abundance was significantly lower for UTA-1 and BGT1 in PDGFR-β$^{+/iCre}$ Cox2$^{fl/fl}$ mice under a high salt diet; other targets did not reach statistical significance (n = 5 for each group); * is p < 0,05*

3.4 Role of Cox-2 in kidney fibrosis

3.4.1 Progression of adenine induced fibrosis in mice deficient for Cox-2

The adenine-induced fibrosis model was chosen due to the inflammatory disease progression in this setting, as Cox-2 is a central player in inflammatory signaling. Furthermore interstitial cells have been shown to contribute greatly to the matrix expressing cells of this model[99,108]. Two stages of this fibrotic model were evaluated for the purpose of this study. The first being the acute fibrotic stimulus, after the mice had been fed a 0,2% adenine containing diet for three consecutive weeks (3wks). In the second approach, the mice were given three additional weeks for recovery from the adenine diet with a normal diet (3wks+3wks). At both time points, the remaining kidney function of the mice was evaluated by measuring their urinary concentrating ability, GFR and hematocrit under the treatment. mRNA abundance for key fibrotic targets was measured to check for differences in disease progression.

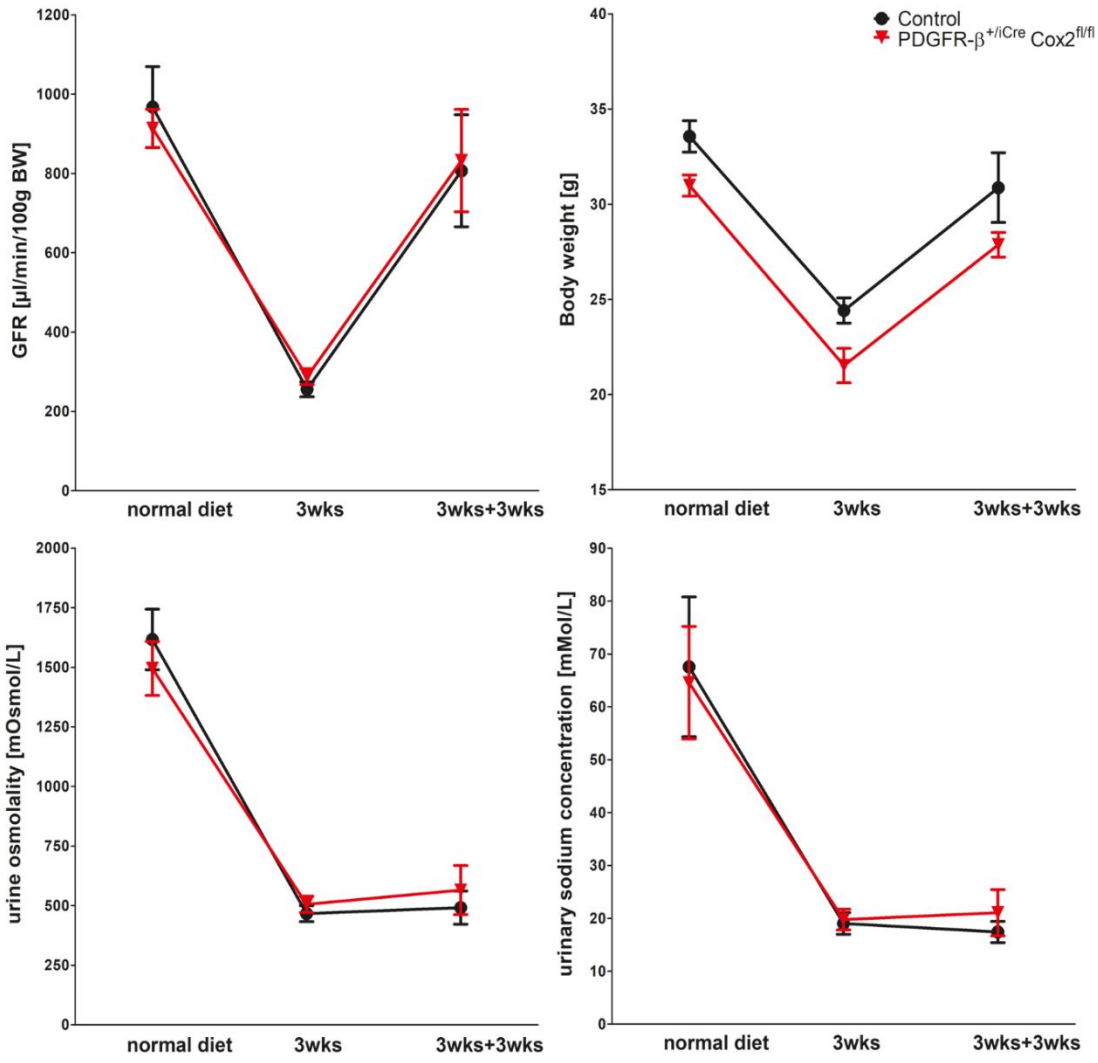

Figure 36: Changes in kidney function during fibrosis induction with an adenine containing diet; between control and PDGFR-β$^{+/iCre}$ Cox2$^{fl/fl}$ mice no difference in the kidney function either directly after 3wks adenine diet or after an additional 3wks recovery period could be detected; the weight loss (upper right) was proportional in both groups; n = 6 for each group

Analysis of the remaining kidney function of PDGFR-β$^{+/iCre}$ Cox2$^{fl/fl}$ mice and their littermate controls after 3wks adenine diet showed no difference in the GFR (287,5 vs. 255,5µl/min/100gBW in controls), urine concentrating ability (505,1 vs. 466,4 mOsmol/L in controls) and sodium excretion (19,7 vs. 19,0 mMol/L in controls) (Figure 36). Although PDGFR-β$^{+/iCre}$ Cox2$^{fl/fl}$ mice were lighter at the beginning of the experiment, their weight loss and gain in the recovery period ran parallel to the control animals. In the recovery period, after the mice were again fed a normal diet, no additional improvement in the kidney function of PDGFR-β$^{+/iCre}$ Cox2$^{fl/fl}$ mice could be observed. Hematocrit values were not significantly different between the experimental groups at any time point of this fibrotic model.

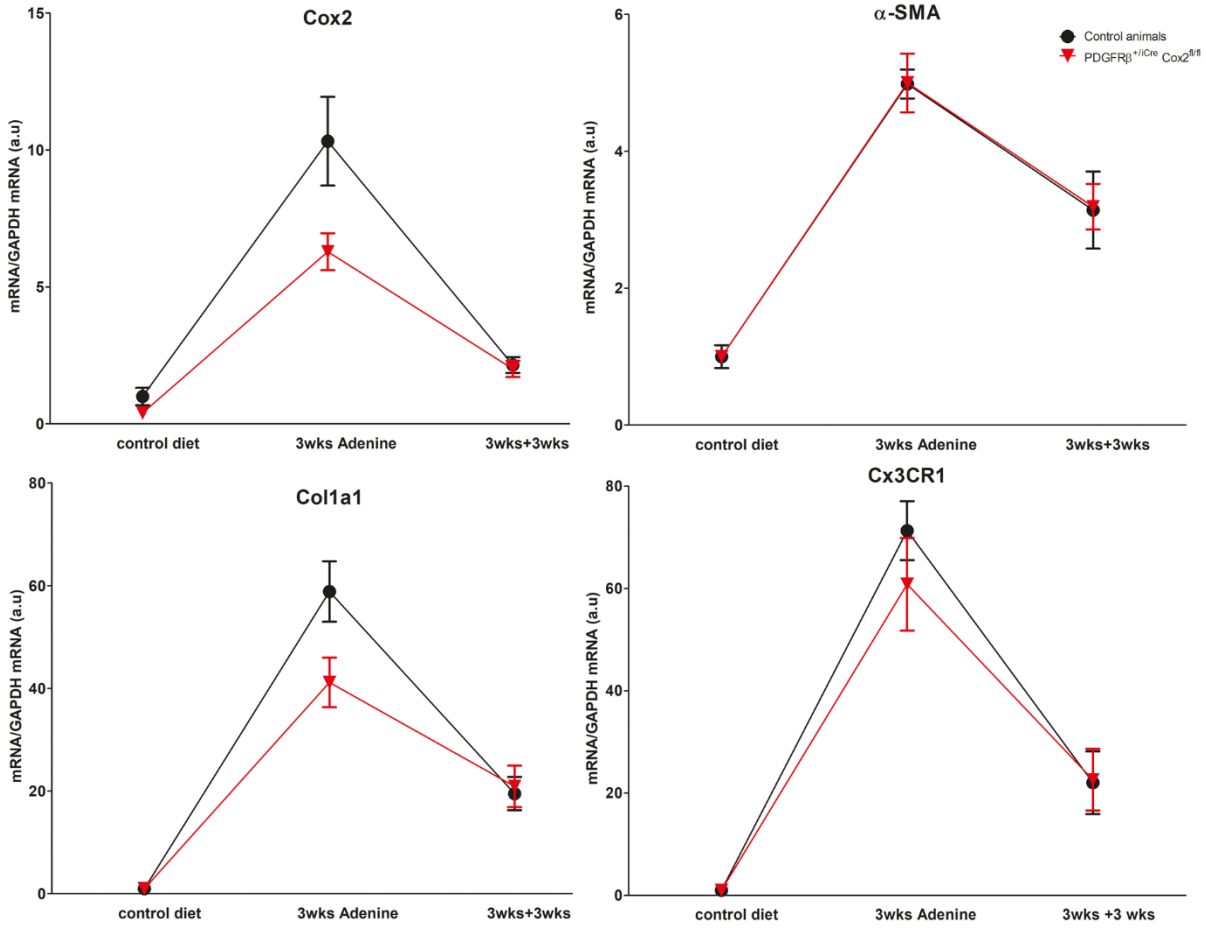

Figure 37: mRNA abundance measured before adenine diet, after 3 weeks of adenine feeding and with additional 3 weeks recovery period for each target; a significant reduction could only be measured for Cox-2 and Col1a1; in all other targets no significant difference in mRNA abundance was observed; (n = 8, for each group in each condition)

Measurement of key fibrotic targets in PDGFR-β$^{+/iCre}$ Cox2$^{fl/fl}$ mice treated with an adenine diet showed a significant change from the control group only for Cox-2 (6,28 vs. 10,32a.u in controls; $p < 0,05$) and Col1a1 mRNA (38,11 vs. 588,8a.u in controls, $p < 0,05$) (Figure 37) after 3wks. Other targets such as α-SMA, Cx3CR1, Col3a1 and fibronectin were unchanged. To localize the residual Cox-2 mRNA expression in

PDGFR-$\beta^{+/iCre}$ $Cox2^{fl/fl}$ mice, I performed co-*in-situ*-hybridization for Cox-2 and several markers. On kidneys of control mice after 3wks adenine diet Cox-2 was detected in the normal expression sites of inner medullary interstitial cells, macula densa cells but also in dense cell clusters around small vessels in fibrotic lesions in the cortex. In PDGFR-$\beta^{+/iCre}$ $Cox2^{fl/fl}$ mice the interstitial Cox-2 expression was absent. The Cox-2^{+} cells around the vessels did not co-express PDGFR-β or Cx3CR1 (Figure 38, top and middle).

Only a small minority of the Col1a1 expressing cells also expressed Cox-2 (Figure 38, bottom). For tissue of mice that were fed a normal diet after the adenine diet, the expression pattern was the same but signal strength was weaker in accordance with the qPCR data.

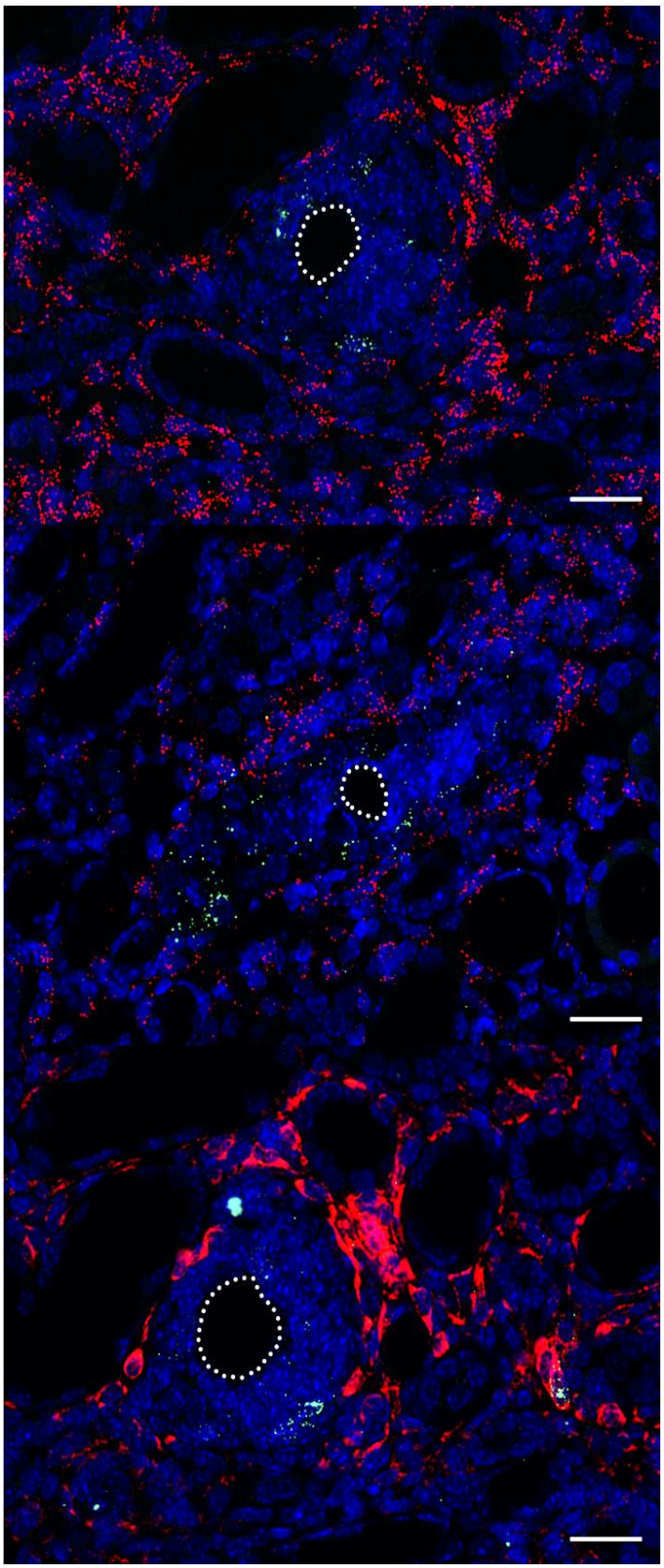

Figure 38: Co-in-situ hybridization for Cox-2 mRNA (green) and different markers (red) on kidney sections of PDGFR-β$^{+/iCre}$ Cox2$^{fl/fl}$ mice fed an adenine diet for 3 weeks; Cox-2 is expressed by probably infiltrating cells around vessels (dotted circles), these cells did not co-express PDGFR-β (red, top); the infiltrating Cox-2^{+} cells also did not express Cx3CR1 mRNA (red, middle); most of the Col1a1 mRNA expressing cells in fibrotic lesions also did not co-express Cox-2 (bottom); scale bar 20µm

3.4.2 Effects of Cox-2 deletion in PDGFR-β^{+} cells in the UUO model

The second model used for the evaluation of the relevance of Cox-2 in PDGFR-β^{+} interstitial cells during kidney fibrosis was the unilateral ureter obstruction (UUO) for 5 days.

Macroscopic evaluation of the kidneys showed no difference in the degree of damage between control mice and PDGFR-β$^{+/iCre}$ Cox2$^{fl/fl}$ mice.

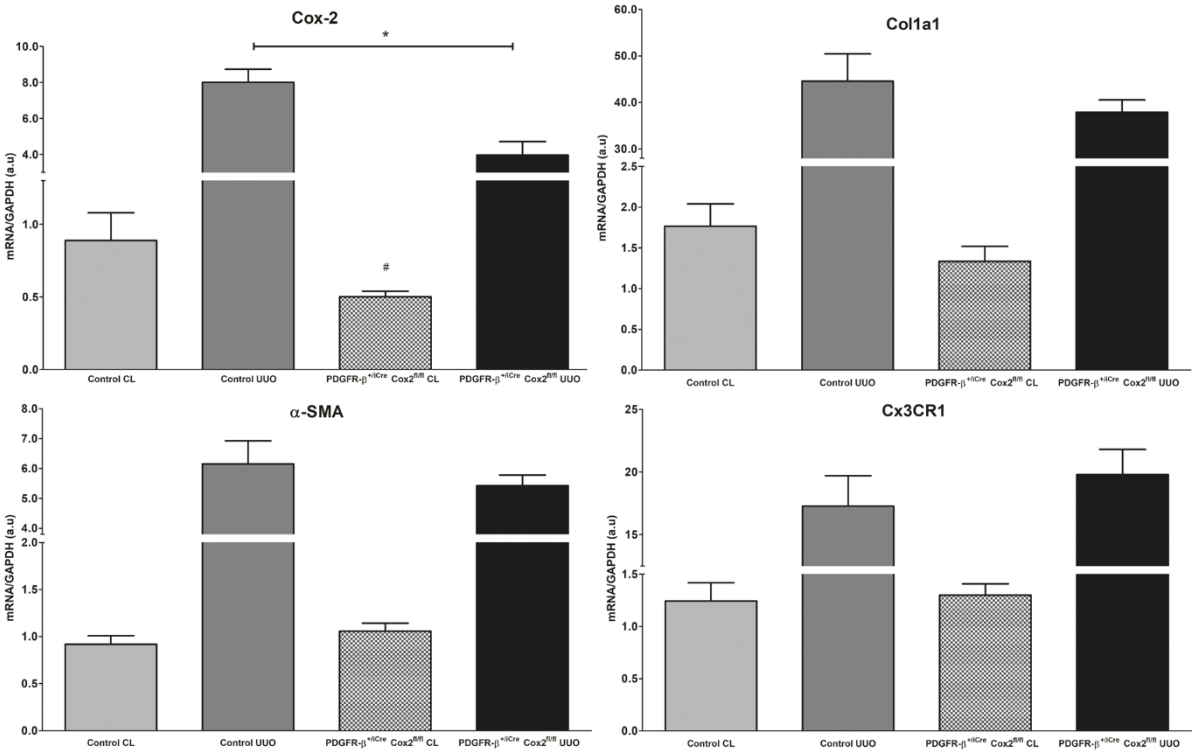

*Figure 39: mRNA abundance for selected fibrotic targets in contralateral (CL) and UUO kidneys; only Cox-2 showed a significant reduction in the CL and UUO kidneys of PDGFR-β$^{+/iCre}$ Cox2$^{fl/fl}$ mice (upper left); for all other measured mRNAs no reduction in the fibrotic pathogenesis could be measured; n = 5 for each group, * is p< 0,05 between UUO; # is p<0,05 between CL*

The undamaged contralateral kidneys of PDGFR-β$^{+/iCre}$ Cox2$^{fl/fl}$ mice showed mRNA levels not different to those of controls, except for Cox-2. Comparing the mRNA abundance of key fibrotic targets between the UUO kidneys of control and PDGFR-β$^{+/iCre}$ Cox2$^{fl/fl}$ mice, Cox-2 mRNA was significantly reduced. Difference in expression for the other measured targets such as α-SMA, Col1a1 and Cx3CR1 to evaluate the degree of fibrosis induced, did not reach significance (Figure 39). EPO mRNA was also not different for PDGFR-β$^{+/iCre}$ Cox2$^{fl/fl}$ mice compared to control mice.

4 Discussion

Of the two major isoforms of cyclooxygenase, Cox-1 has long been described as the constitutively expressed subtype, with a variety of important basal functions and Cox-2 as the inducible form, without particular relevance under basal conditions[4,23,58].

With the widespread use of Cox-inhibitors to treat pain, acute inflammation and chronic inflammatory diseases such as arthritis, a number of side effects became apparent, limiting the usage of these drugs[105,109,110]. Since Cox-1 was believed to be the main housekeeping subtype, great hope was placed in the success of Cox-2 selective inhibitors. But unfortunately these selective drugs, had severe side effects of their own on the renal and cardiovascular system[48,74,105,111,112].

It became clear that Cox-2 must have important functions for the salt and water balance of the body and blood pressure homeostasis[48,53,105]. After the connection between selective Cox-2 inhibition and the salt sensitivity of some hypertensive patients became known, the kidney was investigated more closely[48,53,77,113].

Two expression sites for Cox-2 often have been described in the kidney. One being the cells of the macula densa in the cTAL, where Cox-2 derived prostaglandins influence the renin production and secretion according to the luminal sodium concentration of the urine[4,7,23,34]. The second expression site for Cox-2 has mostly been referred to as “medullary Cox-2 expressing interstitial cells” up to this date[23,46]. No structured investigation into the exact location, regulation, nature and properties of these medullary Cox-2$^+$ cells has been undertaken to my knowledge.

Not much is known about the developmental origin of Cox-2 expressing cells despite the important role of Cox-2 during nephrogenesis[49,81,82]. Furthermore it is unclear whether these cells are a homogenous population or if different cell types, such as collecting duct cells[53,77,77] as well as interstitial cells[23,46,53] are able to express Cox-2 under different conditions. The inducibility of medullary Cox-2 expression has been repeatedly reported[23,74,80] but it remains unclear in which cells exactly this upregulation of Cox-2 takes place. This lack of knowledge until now is most likely due to the lack of a robust detection technique, to reliably locate Cox-2 in cells of the inner medulla. The missing localization of Cox-2 in the inner medulla also leads to the lack of an adequate mouse model for the isolated investigation into the medullary function of Cox-2.

In this study I used the novel RNAscope® technique to reliably localize Cox-2 in cells of the inner medulla of mice and characterize these cells concerning their

developmental path and co-expression of other cellular markers. The further aim of this study was to investigate the function of medullary Cox-2 expression under basal conditions, a high salt stimulus and in the event of kidney fibrosis with a selective deletion of Cox-2 only in the medullary interstitial cells.

4.1 Cox-2 expression and regulation in cells of the kidney

Over the years, many different cell types have been reported to express Cox-2 in the kidney. The expression of TNC in Cox-2$^+$ cells of the medulla has been reported[104,114] as well as the presence of Cox-2 in cells of the collecting duct[53,80,105]. But no convincing prove for or against either has been published to date.

The RNAscope® *in-situ* hybridization technique makes it possible to visualize not only one mRNA target, but also a second different mRNA on the same tissue. This allows the definite co-localization of Cox-2 mRNA with other cellular markers for a closer characterization of Cox-2$^+$ cells.

Cox-2 mRNA expressing cells in the kidney cortex of mice are localized in the characteristic position of macula densa cells close to the vascular pole of glomeruli (Figure 6). No other cells showed a positive signal for Cox-2 mRNA in the cortex.

Evaluation of the basal expression pattern in the inner and outer medulla of the murine kidney showed that only interstitial cells stained positive for Cox-2 mRNA (Figure 6). In accordance with previous findings[46], the Cox-2 expression was restricted to the inner medulla and the inner stripe of the outer medulla. To verify that the Cox-2 signal was localized in interstitial fibroblast-like cells, a co-hybridization with the interstitial marker PDGFR-β was performed. This dual detection of Cox-2 and PDGFR-β also allowed a quantification of the Cox-2/PDGFR-β expressing cells. Nearly all Cox-2 expressing cells in the medulla also express PDGFR-β (Figure 7), and can be classified as interstitial fibroblast-like cells, with their characteristic shape of a small cell body with long processes. The near complete overlap of PDGFR-β and TNC in these cells further supports this characterization (Figure 8). CD73, which is another prominent marker for interstitial cells did not co-localize with Cox-2 due to the different zonal expression. Only PDGFR-β$^+$ cells from the outer stripe of the outer medulla and the cortex co-express CD73, and there no Cox-2 mRNA was detected[17].

Contrary to other groups[53,80,105], I could not detect any Cox-2 mRNA in collecting duct cells, or other non-interstitial cells of the medulla. This contradiction to the multiply

reported presence of Cox-2 in CD cells might on the one hand be due to a differential expression between species, the system used for detection and the experimental setup. With isolated tubules or isolated and cultivated cells an artificial induction of Cox-2 due to the isolation and culture conditions cannot be excluded as Cox-2 is also a major component of the stress reactions in cells[83,115,116]. Co-expression of the two Cox isoforms could only be detected in the medullary interstitial cells (Figure 9). Macula densa cells did not show any Cox-1 expression while the collecting ducts showed a very robust signal for Cox-1 (Figure 40).

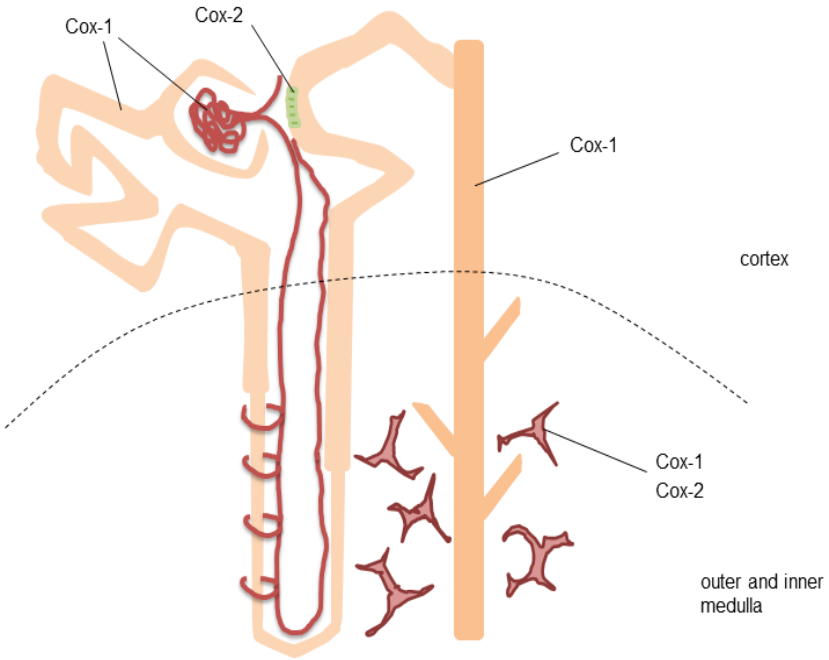

Figure 40: Overview of the expression sites for Cox-1 and Cox-2 along the nephron in the kidney; Cox-1 is expressed in the glomerulus, collecting ducts and the interstitial cells of the medulla; Cox-2 expression is strictly confined to the cells of the macula densa and the interstitial cells of the medulla in all conditions studied for this work

To address the question what cells in the inner and outer medulla are able to express Cox-2 in a stimulated setting, I performed *in-situ* hybridization on tissue of mice either fed a high salt (4%) diet or deprived of water (Figure 12). Both conditions have previously been reported to show a marked increase in the medullary PGE_2 expression (Figure 13)[4,24,30,37,48]. Even under stimulated conditions, high salt treatment showing the strongest recruitment of Cox-2^+ cells, Cox-2 mRNA was strictly confined to PDGFR-β and TNC positive interstitial cells (Figure 14). In the cortex, no Cox-2 mRNA could be detected outside the macula densa cells under these conditions. As under basal conditions, CD cells and other tubular compartments were free of Cox-2 expression.

Hypoxia-signaling is another postulated regulator of medullary Cox-2 expression[55,117]. I used mice with the genetic deletion of Vhl to stabilize the hypoxia inducible factors selectively in PDGFR-β^+ interstitial cells (PDGFR-$\beta^{+/iCre}$ $Vhl^{fl/fl}$ mice)[1,14]. Stabilization of HIF induces permanent activation of hypoxic signaling in these cells. In accordance with previous findings[53,55,56] the induction of hypoxia signaling led to an upregulated Cox-2 expression (Figure 15) compared to wildtype mice. Induction of Cox-2 expression by the hypoxic signaling pathway via HIF might be a protective mechanism designed to improve renal blood flow through the vasodilating actions of PGE_2 under physiological conditions. The additionally recruited Cox-2^+ cells were again exclusively interstitial PDGFR-β^+ cells located in the inner medulla and the inner stripe of the outer medulla, although HIF signaling was induced in all interstitial cells of PDGFR-$\beta^{+/iCre}$ $Vhl^{fl/fl}$ mice. Another effect of the HIF stabilization in PDGFR-β^+ interstitial cells is the strong induction of EPO expression in nearly all of these cells[1]. The recruited EPO producing cells are distributed over all kidney zones, and the question arose whether the medullary PDGFR-β^+ interstitial cells could produce EPO and Cox-2 at the same time. The interstitial cells of the cortex showed only a strong signal for EPO mRNA but no Cox-2 expression (Figure 13, D, Figure 16), in the inner stripe of the outer medulla a large number of Cox-2 expressing cells also expressed EPO.

In principal some Cox-2^+ cells of the inner and most in the outer medulla are able to produce EPO at the same time, while PDGFR-β^+ cells in the cortex can produce EPO, but are inhibited from expressing Cox-2 by a yet undefined mechanism.

From these findings I conclude that the cells of the medulla capable of expressing Cox-2 under basal conditions in the adult kidney, are interstitial PDGFR-β and TNC positive fibroblast-like cells. These cells are the only medullary cells to express Cox-2 even under stimulated conditions and thus represent a functional subpopulation of the large pool of PDGFR-β^+ interstitial cells distributed across the whole kidney (Figure 40).

Comparison of these results in mice with the often used rat kidney[46,74,77] showed a much higher and also different expression of Cox-2 under basal conditions (Figure 11). Rat tissue expressed Cox-2 in glomeruli along with a much stronger medullary expression. The collecting ducts of the rats showed no Cox-2 expression. This much stronger expression of Cox-2 in rat kidneys might be the reason for different results concerning the function of Cox-2 reported between different laboratory species.

4.2 Different functions of Cox-2 in the kidney

4.2.1 Cox-2 in the adult kidney

The models most used to study Cox-2 expression have been either rat kidneys or cultivated cells to date. The rat poses a significantly biased model, as the Cox-2 expression in this species is much higher than in mice and humans (Figure 11)[43]. Cultured cells lack *in vivo* cell-cell interactions that might be relevant for the physiological regulation of gene expression and function. The generation of a complete Cox-2 knockout mouse[81] moved the investigative focus into a species with greater similarities to humans, but it had serious problems. The Cox-2$^{-/-}$ mice showed a severe developmental phenotype in the kidney (Figure 23, A) and other systemic effects[61,81]. While this showed the importance of Cox-2 during nephrogenesis, other findings in adult Cox-2$^{-/-}$ mice are potentially influenced by these defects and cannot solely be attributed to the lack of Cox-2[52,87].

A new model for the cell specific deletion of the Cox-2 gene with the Cre/loxP system has been generated[88]. The investigators inserted loxP sites into the Cox-2 gene, resulting in a stop-codon in exon 6 of the Cox-2 gene after recombination. I used this model to investigate the function of Cox-2 in normally developed adult kidneys (CAG$^{+/iCre}$ Cox2$^{fl/fl}$ mice). This experimental approach had the advantage of excluding any potential developmental effects[81,87,118], since the deletion of the Cox-2 gene was induced after the mice reached adulthood. It also gave insight into the efficiency of the Cox-2 deletion with the Cre/loxP system. All experiments were conducted with mice of a C57BL/6 background. In previously published data this strain showed no hypertension under basal conditions and the least severe phenotype[61]. This background was chosen to exclude as many outside factors as possible, such as an androgen-influenced component with effect on the renin system[61,119].

The CAG$^{+/iCre}$ Cox2$^{fl/fl}$ mice showed no morphological or functional anomalies after the deletion was induced with a tamoxifen containing diet (Figure 19). *In-situ* hybridization, genotyping and mRNA analysis verified the deletion of Cox-2 for nearly all cells (Figure 17). Some investigators found a lower expression of renin[52,87] under basal conditions in Cox-2$^{-/-}$ mice, while others reported no change in the renal renin expression[119]. The basal renin expression in CAG$^{+/iCre}$ Cox2$^{fl/fl}$ mice was unchanged compared to their littermate controls (Figure 20). This is most likely due to the intact glomerular structure in the mice used for this study. Previous studies showed, that the malformation of subcapsular sclerotic glomeruli in Cox-2$^{-/-}$ mice and the varying severity of the renal

phenotype, depending on the background of the mice, are possible reasons for the contradicting published data[10,61,87]. This taken together with the functional data (Figure 19) led me to the conclusion that Cox-2 expression in the normally developed kidney is not essential for basic kidney function and blood pressure homeostasis under normal conditions in this experimental model. The normal blood pressure in CAG$^{+/iCre}$ Cox2$^{fl/fl}$ mice after deletion of Cox-2 in all kidney cells is congruent with findings in previous studies[46,61].

Under stress conditions that activate the RAAS, a low salt diet with application of the ACE-Inhibitor enalapril, the CAG$^{+/iCre}$ Cox2$^{fl/fl}$ mice showed a significantly reduced amount of renal renin mRNA. This strongly reduced recruitment of renin producing cells and the lower PRC in CAG$^{+/iCre}$ Cox2$^{fl/fl}$ mice on LSE treatment is in accordance with previous findings (Figure 20, Figure 21)[43,52,87,119]. The degree to which Cox-2 influences renin release has been discussed controversially in the past[10,43,61]. Low renal perfusion, the activation of the sympathetic nervous system and blood pressure changes have also been postulated to stimulate renin release[6,10]. On the other hand a direct feedback of ANG II via AT1 receptors on renin producing cells has recently been disproven[120]. Due to the normally developed kidneys in CAG$^{+/iCre}$ Cox2$^{fl/fl}$ mice I was able to show that the basal expression of renin is unaffected by a loss of Cox-2 function in all kidney cells, but the renin mRNA recruitment in response to RAAS challenge is greatly dependent on Cox-2 expression in this model. When applying the opposite salt treatment, of 4% sodium, to these mice blood pressure measurement yielded similar results as previously reported in rats[46,61]. There only a medullary infusion of a selective Cox-2 inhibitor led to hypertension, but the systemic application resulted in no change in blood pressure.

4.2.2 Role of Cox-2 in the stromal progenitor compartment

As stated in the introduction, the global deletion of Cox-2 during nephrogenesis leads to a severe renal phenotype. The renal phenotype in Cox-2$^{-/-}$ mice presents with subcapsular, sclerotic glomeruli, interstitial fibrosis at an early age, shortening of the arterial tree and lower renin expression as described above[61,81,87]. In addition it also causes an increased neonatal mortality, shortened lifespan and female sterility[61,81]. To date all investigations into the role of Cox-2 during nephrogenesis were conducted with a systemic approach through global deletion of the Cox-2 gene or application of Cox-2 inhibitors at different time points.

The majority of cells affected by the renal phenotype in Cox-2$^{-/-}$ mice, are interstitial cells, mesangial and vascular cells, all deriving from the FoxD1^{+} compartment of stromal progenitors during nephrogenesis (Figure 3). For a more specific investigation of the involvement of Cox-2 in this compartment during the embryonic phase and immediate postnatal phase, I generated FoxD1$^{+/Cre}$ Cox2$^{fl/fl}$ mice to study their kidney development and function.

In these mice the normal interstitial expression of Cox-2 in the renal medulla is absent, but expression of Cox-2 in cells of the macula densa is unaffected when evaluated by zonal mRNA analysis and *in-situ* hybridization (Figure 22). This selective deletion proves a different developmental path for the two Cox-2 expressing compartments in the kidney. FoxD1$^{+/Cre}$ Cox2$^{fl/fl}$ mice were born in mendelian ratios and both genders were fertile unlike the Cox-2$^{-/-}$ mice[81]. No increased rate of neonatal mortality was observed and basal kidney function and weight of adult FoxD1$^{+/Cre}$ Cox2$^{fl/fl}$ mice was normal (Figure 24). Histological analysis of mature FoxD1$^{+/Cre}$ Cox2$^{fl/fl}$ kidneys showed that the anomalies seen in Cox-2$^{-/-}$ mice were entirely absent. The FoxD1$^{+/Cre}$ Cox2$^{fl/fl}$ mice showed a normal number of glomeruli, none in a subcapsular position (Figure 23) and normal renin expression (Figure 25). Furthermore, the interstitial fibrosis reported for Cox-2$^{-/-}$ mice[61,81] was absent in FoxD1$^{+/Cre}$ Cox2$^{fl/fl}$ mice, pointing to a normal function of renal interstitial fibroblast-like cells even in the absence of Cox-2 (Figure 26) during development.

With this cell specific approach, I could exclude Cox-2 expression in the FoxD1^{+} stromal progenitor compartment as an essential factor for normal kidney development and the post-natal developmental phase in mice. This is in good agreement with recent findings by another group[49,82]. The authors postulate the Cox-2 dependent renin-angiotensin system activation in the immediate postnatal phase as crucial for normal kidney development. This signaling pathway is conserved in FoxD1$^{+/Cre}$ Cox2$^{fl/fl}$ mice as the macula densa expression of Cox-2 is unaffected by this model. Interestingly, the salt reabsorption in the immediate postnatal period that has been described as a factor for the normal glomerular development[82] seems to be independent of Cox-2 signaling in the inner medulla during this developmental stage. Furthermore, while the salt supplementation experiment by Slattery et. al[82] was able to alleviate in part the glomerular malformations caused by the deletion in Cox-2$^{-/-}$ mice, a stunted cortical growth, resulting in thin cortical tissue in adult mice remained. Therefore, the authors speculate that there might be a second pathway for Cox-2, independent of the

activation of the RAAS and AT1 receptors, to influence postnatal kidney development. The normally developed cortex of FoxD1$^{+/Cre}$ Cox2$^{fl/fl}$ mice (Figure 23) points toward either the tubular segments as focal points for the postnatal kidney development or extra-renal factors. The theory of a possible tubular involvement is further supported by combining the findings of Slattery et. al[82], namely the partial phenotype rescue of Cox-2$^{-/-}$ mice with a AT1 receptor agonist, with recent findings in our laboratory. We could show that AT1 receptors in the FoxD1^{+} compartment are not essential for normal kidney development[121]. These findings taken together show that further investigation into the exact localization of RAAS activity during the postnatal kidney development is necessary.

In line with the normally developed kidneys of FoxD1$^{+/Cre}$ Cox2$^{fl/fl}$ mice, no anomalies in their basic functions such as GFR, urinary concentration and blood pressure regulation could be detected. The normal sodium excretion of these animals allows the hypothesis that the missing medullary Cox-2 expression can be compensated under normal conditions. Recruitment of renin producing cells during LSE treatment was also not changed in FoxD1$^{+/Cre}$ Cox2$^{fl/fl}$ mice. These data identifies the macula densa expression of Cox-2 as the expression site responsible for the results obtained with CAG$^{+/iCre}$ Cox2$^{fl/fl}$ mice under LSE and is in good accordance with pervious studies[4,6,10]

4.2.3 Function of medullary Cox-2 expression with different dietary sodium intake

The salt sensitivity of many hypertensive patients is a growing and badly understood problem, especially with the salt loaded diet in industrialized countries. Dietary salt intake has been shown to exacerbate an already existing hypertension and induce formerly normotensive individuals to develop a *de novo* hypertension with the manifold cardiovascular risks involved[73,113].

To investigate the function of medullary Cox-2 expression in the setting of a salt challenge I chose a mouse model to mimic the human circumstances as closely as possible.

PDGFR-β$^{+/iCre}$ Cox2$^{fl/fl}$ mice develop normally with fully functioning Cox-2 expression in all cells, until Cre-recombinase activity is induced with a tamoxifen containing diet. PDGFR-β$^{+/iCre}$ Cox2$^{fl/fl}$ mice express Cox-2 normally except in the interstitial fibroblast-like cells of the inner medulla after recombination. The cells of the macula densa are

unaffected by this model (Figure 6). This is a model allowing the investigation of only medullary Cox-2 function and excluding developmental defects.

On the mRNA level, a strong reduction in medullary Cox-2 could be observed indicating a successfully induced deletion of Cox-2 (Figure 28). Congruent with the results from FoxD1$^{+/Cre}$ Cox2$^{fl/fl}$ mice, the PDGFR-β$^{+/iCre}$ Cox2$^{fl/fl}$ mice showed no morphological or functional anomalies under basal conditions with a balanced salt diet including sodium excretion and blood pressure homeostasis (Figure 29).

While most Cox-2 associated mRNA targets showed a trend toward downregulation, only BGT1 and UTA-1 reached significance (Figure 30). This is similar to results in Cox-2$^{-/-}$ mice, these also showed that BGT1 is strongly controlled by Cox-2 activity, while other small osmolyte transporters, aldose reductase (AR) and sodium dependent myo-inositol cotransporter (SMIT1) seem to have secondary regulators besides Cox-2[24]. These results fit with the observations in humans, that kidney damage through selective Cox-2 inhibitors often requires additional risk factors[67].

It was the aim of this part of my study to investigate what effects the medullary Cox-2 deletion had on kidney function when the animals were challenged by a high dietary sodium intake.

PDGFR-β$^{+/iCre}$ Cox2$^{fl/fl}$ mice treated with a high salt diet showed a rapid and sustained rise in blood pressure (Figure 34). Sodium excretion and GFR increase in these mice was impeded and compensated with a rise in urine volume when compared to the control animals (Figure 33). This lower urinary sodium concentration connects well with a study by Chen et. al[30] that showed PGE_2, when infused medullary, promotes sodium excretion. It is conceivable that through deletion of Cox-2 in the medulla of PDGFR-β$^{+/iCre}$ Cox2$^{fl/fl}$ mice, a lower PGE_2 availability leads to the lower sodium concentration in the urine on a high salt diet. *In-situ* hybridization showed that only few additional Cox-2 expressing cells could be recruited in PDGFR-β$^{+/iCre}$ Cox2$^{fl/fl}$ mice during the high salt diet. Taken together with the lack of increased Cox-2 mRNA abundance, I conclude that PDGFR-β^{+} interstitial cells of the inner medulla are the only cell population in the kidney capable of expressing Cox-2, besides the cells of the macula densa. No other cells can be recruited to compensate the missing Cox-2 expression. Analysis of the zonal mRNA abundance in these mice showed that no compensatory rise in Cox-1 expression took place (data not shown), indicating a specific non-interchangeable function for medullary Cox-2 expression. The strong reduction in

medullary BGT1 mRNA abundance is in good accordance with previous works (Figure 35)[24]. AR and SMIT1 on the other hand seem to have secondary regulatory mechanisms and are not significantly affected by the lack of medullary Cox-2 expression[51,77], this is in good accordance with the data of this work.

The persistent rise in blood pressure of PDGFR-$\beta^{+/iCre}$ $Cox2^{fl/fl}$ mice led me to question the possible mechanism for this change. Very recently, other investigators have also described elevated blood pressure in mice lacking Cox-2 in medullary cells on a high salt diet[104]. In this study, the authors hypothesized that a rise in medullary AQ2 and ENACα mRNA abundance leads to a volume challenge and subsequent rise in blood pressure for these mice.

My data could not confirm these findings, as the mRNA abundance for AQ2 and ENACα showed no significant changes when compared to the control mice (Figure 35). The mice in the study by Zhang et. al[104] showed a much slower increase in blood pressure, reaching significance only after 4 weeks, than it was observed in the mice of this study (Figure 34). The above mentioned study and others have also postulated an important role for Cox-2 expression in the survival of medullary cells under stress[24,51,104]. In PDGFR-$\beta^{+/iCre}$ $Cox2^{fl/fl}$ mice no pathological changes or necrotic lesions could be detected even after maintaining the high salt diet for a prolonged time (data not shown). A possible explanation for these different results is the much higher concentration of sodium (8%) fed in the study by Zhang et. al[104] compared to the 4% sodium in the high salt diet used for this study. To sum up the lower salt concentration and the not significantly changed mRNA expressions for AQ2, ENACα and two of the three investigated osmolyte transporters might explain the intact kidney tissue in PDGFR-$\beta^{+/iCre}$ $Cox2^{fl/fl}$ mice.

Taking together the intact kidney structure, lack of sodium and water retention, the unchanged levels for AQ2 and other targets in the PDGFR-$\beta^{+/iCre}$ $Cox2^{fl/fl}$ mice, the lack of medullary prostaglandins balancing the action of ANGII might be the reason for the blood pressure rise in this model. The vasoconstrictive effects of ANGII have previously been reported to play an important role in Cox-2 inhibitor mediated hypertension and reduced renal blood flow[4,45,74,84,122]. The hypothesis of renal ANGII vasoconstriction is supported by considering further points. On the one hand when comparing this study with data of a study by Yu et. al[64], their results could not be confirmed. Yu et. al postulated that the salt sensitivity under Cox-2 selective inhibitors was attributed to a lack of Cox-2 derived prostaglandins in the aorta. *In-situ*

hybridization for Cox-2 and PDGFR-β was performed on aortae of wildtype mice with a normal and high salt diet to exclude this possibility. In both cases the presence of PDGFR-β mRNA could be confirmed, but no signal for Cox-2 mRNA was observed (data not shown). Another point arguing against a systemic effect of Cox-2 as the reason for the hypertension is the short stability of PGE_2[35]. It seems unlikely that the medullary Cox-2 products would exert their main function outside the kidney in such a short time. In the review of Cowley, Jr.[84] an increased responsiveness to ANGII of rats pretreated with Cox-2 inhibitors was discussed, along with the possible influence of medullary pericytes on renal blood flow. The renal pericytes are targeted by the deletion of Cox-2 in this study and might thus be in part responsible for the observed hypertension.

Taking these points together, I can conclude that Cox-2 expression in PDGFR-β^+ interstitial fibroblast-like cells is essential for renal blood pressure homeostasis under a high sodium challenge. This study was focused on identifying, localizing and characterizing the cells in the inner medulla expressing Cox-2 and the functional consequences of a targeted deletion. But the elucidation of the one or possibly different mechanisms following Cox-2 deletion and contributing to the salt sensitive hypertension needs further investigation.

4.5 Cox-2 in two models of kidney fibrosis

Many different models to mimic the human pathology of kidney fibrosis have been established over the years[98,99,108]. In this work two mechanistically different models have been chosen to evaluate the involvement of Cox-2 in resident PDGFR-β^+ interstitial fibroblast-like cells of the kidney in the pathological disease progression.

4.5.1 Influence of Cox-2 deletion in PDGFR-β^+ cells on adenine-induced nephropathy

The model of adenine induced nephropathy is characterized by considerable interstitial inflammation and fibrosis, tubular atrophy and cardiovascular effects that closely mirror the symptoms seen in human patients with CKD[99,100,108]. Cox-2 has been described as a major player in the inflammatory pathway[68,72,123]. The adenine-induced fibrosis was chosen due to the contribution of interstitial inflammation and fibrosis in the phenotype of this model. It was the aim of this experimental setup to determine whether the lack of Cox-2 in PDGFR-β^+ interstitial cells in this model had any effect on the progression

of kidney damage inflicted by adenine feeding or if it changed the recovery of mice after they returned to a normal diet.

Evaluation of GFR and kidney function showed neither adverse nor protective effects for a lack of Cox-2 in PDGFR-β^+ interstitial fibroblast-like cells. PDGFR-$\beta^{+/iCre}$ $Cox2^{fl/fl}$ mice showed the same decrease and recovery of the analyzed kidney parameters as their littermate controls over the entire experiment (Figure 36). Concerning the anemia caused by the loss of EPO production in the kidneys observed in this model and human CKD patients, the deletion of Cox-2 had no effect on hematocrit values after 3 weeks (3wks) of the adenine diet or after additional 3 weeks recovery.

On the mRNA level the increase of Cox-2 mRNA was significantly lower in PDGFR-$\beta^{+/iCre}$ $Cox2^{fl/fl}$ mice after 3 weeks adenine than in control mice. These data signify that the PDGFR-β^+ interstitial fibroblast-like cells contribute to the proinflammatory reaction after 3wks adenine, but are not the only cell type expressing Cox-2 under these conditions. *In-situ* hybridization located the residual Cox-2 expression in non PDGFR-β^+ cells grouped around small vessels in fibrotic lesions of the kidney cortex after 3wks adenine (Figure 38, top). As these do not express PDGFR-β and are localized so strikingly in dense clusters around vessels, they are most likely not resident fibroblast-like cells of the kidney, but infiltrating cells. To gain more information about these infiltrating cells co-localization of Cox-2 with Cx3CR1 was performed. Cx3CR1 is a chemokine receptor associated with leukocyte migration and adhesion[124,125]. However there was no overlap between Cx3CR1 and Cox-2 mRNA, but Cx3CR1 positive cells were clustered around the Cox-2 expressing cells (Figure 28, middle). The mRNA abundance of Col1a1 was also reduced in PDGFR-$\beta^{+/iCre}$ $Cox2^{fl/fl}$ mice after 3wks adenine and Col1a1 expressing cells were clustered in a pattern similar to Cx3CR1 around the infiltrating Cox-2 expressing cells (Figure 38, bottom). Recent studies showed that a large percentage of the Col1a1 production in adenine-induced fibrosis stems from hematopoietic cells, these cells are mostly responsible for the residual Col1a1 expression[100]. This and the unchanged abundance of other markers explains the lack of functional improvement in the PDGFR-$\beta^{+/iCre}$ $Cox2^{fl/fl}$ mice. The mRNA results of PDGFR-$\beta^{+/iCre}$ $Cox2^{fl/fl}$ mice might also show that there are different pathways inducing the expression of the classical fibrosis markers Col1a1 and α-SMA in the acute phase, as the abundance of α-SMA was unchanged. This detailed mechanism of differential induction between different fibrosis markers needs further investigation.

Cox-2 expression in resident PDGFR-β^{+} interstitial fibroblast-like cells might play a small role in the inflammatory response of the kidney in the model of adenine-induced nephropathy, but it is not a focal point for the disease progression. Local Cox-2 expression seems to be only one component inducing the expression of fibrotic markers. The localization of infiltrating Cox-2^{+} cells with pro-fibrotic cells grouped around them gives rise to the idea that these cells play a role in cell migration and transformation during fibrosis and are not resident kidney cells.

4.5.2 Role of Cox-2 in PDGFR-β^{+} interstitial cells during 5d UUO

The second model I chose for the investigation of Cox-2 in resident PDGFR-β^{+} interstitial cells during fibrosis was the unilateral ureter obstruction (UUO). In this model, one ureter is surgically ligated and the resulting pressure and urine backflow induces fibrotic changes in the kidney tissue. Compared to the model of adenine-induced nephropathy the progression is much more rapid, with greater structural damage to the ligated kidney. But with the UUO model, only one kidney is affected, while the other remains functional[126]. In this study a medium duration of 5 days for UUO was chosen. Previous studies have reported a beneficial role for Cox-2 in the UUO model and a more severe progression if Cox-2 is inhibited[90,127]. Others have reported a more controversial role for Cox-2 depending on the mode of inhibition[91,92].

In PDGFR-β$^{+/iCre}$ Cox2$^{fl/fl}$ mice no effect on the progression of the UUO induced damage could be observed. Histological analysis showed no difference in the damage by 5d UUO between Cox-2 deficient mice and their controls. In line with this, the mRNA abundance for key fibrotic markers Col1a1, α-SMA and Cx3CR1 were unchanged in the UUO kidneys when compared to the UUO kidneys of control animals. The mRNA abundance for Cox-2 was again significantly lower in PDGFR-β$^{+/iCre}$ Cox2$^{fl/fl}$ mice. Comparable mRNA levels for Col1a1 in both groups might be an indication that different pathways for the Col1a1 induction are active in different fibrotic models.

The unchanged progression of the fibrotic changes in the UUO kidneys of PDGFR-β$^{+/iCre}$ Cox2$^{fl/fl}$ mice contradicts with the above mentioned studies[90,127], postulating a protective role for Cox-2 during UUO. These different results are most likely due to major differences in the experimental approach. In the mentioned studies, the investigators used either the Cox-2$^{-/-}$ mice with their inherent histological and functional deficiencies or a pharmacological inhibition of Cox-2 affecting a systemic block of all

Cox-2 activity. I used a cell specific approach for the first time to my knowledge with the targeted deletion of Cox-2. I could show that the protective effect of Cox-2 seen in other studies must be exerted by a source outside the normal interstitial Cox-2 expressing cells in the kidney. A most likely hypothesis would be the overall reduction in proinflammatory stimuli achieved by global Cox-2 deletion or pharmacological inhibition.

5 Summary

Cyclooxygenase 2 is a key enzyme in the production of prostaglandins. The widespread application of Cox-2 selective inhibitors to treat pain and inflammation has shown severe renal side effects for these drugs. But the exact expression sites for Cox-2 and its normal function in the kidney is not yet clear.

Utilizing a novel *in-situ* hybridization technique Cox-2 could be distinctly located in two developmentally different cell populations of the murine kidney. In the cortex only specialized macula densa cells of the cTAL express Cox-2. In the renal medulla, interstitial fibroblast-like cells, characterized by the expression of PDGFR-β and TNC, produce Cox-2 mRNA.

Stimulating Cox-2 expression in the kidneys of mice, through a high dietary sodium intake, Cox-2 expression was induced only in the inner medulla and the inner stripe of the outer medulla. This recruitment of Cox-2 expressing cells only took place in interstitial PDGFR-β^{+}/TNC^{+} cells. In mice deprived of water for 24h the recruitment pattern and cell type was the same, but the total number of Cox-2 expressing cells was on average lower than in high salt treated mice. The model of genetic stabilization of the HIF pathway in PDGFR-$\beta^{+/iCre}$ Vhl$^{fl/fl}$ mice not only showed that Cox-2 is a hypoxia inducible gene, but that an overlap between Cox-2 and EPO expression in the same cell is possible. The locally very restricted inducible expression of medullary interstitial Cox-2 led me to classify these cells as a functional subpopulation of the large pool of PDGFR-β^{+} interstitial cells. No Cox-2 expression could be detected in non-interstitial cells or in interstitial cells of the cortex in the conditions investigated in the scope of this work.

The medullary Cox-2^{+} cells, as well as most cells involved in the severe phenotype of global Cox-2 deficient mice, namely mesangial cells and vascular smooth muscle cells derive from the FoxD1^{+} stromal progenitor compartment. The role of Cox-2 during nephrogenesis was evaluated with a selective deletion in this compartment with FoxD1$^{+/Cre}$ Cox2$^{fl/fl}$ mice. The mice with a targeted Cox-2 deletion in the stromal compartment, but intact Cox-2 function in the cells of the macula densa, showed no developmental or functional defects. In FoxD1$^{+/Cre}$ Cox2$^{fl/fl}$ mice the recruitment of renin on a low salt stimulus was normal unlike in the mice with a total deletion of Cox-2.

In adult mice, the strong medullary induction of Cox-2 with a high dietary sodium intake implicates a functional connection between Cox-2 and the salt handling capability of

the kidney. The lack of an adequate model made the distinction between the functions of the different Cox-2 expression sites difficult. With the use of PDGFR-$\beta^{+/iCre}$ $Cox2^{fl/fl}$ mice, it was possible to study the functional consequences of the isolated deletion of Cox-2 only in medullary interstitial cells under different conditions. This model showed that missing Cox-2 expression in the renal medulla led to reduced concentrating ability for sodium with a compensatory rise in urine volume and persistent hypertension under a high salt diet.

Experiments performed, concerning the role of Cox-2 in PDGFR-β^{+} cells during fibrosis, showed a dependence on the fibrotic model used. In the adenine-induced nephropathy Cox-2 seems to play some role in the induction of Col1a1 mRNA expression. But a deletion of Cox-2 in PDGFR-β^{+} cells had no effect on the expression of fibrotic markers in the UUO model.

The characterization of markers for Cox-2 expressing cells in the kidney is the basis for a targeted deletion in sub-compartments and their functional investigation. While Cox-2 expression in medullary interstitial cells is not essential for normal kidney development, it is necessary for blood pressure homeostasis during a high salt challenge.

6 Bibliography

1. Gerl, K. *et al.* Erythropoietin production by PDGFR-β+ cells. *Pflüg. Arch. - Eur. J. Physiol.* **468**, 1479–1487 (2016).
2. Pavlovic, D., Katicic, D., Gulin, T. & Josipovic, J. Vitamin D in the Patients with Chronic Kidney Disease: When, to Whom and in Which Form. *Mater. Socio-Medica* **27**, 122–124 (2015).
3. McMahon, A. P. Development of the Mammalian Kidney. *Curr. Top. Dev. Biol.* **117**, 31–64 (2016).
4. Harris, R. C. & Breyer, M. D. Physiological regulation of cyclooxygenase-2 in the kidney. *Am. J. Physiol.-Ren. Physiol.* **281**, F1–F11 (2001).
5. Schweda, F., Klar, J., Narumiya, S., Nüsing, R. M. & Kurtz, A. Stimulation of renin release by prostaglandin E2 is mediated by EP2 and EP4 receptors in mouse kidneys. *Am. J. Physiol.-Ren. Physiol.* **287**, F427–F433 (2004).
6. Peti-Peterdi, J. & Harris, R. C. Macula Densa Sensing and Signaling Mechanisms of Renin Release. *J. Am. Soc. Nephrol.* **21**, 1093–1096 (2010).
7. Castrop, H. *et al.* Physiology of Kidney Renin. *Physiol. Rev.* **90**, 607–673 (2010).
8. Brewster, U. C. & Perazella, M. A. The renin-angiotensin-aldosterone system and the kidney: effects on kidney disease. *Am. J. Med.* **116**, 263–272 (2004).
9. Streatfeild-James, R. M. *et al.* Angiotensinogen cleavage by renin: importance of a structurally constrained N-terminus. *FEBS Lett.* **436**, 267–270 (1998).
10. Schweda, F. Salt feedback on the renin-angiotensin-aldosterone system. *Pflüg. Arch. - Eur. J. Physiol.* **467**, 565–576 (2015).
11. Humphreys, B. D. *et al.* Fate tracing reveals the pericyte and not epithelial origin of myofibroblasts in kidney fibrosis. *Am. J. Pathol.* **176**, 85–97 (2010).

12. Armulik, A., Genové, G. & Betsholtz, C. Pericytes: Developmental, Physiological, and Pathological Perspectives, Problems, and Promises. *Dev. Cell* **21**, 193–215 (2011).
13. Kida, Y. & Duffield, J. S. Pivotal role of pericytes in kidney fibrosis. *Clin. Exp. Pharmacol. Physiol.* **38**, 467–473 (2011).
14. Gerl, K. *et al.* Inducible glomerular erythropoietin production in the adult kidney. *Kidney Int.* **88**, 1345–1355 (2015).
15. Duffield, J. S. Cellular and molecular mechanisms in kidney fibrosis. *J. Clin. Invest.* **124**, 2299–2306 (2014).
16. Li, W., Hartwig, S. & Rosenblum, N. D. Developmental origins and functions of stromal cells in the normal and diseased mammalian kidney. *Dev. Dyn. Off. Publ. Am. Assoc. Anat.* **243**, 853–863 (2014).
17. Gerl, K. A.-E. Erythropoietin-Expression in Stromazellen der Niere. (2018).
18. DeWitt, D. L. & Smith, W. L. Primary structure of prostaglandin G/H synthase from sheep vesicular gland determined from the complementary DNA sequence. *Proc. Natl. Acad. Sci. U. S. A.* **85**, 1412–1416 (1988).
19. Park, J. Y., Pillinger, M. H. & Abramson, S. B. Prostaglandin E2 synthesis and secretion: The role of PGE2 synthases. *Clin. Immunol.* **119**, 229–240 (2006).
20. Kujubu, D. A., Fletcher, B. S., Varnum, B. C., Lim, R. W. & Herschman, H. R. TIS10, a phorbol ester tumor promoter-inducible mRNA from Swiss 3T3 cells, encodes a novel prostaglandin synthase/cyclooxygenase homologue. *J. Biol. Chem.* **266**, 12866–12872 (1991).
21. Xie, W. L., Chipman, J. G., Robertson, D. L., Erikson, R. L. & Simmons, D. L. Expression of a mitogen-responsive gene encoding prostaglandin synthase is regulated by mRNA splicing. *Proc. Natl. Acad. Sci. U. S. A.* **88**, 2692–2696 (1991).

22. Chandrasekharan, N. V. *et al.* COX-3, a cyclooxygenase-1 variant inhibited by acetaminophen and other analgesic/antipyretic drugs: Cloning, structure, and expression. *Proc. Natl. Acad. Sci. U. S. A.* **99**, 13926–13931 (2002).
23. Harris, R. C. Cyclooxygenase-2 in the Kidney. *J. Am. Soc. Nephrol.* **11**, 2387–2394 (2000).
24. Moeckel, G. W. *et al.* COX2 Activity Promotes Organic Osmolyte Accumulation and Adaptation of Renal Medullary Interstitial Cells to Hypertonic Stress. *J. Biol. Chem.* **278**, 19352–19357 (2003).
25. Kirtikara, K. *et al.* Compensatory Prostaglandin E2 Biosynthesis in Cyclooxygenase 1 or 2 Null Cells. *J. Exp. Med.* **187**, 517–523 (1998).
26. Gene: PTGS1 (ENSG00000095303) - Summary - Homo sapiens - Ensembl genome browser 95. Available at: https://www.ensembl.org/Homo_sapiens/Gene/Summary?g=ENSG00000095303;r=9:122370530-122395703. (Accessed: 2nd April 2019)
27. Gene: PTGS2 (ENSG00000073756) - Summary - Homo sapiens - Ensembl genome browser 95. Available at: https://www.ensembl.org/Homo_sapiens/Gene/Summary?db=core;g=ENSG00000073756;r=1:186671791-186680427. (Accessed: 2nd April 2019)
28. Morita, I. Distinct functions of COX-1 and COX-2. *Prostaglandins Other Lipid Mediat.* **68–69**, 165–175 (2002).
29. Hao, C.-M. & Breyer, M. D. Physiological Regulation of Prostaglandins in the Kidney. *Annu. Rev. Physiol.* **70**, 357–377 (2008).
30. Chen, J. *et al.* Increased dietary NaCl induces renal medullary PGE2 production and natriuresis via the EP2 receptor. *Am. J. Physiol. - Ren. Physiol.* **295**, F818–F825 (2008).

31. Jia, Z. *et al.* Role of COX-2/mPGES-1/Prostaglandin E2 Cascade in Kidney Injury. *Mediators of Inflammation* (2015). doi:10.1155/2015/147894
32. Reid, G. *et al.* The human multidrug resistance protein MRP4 functions as a prostaglandin efflux transporter and is inhibited by nonsteroidal antiinflammatory drugs. *Proc. Natl. Acad. Sci. U. S. A.* **100**, 9244–9249 (2003).
33. Breyer, M. D. & Breyer, R. M. Prostaglandin E receptors and the kidney. *Am. J. Physiol.-Ren. Physiol.* **279**, F12–F23 (2000).
34. Karger, C. *et al.* COX-2-derived PGE2 triggers hyperplastic renin expression and hyperreninemia in aldosterone synthase-deficient mice. *Pflugers Arch.* **470**, 1127–1137 (2018).
35. Markovič, T., Jakopin, Ž., Dolenc, M. S. & Mlinarič-Raščan, I. Structural features of subtype-selective EP receptor modulators. *Drug Discov. Today* **22**, 57–71 (2017).
36. Hla, T., Bishop-Bailey, D., Liu, C. H., Schaefers, H. J. & Trifan, O. C. Cyclooxygenase-1 and -2 isoenzymes. *Int. J. Biochem. Cell Biol.* **31**, 551–557 (1999).
37. He, W. *et al.* Increased Dietary Sodium Induces COX2 Expression by activating NFκB in Renal Medullary Interstitial Cells. *Pflugers Arch.* **466**, 357–367 (2014).
38. Kirkby, N. S. *et al.* Systematic study of constitutive cyclooxygenase-2 expression: Role of NF-κB and NFAT transcriptional pathways. *Proc. Natl. Acad. Sci. U. S. A.* **113**, 434–439 (2016).
39. Inoue, H. & Tanabe, T. Transcriptional Role of the Nuclear Factor κB Site in the Induction by Lipopolysaccharide and Suppression by Dexamethasone of Cyclooxygenase-2 in U937 Cells. *Biochem. Biophys. Res. Commun.* **244**, 143–148 (1998).
40. Transcriptional Regulation of Human Prostaglandin-endoperoxide Synthase-2 Gene by Lipopolysaccharide and Phorbol Ester in Vascular Endothelial Cells.

Available at: http://www.jbc.org/content/270/42/24965.long. (Accessed: 2nd April 2019)

41. Ristimäki, A., Narko, K. & Hla, T. Down-regulation of cytokine-induced cyclo-oxygenase-2 transcript isoforms by dexamethasone: evidence for post-transcriptional regulation. *Biochem. J.* **318**, 325–331 (1996).
42. IL-1 beta stabilizes COX II mRNA in renal mesangial cells: role of 3'-untranslated region | American Journal of Physiology-Renal Physiology. Available at: https://www.physiology.org/doi/abs/10.1152/ajprenal.1994.267.3.F504. (Accessed: 2nd April 2019)
43. Wagner, C. *et al.* Differential regulation of renin and Cox-2 expression in the renal cortex of C57Bl/6 mice. *Pflüg. Arch.* **447**, 214–222 (2003).
44. Khan, K. N. M., Paulson, S. K., Verburg, K. M., Lefkowith, J. B. & Maziasz, T. J. Pharmacology of cyclooxygenase-2 inhibition in the kidney. *Kidney Int.* **61**, 1210–1219 (2002).
45. Jia Zhanjun *et al.* Microsomal Prostaglandin Synthase-1–Derived Prostaglandin E2 Protects Against Angiotensin II–Induced Hypertension via Inhibition of Oxidative Stress. *Hypertension* **52**, 952–959 (2008).
46. Zewde Tewabech & Mattson David L. Inhibition of Cyclooxygenase-2 in the Rat Renal Medulla Leads to Sodium-Sensitive Hypertension. *Hypertension* **44**, 424–428 (2004).
47. Nissen, H. M. & Bojesen, I. On lipid droplets in renal interstitial cells. *Z. Für Zellforsch. Mikrosk. Anat.* **97**, 274–284 (1969).
48. Hao Chuan-Ming & Breyer Matthew D. Hypertension and Cyclooxygenase-2 Inhibitors. *Hypertension* **44**, 396–397 (2004).

49. Frölich, S. *et al.* Angiotensin II-AT1–receptor signaling is necessary for cyclooxygenase-2–dependent postnatal nephron generation. *Kidney Int.* **91**, 818–829 (2017).
50. Murakami, M. *et al.* Regulation of Prostaglandin E2 Biosynthesis by Inducible Membrane-associated Prostaglandin E2 Synthase That Acts in Concert with Cyclooxygenase-2. *J. Biol. Chem.* **275**, 32783–32792 (2000).
51. Neuhofer, W., Steinert, D., Fraek, M.-L. & Beck, F.-X. Prostaglandin E2 stimulates expression of osmoprotective genes in MDCK cells and promotes survival under hypertonic conditions. *J. Physiol.* **583**, 287–297 (2007).
52. Yang, T. *et al.* Renin expression in COX-2-knockout mice on normal or low-salt diets. *Am. J. Physiol.-Ren. Physiol.* **279**, F819–F825 (2000).
53. Yang, T. & Liu, M. REGULATION AND FUNCTION OF RENAL MEDULLARY CYCLOOXYGENASE-2 DURING HIGH SALT LOADING. *Front. Biosci. Landmark Ed.* **22**, 128–136 (2017).
54. Hermann Matthias *et al.* Selective COX-2 Inhibitors and Renal Injury in Salt-Sensitive Hypertension. *Hypertension* **45**, 193–197 (2005).
55. Xue, X. & Shah, Y. M. Hypoxia-inducible factor-2α is essential in activating the COX2/mPGES-1/PGE2 signaling axis in colon cancer. *Carcinogenesis* **34**, 163–169 (2013).
56. Zhu, Q. *et al.* Overexpression of HIF prolyl-hydoxylase-2 transgene in the renal medulla induced a salt sensitive hypertension. *J. Cell. Mol. Med.* **16**, 2701–2707 (2012).
57. Li, N., Chen, L., Yi, F., Xia, M. & Li, P.-L. Salt-sensitive hypertension induced by decoy of transcription factor hypoxia-inducible factor-1alpha in the renal medulla. *Circ. Res.* **102**, 1101–1108 (2008).

58. Ehmke, H. & Kurtz, A. Deciphering the physiological roles of COX-2. *Am. J. Physiol.-Regul. Integr. Comp. Physiol.* **284**, R486–R487 (2003).
59. Catella-Lawson, F. *et al.* Effects of Specific Inhibition of Cyclooxygenase-2 on Sodium Balance, Hemodynamics, and Vasoactive Eicosanoids. *J. Pharmacol. Exp. Ther.* **289**, 735–741 (1999).
60. Qi, Z. *et al.* Opposite effects of cyclooxygenase-1 and -2 activity on the pressor response to angiotensin II. *J. Clin. Invest.* **110**, 61–69 (2002).
61. Yang, T. *et al.* Influence of genetic background and gender on hypertension and renal failure in COX-2-deficient mice. *Am. J. Physiol.-Ren. Physiol.* **288**, F1125–F1132 (2005).
62. Elliott, W. J. Do the Blood Pressure Effects of Nonsteroidal Antiinflammatory Drugs Influence Cardiovascular Morbidity and Mortality? *Curr. Hypertens. Rep.* **12**, 258–266 (2010).
63. Kohsaka, S. *et al.* Increased risk of incident stroke associated with the cyclooxygenase 2 (COX-2) G−765C polymorphism in African-Americans: The Atherosclerosis Risk in Communities Study. *Atherosclerosis* **196**, 926–930 (2008).
64. Yu, Y. *et al.* Vascular COX-2 Modulates Blood Pressure and Thrombosis in Mice. *Sci. Transl. Med.* **4**, (2012).
65. Hörl, W. H. Nonsteroidal Anti-Inflammatory Drugs and the Kidney. *Pharmaceuticals* **3**, 2291–2321 (2010).
66. Kaewput, W., Disorn, P. & Satirapoj, B. Selective cyclooxygenase-2 inhibitor use and progression of renal function in patients with chronic kidney disease: a single-center retrospective cohort study. *Int. J. Nephrol. Renov. Dis.* **9**, 273–278 (2016).
67. Perazella, M. A. & Tray, K. Selective cyclooxygenase-2 inhibitors: a pattern of nephrotoxicity similar to traditional nonsteroidal anti-inflammatory drugs. *Am. J. Med.* **111**, 64–67 (2001).

68. Østensen, M. E. & Skomsvoll, J. F. Anti-inflammatory pharmacotherapy during pregnancy. *Expert Opin. Pharmacother.* **5**, 571–580 (2004).
69. Nakhai-Pour, H. R. & Bérard, A. Major malformations after first trimester exposure to aspirin and NSAIDs. *Expert Rev. Clin. Pharmacol.* **1**, 605–616 (2008).
70. Akhund, L., Quinet, R. J. & Ishaq, S. Celecoxib-related renal papillary necrosis. *Arch. Intern. Med.* **163**, 114–115 (2003).
71. Sanders, P. W. Vascular consequences of dietary salt intake. *Am. J. Physiol.-Ren. Physiol.* **297**, F237–F243 (2009).
72. Cheng, H. F. & Harris, R. C. Renal effects of non-steroidal anti-inflammatory drugs and selective cyclooxygenase-2 inhibitors. *Curr. Pharm. Des.* **11**, 1795–1804 (2005).
73. Morgan, T. O., Anderson, A. & Bertram, D. Effect of indomethacin on blood pressure in elderly people with essential hypertension well controlled on amlodipine or enalapril. *Am. J. Hypertens.* **13**, 1161–1167 (2000).
74. Höcherl, K., Endemann, D., Kammerl, M. C., Grobecker, H. F. & Kurtz, A. Cyclo-oxygenase-2 inhibition increases blood pressure in rats. *Br. J. Pharmacol.* **136**, 1117–1126 (2002).
75. Mishra, S., Ingole, S. & Jain, R. Salt sensitivity and its implication in clinical practice. *Indian Heart J.* **70**, 556–564 (2018).
76. Matzdorf, C., Kurtz, A. & Höcherl, K. COX-2 activity determines the level of renin expression but is dispensable for acute upregulation of renin expression in rat kidneys. *Am. J. Physiol.-Ren. Physiol.* **292**, F1782–F1790 (2007).
77. Neuhofer, W. *et al.* Chronic COX-2 inhibition reduces medullary HSP70 expression and induces papillary apoptosis in dehydrated rats11.See Editorial by Aufricht, p. 739. *Kidney Int.* **65**, 431–441 (2004).

78. Ye, W. *et al.* Expression and function of COX isoforms in renal medulla: evidence for regulation of salt sensitivity and blood pressure. *Am. J. Physiol.-Ren. Physiol.* **290**, F542–F549 (2006).
79. Hao, S., DelliPizzi, A., Quiroz-Munoz, M., Jiang, H. & Ferreri, N. R. The EP3 receptor regulates water excretion in response to high salt intake. *Am. J. Physiol.-Ren. Physiol.* **311**, F822–F829 (2016).
80. Liu, Y., Flores, D., Carrisoza-Gaytán, R. & Rohatgi, R. Biomechanical regulation of cyclooxygenase-2 in the renal collecting duct. *Am. J. Physiol. - Ren. Physiol.* **306**, F214–F223 (2014).
81. Dinchuk, J. E. *et al.* Renal abnormalities and an altered inflammatory response in mice lacking cyclooxygenase II. *Nature* **378**, 406 (1995).
82. Slattery, P., Frölich, S., Goren, I. & Nüsing, R. M. Salt supplementation ameliorates developmental kidney defects in COX-2−/− mice. *Am. J. Physiol.-Ren. Physiol.* **312**, F1044–F1055 (2017).
83. Januszyk, M. *et al.* Evaluating the Effect of Cell Culture on Gene Expression in Primary Tissue Samples Using Microfluidic-Based Single Cell Transcriptional Analysis. *Microarrays* **4**, 540–550 (2015).
84. Cowley, A. W. Renal Medullary Oxidative Stress, Pressure-Natriuresis, and Hypertension. *Hypertension* **52**, 777–786 (2008).
85. Facemire Carie S., Griffiths Robert, Audoly Laurent P., Koller Beverly H. & Coffman Thomas M. The Impact of Microsomal Prostaglandin E Synthase 1 on Blood Pressure Is Determined by Genetic Background. *Hypertension* **55**, 531–538 (2010).
86. Zhang, D. *et al.* Enhanced pressor response to acute Ang II infusion in mice lacking membrane-associated prostaglandin E2 synthase-1. *Acta Pharmacol. Sin.* **31**, 1284–1292 (2010).

87. Gerl, M. COX-2 und TGF-β als potentielle Faktoren zur Steuerung der Reninzellrekrutierung - Untersuchungen in COX-2- und reninzellspezifischen TGF-βRII-Knockoutmäusen. (2011).
88. Ishikawa, T. & Herschman, H. R. Conditional knockout mouse for tissue-specific disruption of the cyclooxygenase-2 (Cox-2) gene. *genesis* **44**, 143–149 (2006).
89. Nilsson, L. *et al.* Disruption of cyclooxygenase-2 prevents downregulation of cortical AQP2 and AQP3 in response to bilateral ureteral obstruction in the mouse. *Am. J. Physiol.-Ren. Physiol.* **302**, F1430–F1439 (2012).
90. He, W. *et al.* Sirt1 activation protects the mouse renal medulla from oxidative injury. *J. Clin. Invest.* **120**, 1056–1068 (2010).
91. Yang, T. & Li, C. Role of COX-2 in unilateral ureteral obstruction: what is new? *Am. J. Physiol. - Ren. Physiol.* **310**, F746–F747 (2016).
92. Yang, C. *et al.* Chitosan/siRNA Nanoparticles Targeting Cyclooxygenase Type 2 Attenuate Unilateral Ureteral Obstruction-induced Kidney Injury in Mice. *Theranostics* **5**, 110–123 (2015).
93. Indra, A. K. *et al.* Temporally-controlled site-specific mutagenesis in the basal layer of the epidermis: comparison of the recombinase activity of the tamoxifen-inducible Cre-ER(T) and Cre-ER(T2) recombinases. *Nucleic Acids Res.* **27**, 4324–4327 (1999).
94. Kobayashi, A. *et al.* Identification of a Multipotent Self-Renewing Stromal Progenitor Population during Mammalian Kidney Organogenesis. *Stem Cell Rep.* **3**, 650–662 (2014).
95. Mederacke, I. *et al.* Fate-tracing reveals hepatic stellate cells as dominant contributors to liver fibrosis independent of its etiology. *Nat. Commun.* **4**, 2823 (2013).

96. Feil, R., Wagner, J., Metzger, D. & Chambon, P. Regulation of Cre Recombinase Activity by Mutated Estrogen Receptor Ligand-Binding Domains. *Biochem. Biophys. Res. Commun.* **237**, 752–757 (1997).

97. Haase, V. H., Glickman, J. N., Socolovsky, M. & Jaenisch, R. Vascular tumors in livers with targeted inactivation of the von Hippel-Lindau tumor suppressor. *Proc. Natl. Acad. Sci. U. S. A.* **98**, 1583–1588 (2001).

98. Rahman, A. *et al.* A novel approach to adenine-induced chronic kidney disease associated anemia in rodents. *PLoS ONE* **13**, (2018).

99. Jia, T. *et al.* A novel model of adenine-induced tubulointerstitial nephropathy in mice. *BMC Nephrol.* **14**, 116 (2013).

100. Buchtler, S. *et al.* Cellular Origin and Functional Relevance of Collagen I Production in the Kidney. *J. Am. Soc. Nephrol.* **29**, 1859–1873 (2018).

101. Rieg, T. A High-throughput Method for Measurement of Glomerular Filtration Rate in Conscious Mice. *J. Vis. Exp. JoVE* (2013). doi:10.3791/50330

102. Wang, F. *et al.* RNAscope. *J. Mol. Diagn. JMD* **14**, 22–29 (2012).

103. Chomczynski, P. & Sacchi, N. Single-step method of RNA isolation by acid guanidinium thiocyanate-phenol-chloroform extraction. *Anal. Biochem.* **162**, 156–159 (1987).

104. Zhang Ming-Zhi *et al.* Renal Medullary Interstitial COX-2 (Cyclooxygenase-2) Is Essential in Preventing Salt-Sensitive Hypertension and Maintaining Renal Inner Medulla/Papilla Structural Integrity. *Hypertension* **72**, 1172–1179 (2018).

105. Gambaro, G. & Perazella, M. A. Adverse renal effects of anti-inflammatory agents: evaluation of selective and nonselective cyclooxygenase inhibitors. *J. Intern. Med.* **253**, 643–652 (2003).

106. Lin, S.-L., Kisseleva, T., Brenner, D. A. & Duffield, J. S. Pericytes and Perivascular Fibroblasts Are the Primary Source of Collagen-Producing Cells in Obstructive Fibrosis of the Kidney. *Am. J. Pathol.* **173**, 1617–1627 (2008).

107. Gomez, I. G. & Duffield, J. S. The FOXD1 lineage of kidney perivascular cells and myofibroblasts: functions and responses to injury. *Kidney Int. Suppl.* **4**, 26–33 (2014).

108. Diwan, V., Brown, L. & Gobe, G. C. Adenine-induced chronic kidney disease in rats. *Nephrology* **23**, 5–11 (2018).

109. Johnson, A. G., Nguyen, T. V. & Day, R. O. Do nonsteroidal anti-inflammatory drugs affect blood pressure? A meta-analysis. *Ann. Intern. Med.* **121**, 289–300 (1994).

110. Harirforoosh, S. & Jamali, F. Renal adverse effects of nonsteroidal anti-inflammatory drugs. *Expert Opin. Drug Saf.* **8**, 669–681 (2009).

111. Whelton, A., Maurath, C. J., Verburg, K. M. & Geis, G. S. Renal Safety and Tolerability of Celecoxib, a Novel Cyclooxygenase-2 Inhibitor. *Am. J. Ther.* **7**, 159 (2000).

112. Yu, Y. *et al.* Cyclooxygenase-2–Dependent Prostacyclin Formation and Blood Pressure Homeostasis. *Circ. Res.* (2010). doi:10.1161/CIRCRESAHA.109.204529

113. Fierro-Carrion, G. A. & Ram, C. V. S. Nonsteroidal Anti-Inflammatory Drugs (NSAIDs) and Blood Pressure. *Am. J. Cardiol.* **80**, 775–776 (1997).

114. He, W. *et al.* Generation of a Tenascin-C-CreER2 Knockin Mouse Line for Conditional DNA Recombination in Renal Medullary Interstitial Cells. *PLoS ONE* **8**, (2013).

115. Srivastava, T. *et al.* Cyclooxygenase-2, prostaglandin E2, and prostanoid receptor EP2 in fluid flow shear stress-mediated injury in the solitary kidney. *Am. J. Physiol.-Ren. Physiol.* **307**, F1323–F1333 (2014).

116. Ogasawara, A. *et al.* Fluid Shear Stress-induced Cyclooxygenase-2 Expression Is Mediated by C/EBP β, cAMP-response Element-binding Protein, and AP-1 in Osteoblastic MC3T3-E1 Cells. *J. Biol. Chem.* **276**, 7048–7054 (2001).

117. Wang Zhengchao *et al.* Hypoxia-Inducible Factor Prolyl-Hydroxylase 2 Senses High-Salt Intake to Increase Hypoxia Inducible Factor 1α Levels in the Renal Medulla. *Hypertension* **55**, 1129–1136 (2010).

118. Norwood, V. F., Morham, S. G. & Smithies, O. Postnatal development and progression of renal dysplasia in cyclooxygenase-2 null mice. *Kidney Int.* **58**, 2291–2300 (2000).

119. Cheng, H.-F. *et al.* Genetic deletion of COX-2 prevents increased renin expression in response to ACE inhibition. *Am. J. Physiol.-Ren. Physiol.* **280**, F449–F456 (2001).

120. Neubauer Bjoern *et al.* Angiotensin II Short-Loop Feedback. *Hypertension* **71**, 1075–1082 (2018).

121. Schrankl, J. *et al.* Apparently normal kidney development in mice with conditional disruption of ANGII-AT1 receptor genes in FoxD1 positive stroma cell precursors. *Am. J. Physiol.-Ren. Physiol.* (2019). doi:10.1152/ajprenal.00305.2018

122. Qi Zhonghua, Cai Hui, Morrow Jason D. & Breyer Matthew D. Differentiation of Cyclooxygenase 1- and 2–Derived Prostanoids in Mouse Kidney and Aorta. *Hypertension* **48**, 323–328 (2006).

123. Nørregaard, R., Kwon, T.-H. & Frøkiær, J. Physiology and pathophysiology of cyclooxygenase-2 and prostaglandin E2 in the kidney. *Kidney Res. Clin. Pract.* **34**, 194–200 (2015).

124. Imai, T. *et al.* Identification and Molecular Characterization of Fractalkine Receptor CX3CR1, which Mediates Both Leukocyte Migration and Adhesion. *Cell* **91**, 521–530 (1997).

125. Brand, S., Sakaguchi, T., Gu, X., Colgan, S. P. & Reinecker, H. Fractalkine-mediated signals regulate cell-survival and immune-modulatory responses in intestinal epithelial cells. *Gastroenterology* **122**, 166–177 (2002).

126. Chevalier, R. L., Forbes, M. S. & Thornhill, B. A. Ureteral obstruction as a model of renal interstitial fibrosis and obstructive nephropathy. *Kidney Int.* **75**, 1145–1152 (2009).

127. Nilsson, L. *et al.* Disruption of cyclooxygenase type 2 exacerbates apoptosis and renal damage during obstructive nephropathy. *Am. J. Physiol.-Ren. Physiol.* **309**, F1035–F1048 (2015).

7 Annex

7.1 Abbreviations

°C	degree Celsius
AA	arachidonic acid
AB	antibody
ACE	Angiotensin converting enzym
ANG I	Angiotensin I
AR	aldose reductase
BGT1	sodium and chloride dependent betain/GABA transpoter 1
bp	base pair
BSA	Bovine Serum Albumin
BW	body weight
CAGG	artificial CAG Promotor
cAMP	cyclic adenosine monophosphate
CD	collecting duct
CD73	ecto-5'-nucleotidase
CKD	Chronic kidney disease
Col1a1	Collagen, type I, alpha 1
Cox-2	Cyclooxygenase 2
$CreER^{T2}$	tamoxifen-inducible Cre-ERT2 fusion protein
cTAL	cortical thick ascending limp of the loop of Henle
Cy	Cyanine
DAPI	4′,6-Diamidin-2-phenylindol
DNA	Deoxyribonucleic acid
ENAC	Epithelial sodium channel
EPO	Erythropoetin
FoxD1	forkhead box D1
FSB	first strand buffer 5x
gDNA	genomic DNA
GFR	glomerular filtration rate
h	hour
HEPES	(4-(2-hydroxyethyl)-1-piperazineethanesulfonic acid)
HIF	hypoxia inducible factor
HoxB7	homebox protein B7
HS	Horse Serum
HSP70	heat shock protein 70
i.p	inter peritoneal
IF	Immunofluorescence
IL	interleukin
ISH	*In-situ* hybridization

JGA	juxtaglomerular apparatus
MEF2	myocyte enhancer factor-2
min	minute
mMol/l	million moles per liter
mOsmol/l	million osmoles per liter
mPGES	membrane associated prostaglandin E synthase
mRNA	Messenger ribonucleic acid
NBF	Neutral buffered formalin
NF	nuclear factor
NFAT	Nuclear factor of activated T-cells
NFκB	nuclear factor kappa-light-chain-enhancer of activated B cells specificity protein 1
NG2	Neural/glial antigen 2
NKCC2	Na^+-K^+-Cl^- cotransporter
nm	nanometer
NSAID	non steroidal anti-inflammatory drug
PBS	Phosphate buffered saline
PDGF	platelet derived growth factor
PG	prostaglandin
PMSF	Phenylmethylsulfonylfluorid
PTGS	prostaglandin endoperoxide synthase
RNA	ribonucleic acid
RPL32	Ribosomal Protein L32
rpm	revolutions per minute
RT	room temperature
s	second
Six2	six homebox 2
SMIT	sodium dependent myo-inositol cotransporter
SM-MHC	Smooth Muscle Myosin Heavy Chain
SP1	specificity protein 1
SR	picro-sirius red staining
TNC	tenascin – C
TRITC	5(6)-Tetramethylrhodaminisothiocyanat
TX	thromboxane
UTA1	Urea transporter A1
UUO	unilateral ureter obstruction
V	Volt
Vhl	von-Hippel-Lindau
wks	weeks
WT	wildtype
MWF rat	Munich Wistar Frömter rat

7.2 Congress contributions

Europhysiology London 2018 – Poster price in Metabolism & Endocrinology

"The importance of Cox-2 in interstitial cells of the renal medulla for kidney function and salt handling"

Kongress für Nephrologie 2018

"Charakterisierung der Rolle von Cyclooxygenase-2 in PDGFR-β^{+} intersitiellen Zellen der renalen Medulla"

7.3 Declaration

I declare that this work has been authored by myself without the undue and inadmissible help by other persons and no other aids as those listed were used. The persons mentioned in the acknowledgement kindly provided their help without direct or indirect payment from myself. No other forms of payment, direct or indirect, were given out in connection with this work.

No other persons have helped me with the conception and realization of this work. No professional services or agencies were involved in the experimental or writing process of this work.

This thesis has not been submitted in part or as a whole in this country or abroad to any other committee.

Regensburg 10.07.2019

Michaela Fuchs

8 Acknowledgement

I would like to take this opportunity to thank all the people who supported me during my thesis.

Special thanks is due to Prof. Dr. Armin Kurtz who gave me the opportunity to work on this engaging and interesting topic in his laboratory. Prof. Kurtz was an invaluable help, always ready with advice and the engaging discussions provided essential insight and encouragement that made this work a success.

I would also like to thank my dear colleagues Dr. Katharina Gerl and Julia Schrankl. Thank you both for the time you took to let me spin my ideas out loud. Katharina thank you for the endless patience and the support through all ups and downs. Julia, thanks for the friendship, perseverance, help and support. Thank you both: This journey would not have been half as much fun without you inside the lab and with the great time we had outside of it!

Dr. Birgül Kurt helped me find my way in the beginning and always had a helpful tip and an endless well of expertise.

Susanne Fink, Ramona Steppan and Gerda Treuner were a great help with their excellent technical expertise and assistance.

Without the unconditional support of my parents, Johann and Ingrid, I could have never chosen this path. Thank you both for letting me chose my own way and always doing everything in your power to make it possible.

To my brother Andreas: There is no way to list all the ways in which you have helped me and been there for me through the years. None of this would have been possible without you and I would not be the person I am today.